1-16-2017

Real-time Damage Detection for Civil Structures using Big Data

Chenhao Jin
University of Connecticut - Storrs, chenhao.jin@uconn.edu

Real-time Damage Detection for Civil Structures using Big Data

Chenhao Jin, PhD

University of Connecticut, 2017

The overall goal of the research in this dissertation is to develop efficient and accurate algorithms to detect damages in real time for civil structures using large scale of monitoring data. First, big data analysis is performed using one-year monitoring weigh-in-motion data collected from an in-service highway bridge located in Meriden, Connecticut. In order to quickly evaluate the structural condition from large scale of weight-in-motion data, two structural reliability-based methods were developed based on yield strength limit state and fatigue limit state. Then, in order to estimate structural parameter from structural dynamic response data, extended Kalman filter is used to estimate stiffness for a three-story building with MR damper. All the above methodology will be further developed for real-time damage detection for building structure as well as bridge structures.

For building structures, a novel real-time structural damage detection method is developed for building structures that can be represented using structural dynamic models by integrating extended Kalman filter and dynamic statistical process control. The numerical validation is performed on a three-story linear building structure and a two-story nonlinear hysteric building structure, considering different damage scenarios during earthquake excitation. The simulation results demonstrate high detection accuracy rate and light computational costs of this method.

The EKF-based method is further developed for full-scale implementation on bridge structures. An extended Kalman filter-trained artificial neural network (EKFNN) method is developed to eliminate the temperature effects and detect damage for a long-term monitored highway bridge. Numerical testing results show that the temperature-induced changes in natural frequencies have been considered prior to the establishment of the bridge damage warning thresholds, and the simulated damages have been successfully captured in real time.

The research work in this thesis can provide engineers and scientists a thorough understanding of how to process and analyze big data collected from structural health monitoring systems for real-time structural damage detection purpose. This study will also have practical importance for infrastructure owners (e.g., Department of Transportation, building owners, etc.) and first responders (e.g., policemen, fire fighters, rescuers, etc.) to make rapid decisions after structural damage events.

Real-time Damage Detection for Civil Structures using Big Data

Chenhao Jin

M.S., Carnegie Mellon University, 2012

B.S., Hohai University, 2010

A Dissertation

Submitted in Partial Fulfillment of the

Requirements for the Degree of

Doctor of Philosophy

at the

University of Connecticut

2017

Approval Page

Doctor of Philosophy Dissertation

Real-time Damage Detection for Civil Structures using Big Data

Presented by

Chenhao Jin, B.S., M.S.

Major Advisor: _____

Dr. Shinae Jang

Associate Advisor: _____

Dr. Richard Christenson

Associate Advisor: _____

Dr. Jeongho Kim

University of Connecticut

2017

ACKNOWLEDGEMENT

It is my great fortunate to have the opportunity to study and pursue PhD degree in civil engineering at University of Connecticut. The past four years will become one of the most beautiful experiences and memories in my life.

First of all, I would like to thank my major advisor, Prof. Shinae Jang. Prof. Jang provides all the resources and support for me to reach my goal in research as well as in career. I can always get her professional guidance in my research, paper publication and presentations. I appreciate all her generous support on graduate student assistantship, scholarship application and conference participations.

I am truly thankful for the advice, comments and suggestions from my associate advisors and dissertation committee members. Prof. Christenson's bridge monitoring project provided me an excellent test bed to verify my damage detection methods using big data. My knowledge of finite element analysis is the result of taking Prof. Kim's finite element mechanics classes. Prof. Malla's research on dynamics and vibrations of structures and applied mechanics, especially on the long-span railroad bridge monitoring gave me lots of inspirations on my research, and I also got his supervise for teaching assistant and volunteering at Connecticut Innovation Conference (CIC). Chapter 3 in this dissertation is initialized based on my course project in the Structural Reliability course I took with Prof. Zhang. I also would like to thank Prof. Zhaoshuo Jiang, Prof. Sarira Motaref, Dr. Hao Sun, Jin Zhu, Masoud Mehr and Sergio Lobo-Aguilar for their collaboration and help on my research projects.

I thank all my fellow graduate student friends in Department of Civil & Environmental Engineering and School of Engineering at University of Connecticut, especially my colleagues at Prof. Jang's Smart Infrastructure Lab: Edward Eskew, Jingcheng Li, Valeri I. Kolev and Rosana Martinez-Castro.

The last but not the least, I am very grateful for my family, my wife Iris Xiaorong Sun and our new born son. All my recent achievements cannot be made without my wife's strong support and encouragement. Without her, my life would be incomplete.

TABLE OF CONTENTS

LIST OF FIGURES

LIST OF TABLES

CHAPTER 1 INTRODUCTION

Civil structures such as bridges and buildings are essential for the economic development and public safety, and must be under good maintenance. However, the current condition and performance of the infrastructure systems in United States is in urgent need to be improved. According to ASCE 2013 report card, one in nine of the nation's bridges are rated as structurally deficient, while the average age of the nation's 607,380 bridges is currently 42 years (ASCE Report Card, 2013). There are nearly 204 million daily crossings on 58,495 U.S. structurally deficient bridges in need of repair (Federal Highway Administration, 2016). Statistical study showed that 1,062 failed bridges in U.S. were reported during recent two decades from 1980 to 2012 (Lee *et al.*, 2013). Thus, it is of great importance to find damage or defects on civil structures beforehand to prevent structural failures.

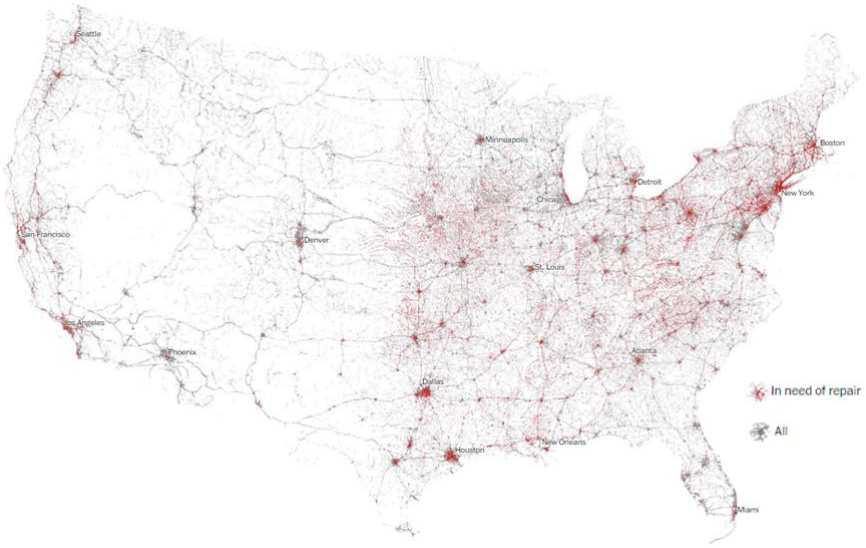

Figure 1.1 Map of all bridges and bridges in need of repair in US (Meko, 2016)

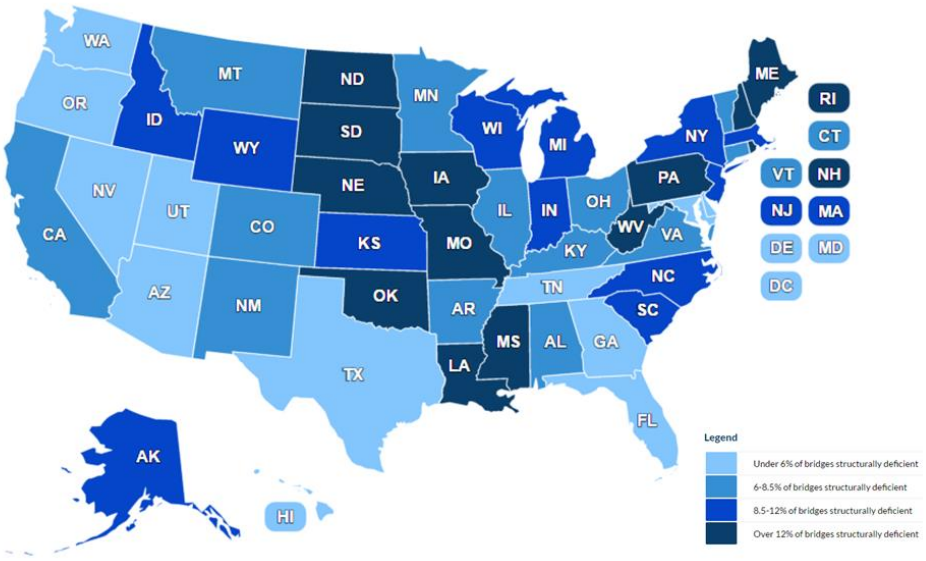

Figure 1.2 Map of 2016 structural deficient bridges in US by state (American Road & Transportation Builders Association, 2016)

Maintaining civil engineering structures in good condition through structural health monitoring (SHM) has become an increasingly viable option in the past two decades. Many structural health monitoring systems have been developed and implemented to obtain reliable information regarding the condition and the integrity of the structures. Through analyzing and extracting key information using data collected from various sensors installed on a structure, structural conditions can be assessed in an automatic, objective and remote way. With the rapid progress of smart sensor technology and decreasing cost of online monitoring, large volume of raw data can be collected from the data acquisition system. More and more SHM systems are targeted to monitor the whole structure instead of some specific hot-spot areas. This current trend brought new challenges for the capacity of traditional data process and analysis approaches. For example, SHM project for Vincent Thomas Bridge in San Pedro, California collected 3 TB data per year (Kallinikidou *et al.*, 2013); 300 GB acoustic data were collected during 6 months for wind turbine monitoring (Anastasopoulos *et al.*, 2012); 7 GB data were obtained per day for Confederation Bridge in Canada (Desjardins *et al.*, 2006); over 20 GB were received for automated railway inspection in Brockton, Massachusetts (Zhang *et al.*, 2014); In the bridge weight-in-motion highway bridge monitoring project in

Meriden Connecticut, more than 4 GB data are collected daily (Christenson *et al.*, 2016). All the above SHM applications call for the use of big data techniques into structural health monitoring. Some good literature about big data analytics for structural health monitoring can be found in Cai and Mahadevan (2016) and Liang *et al.* (2016).

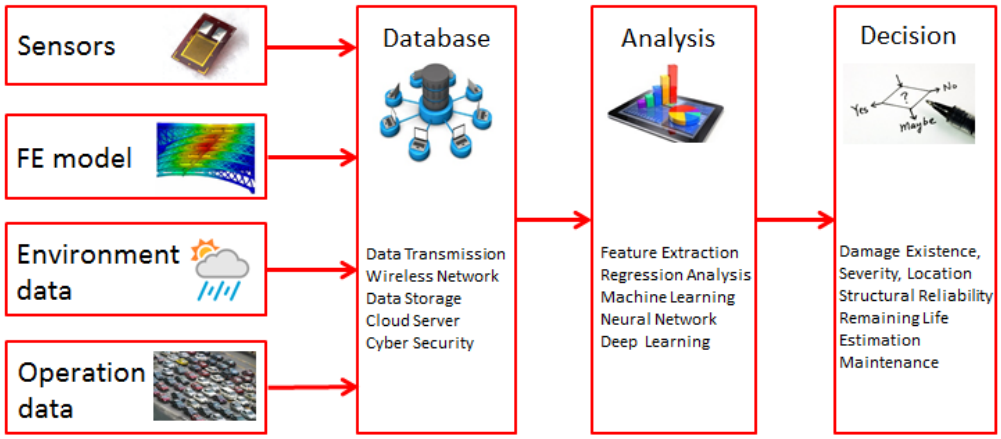

Figure 1.3 Workflow of structural health monitoring

Table 1.1 Example of recent SHM projects

SHM Projects	**Data Size**	**Year**
Confederation Bridge, Canada	7 GB/ Day	2006
Wind Turbine, Greece	300 GB/ 6 Months	2012
Vincent Thomas Bridge, San Pedro, CA	3 TB/ Year	2013
Railway Inspection, Brockton, MA	20 GB	2014
I-91 Highway Bridge, Meriden, CT	16 GB/ Day	2016

The big data problem associated with SHM mainly affects two areas: data acquisition and data analytics. In data acquisition, critical problems include data transmission, data synchronization and wireless sensor network, etc. This research focus on data analytics issues in SHM, in the presence of big data.

1.1 Motivation

1.1.1 Efficient structural condition assessment using big data

The heavy traffic and operation of bridge structures also influence the quality and accuracy of structural health monitoring. Bridge weight-in-motion systems have been developed to estimate the weight of vehicles travelling through bridges. Most damage detection methods are based on acceleration data. It will be helpful to assess the condition of structures based on strain data.

1.1.2 Structural parameter estimation for structures equipped with control devices

Structural health monitoring can be used to identify the existence, location and severity of structural damage, and help to estimate the remaining service life based on fatigue theory. Structural control devices have the ability to protect the structure and reduce the damage from earthquake, wind and waves by using structural control devices. In an ideal system, civil structures have both structural health monitoring system and structural control systems. In structural health monitoring, many damage detection methods are based on structural dynamic models. However, the installation of structure control system will change the structural dynamic model itself, make it unrepresentative of the current condition of the structure, and add difficulty for damage detection. With structural control devices more and more widely used in civil structures, it is important to develop achieve real time parameter estimation for structures equipped with control devices.

1.1.4 Real time damage detection for building structures

After disasters such as earthquake, tsunami, surface subsidence, fire or blasts, post-disaster evaluations are of great importance to assess structural conditions for damaged buildings. Decision about whether the building is structural deficient is valuable for building owners or authority to decide whether the building should be evacuated, repaired, demolished or still being in use.

1.1.4 Real time damage detection for bridges

The modal parameters of bridge structures are affected by many operational and environmental factors. Among these factors, temperature is the dominant factor affecting the modal parameters of the bridge under normal condition. One important goal of structural health monitoring is to detect the damage when it occurs. A challenge for vibration based damage detection method is that the changes of modal property due to temperature effect might be larger than due to structural damage. If the temperature effect is not considered and accounted in the damage detection rules, false alarm problems may arise and limit the effectiveness of structural health monitoring for in-service structures. It is critical to develop effective structural damage detection method and consider temperature effect in damage detection rule for in-service bridge structures.

1.2 Research objectives

The objective of this dissertation is to develop efficient and accurate algorithms to analyze big data collected from structural health monitoring systems for real time structural damage detection purpose. The objectives of the research are listed as follows:

(1) On the basis of statistical analysis of bridge weight-in-motion data, propose an efficient method to evaluate the condition of the whole bridge structure in fast speed.

(2) Develop a structural stiffness estimation method for civil structures equipped with structural control devices. MR damper will be used in this research due to its promising advantages.

(3) Extend the method developed in objective 2 to develop a real time damage detection method for building structures. This research should consider how to deal with the uncertain effects in the dynamic system in order to decrease false alarm rate.

(4) Develop a real time damage detection method for bridge structures from historical data. One-year monitoring data from a highway bridge in Meriden CT will be used as testbed. This real time damage detection method should consider both severe temperature effects and real bridge damage scenarios.

1.3 Organization of Dissertation

The following paragraphs outline the contents of the research presented in this dissertation. Chapter 2 will provide background literature review on structural health monitoring, structural control, structural parameter estimation and neural network method. Chapter 3 will implement a pilot study through analyzing bridge monitoring data from Meriden Bridge to implement a quick assessment of structural reliability. Chapter 4 will explore structural parameter estimation using extended Kalman filter method for a special structure equipped with control devices. Chapter 5 will extend the previous EKF method to achieve the goal of real-time structural damage detection for building structures. In Chapter 6, the above methods will be further developed to a machine learning algorithm for real-time damage detection for a highway bridge based on one-year monitoring data. In the end, conclusion and recommendations for future work will be highlighted.

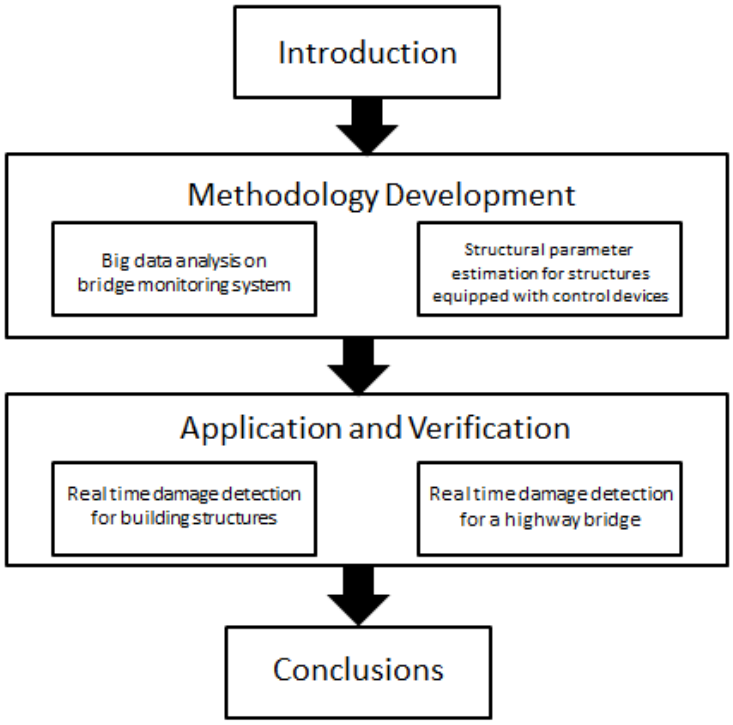

Figure 1.4 Flowchart for organization of research

CHAPTER 2 LITERATURE REVIEW

In this chapter, a summary of literature review of the proposed work has been provided. First, the bridge reliability assessment methods using weight-in-motion data are reviewed. Secondly, dynamic models for MR damper are surveyed in order to understand the behavior of structure control device equipped structures. Thirdly, in order to achieve real time damage detection, extend Kalman filter-based methods are studied. Fourthly, temperature effects on natural frequency of bridge structures are studied. In the end, in order to eliminate the temperature effects on structural properties, neural network-based methods used in bridge monitoring projects will be surveyed.

2.1 Bridge weight-in-motion based reliability assessment

In the field of structural health monitoring, strain gauges are widely used in monitoring systems. They are inexpensive, easy to install, and sensitive enough to detect the potential danger of a structure. Based on the strain data history, a lot of investigations and applications have been done on fatigue damage evaluation and life prediction of bridge structures. Two traditional approaches are commonly used: (1) S-N curve method, which focus on the relationship between the constant-amplitude stress range and the number of cyclic loadings; (2) fracture mechanics, which is dedicated to explore the characteristics of crack initialization and growth.

Over the past several decades, the concepts and methods of structural reliability have developed rapidly and widely accepted. Most of the research work on reliability-based fatigue analysis has focused on steel bridges. The general approach is to formulate a mathematical model, usually the lognormal and Weibull distribution are used for load distribution. The fatigue reliability assessment of steel bridges can be performed by using the probability density function of the equivalent stress range (Kim, *et al.* 2001) and a continuous probabilistic formulation of Miner's rule (Kwon and Frangopol, 2010).

Professor Dan M. Frangopol has extensive research work in the field of Bridge reliability assessment. He proposed an efficient approach to use monitoring data to evaluate structural reliability (Frangopol *et al.*

2008). Ming Liu and Dan M. Frangopol also presented a system reliability-based approach using SHM data (Liu *et al.* 2009). The two papers provide a solid basis for integrating monitoring data into bridge reliability assessment, which will be adopted in this research.

2.2 Dynamic models for MR damper

MR damper's dynamic behavior show highly nonlinear properties, which makes it difficult to find a universal model to represent and control effectively. Many mathematical models have been proposed and verified to determine the values of MR damper force as a function of current, displacement and velocity of the damper: Bouc-Wen model (Rodriguez, *et al.* 2008), hyperbolic tangent model (Bass and Christenson, 2007), viscous plus Dahl model (Aguirre *et al.* 2012), Bingham model and LuGre model (Shirazi, *et al.* 2012), etc. The hyperbolic tangent model was proposed by Bass and Christenson in 2007. In the hyperbolic tangent model, MR damper can be described by two sets of spring-dashpot elements connected by an inertial mass element. All parameters in MR damper can be represented as pre-identified functions of current. The dynamics of the system and force output can be described in state space form, which can be combined with structural dynamic model in a new state space model.

2.3 Extended Kalman filter based real-time damage detection

Many structural parameter identification methods have been developed in order to estimate system parameters based on the measurements of structural response data directly, including extended Kalman filter (EKF), unscented Kalman filter (UKF) and Particle filter. These methods can estimate structural parameters straightly, so that they can provide more detailed information and understanding about the existence, location, and severity of the structural damage. Recently EKF is widely used in state estimation and structural parameter estimation for civil engineering problems (Yang *et al.* 2006, 2007; Soyoz and Feng, 2008; Lei *et al.* 2012; Liu *et al.* 2009; Yin *et al.* 2013) due to its high updating frequency, fast convergence speed, and low computational costs.

Statistical process control (SPC) has been widely used to monitor and control processes due to its advantages of early detection and prevention capability. The SPC attempts to differentiate additional sources of variation from natural sources in a process by using control limits. When the process data deviate from their normal range and trigger the control limits, the excessive variation of data indicates the presence of faults or damage in the system. SPC has been applied to many solve damage detection problems in the field of SHM, especially in long-term bridge monitoring research projects (Sohn *et al.* 2000; Fugate *et al.* 2001; Kullaa 2003; Deraemaeker *et al.* 2008; Zapico-Valle, *et al.* 2011; Magalhaes, *et al.* 2012).

2.4 Temperature effects on bridge natural frequency

The temperature effects on modal properties of bridge structures have been intensively investigated. For example, the natural frequencies of Alamos Canyon Bridge (Cornwell, *et. al.* 1999) were discovered to vary 5% during a 24-hour period, and the natural frequencies of Z-24 Bridge (Peeters, *et al.* 2001) were found to fluctuate 14%-18% in one-year period. The freezing effect is also found on the relationship between natural frequencies and temperature when the temperature is below the freezing point (0ºC or 32ºF) (Gonzales, *et al.* 2013; Li, 2014).

Different methods have been developed for structural damage detection for in-service bridges considering temperature effects, including statistical regression models and artificial neural networks. Linear regression model assumes a linear function to describe relationships between modal parameter and affecting factors. The coefficients of the function are estimated based on historical data, and the adequacy of the model is then verified by analyzing model residuals. Peeters presented a dynamic linear regression analysis method based on an Autoregressive and Exogenous model to filter out temperature effects on natural frequencies for the Z-24 Bridge (Peeters, *et al.* 2001). Ding and Li presented a polynomial regression model to fit frequency-temperature relations for Runyang Suspension Bridge (Ding and Li, 2011). However, the disadvantage of regression analysis is that many real-world phenomena are not simply represented as a single equation with sure estimators, especially when the regression functions do not contain all potential independent variables.

2.5 Neural network-based structural damage detection

Artificial neural networks (NNs) have been widely used in structural damage detection because of their strong capability to approximate the nonlinear functions between inputs and outputs through learning from historical data. Sohn *et al.* developed an auto-associative neural network (AANN)-based method considering environmental and operational conditions for structural damage detection, which selected linear regression model parameters as input and output (Sohn, *et al.* 2002). Zhou *et al*. developed a back propagation neural network (BPNN)-based approach which picked normalized modal frequency as input, and generated novelty index as output to detect damage (Zhou, *et al.* 2010, 2011). Xu *et al.* used BPNN-based approach to predict damage magnitude based on modal energy-based damage index for Crowchild Bridge (Xu and Humar, 2006). Mata developed a neural network model that uses environmental factors as input and displacement as output to analyze behavior for a concrete dam (Mata, 2011). These papers focused on the estimation of the relationship between environmental factors and modal properties, and shared insights on input parameters selection for neural network models. However, based on the authors' best knowledge, none of them used the historical data to predict the natural frequency. Moreover, using AANN or BPNN might suffer from slow convergence in view of the nature of first order learning algorithm. In addition, the confidence intervals of the predictions were not given, which means the quality of damage detection was hard to evaluate.

2.6 Challenges

In this section, the challenges and difficulties of each topic are discussed and explained. First, the challenges of using neural network methods in structural damage detection will be discussed. Secondly, the difficulties of bridge weight-in-motion will be discussed. The third part focus on structural dynamic model based damage detection. The fourth part covers damage detection for structure with MR dampers.

2.6.1 Bridge weight-in-motion based structural health monitoring

In early stage of structural health monitoring, only short period (several hours) of data can be monitored using limited number of sensors. The latest development in sensor technology and computer hardware make equipment much cheaper and smaller than before, and make long-term structural health monitoring possible. Nowadays, a typical structural health monitoring system contains multiple types of sensors and up to hundreds of sensors. And data acquisition systems usually operate 24 hours a day, 7 days a week continuously. Such structural health monitoring system collects several GB of data every day, which makes data analytics work more challenge than before. Moreover, considering the tendency that SHM systems will be installed on more and more bridge structures in the infrastructure networks, how to use techniques in big data analytics to solve structural damage detection problem from bridge monitoring data will become an urgent problem for structural engineers and infrastructure authorities (e.g., National Highway Authority, State Department of Transportation).

With the development of sensing technology, civil engineers will have more choices for structural health monitoring. On the other hand, more advanced technology means bigger data collected and superior algorithm needed for structural damage detection. The next generation of structural health monitoring system will be smarter to be able to process all data on site. With more and more big data available for various types of bridges, selecting proper big damage processing methods will be a challenge to help us recognize the pattern of bridge monitoring data and detect damage before bridge failure happens. Another challenge of big data analytics for bridge weight-in-motion monitoring will be sensor fusion. Multiple sensor displacement has already become common for bridge monitoring. Some large scale bridges even have hundreds of sensors. Developing methods of information fusion using diverse set of devices to improve accuracy and robustness for bridge monitoring will also be a challenge.

2.6.2 SHM for structures equipped with MR damper

Structural damage detection for MR damper equipped structure is difficult in view of the complex nonlinear model MR damper model and interaction between two subsystems in structure and damper. Many MR damper models have complex nonlinear terms, which make it difficult to incorporate with structural

dynamic model. Moreover, all the structural parameters and MR damper parameters need to be estimated at the same time in each time step. The estimation of these parameters is difficulty because any error in any parameter will cause error in the whole system. Thus, the two problems must be appropriately addressed in the structural damage detection problems.

2.6.3 State-space model based structural parameter estimation

In many structural parameter identification studies, the structural parameters are all assumed constant values throughout time. That is, if the identified values of structural parameters deviate from their constant values, then the structural damage is identified. However, this assumption does not consider the influence of varying environmental and operational conditions, which may trigger false alarms when data points are falling outside static control limits but the structure has not been damaged, which decrease the usefulness and effectiveness of structural health monitoring systems. Developing high-confidence level real-time damage detection methods considering environmental and operational effects for in-service civil structures is another challenge needs to be solved.

2.6.4 Structural damage detection using neural network

Most current neural network models about bridge monitoring focused on the estimation of the relationship between environmental factors and modal properties, which is using one environmental factor as input and one modal parameter as output in the neural network model. These research shared insights on input parameters selection for neural network models, however, the real model for structural modal property is not single-input-single-output model. The model with only one input factor is not accurate enough to represent the features of the changes of structural property. How to select proper input factor is a challenge work needs investigation.

Using traditional AANN or BPNN algorithm to train the weights of neural network model might suffer from slow convergence in view of the nature of first order learning algorithm. Considering the demands of real-time structural damage detection, faster weight training algorithm is preferred for neural network-based

methods. Developing better algorithms for online structural damage detection with less storage demand and more computationally efficiency is of great importance for SHM.

Traditionally structural damage detection is implemented by civil engineers after all data are collected using sensors during field tests, but this post-processing approach causes significant time delay and expensive labor cost. An ideal smart structural health monitoring system is desirable to collect data, analyze and detect damage online on board. As to the damage detection criteria to detect the occurrence of damage, it is usually performed by engineer's object experience to set some fixed limits or thresholds.

CHAPTER 3 BIG DATA ANALYSIS FOR BRIDGE MONITORING SYSTEMS

3.1 Introduction

The aim for author to write this paper is to study the latest development of bridge reliability assessment based on monitoring, and use these methods to analyze the monitoring data on Meriden Bridge, Connecticut. The expectation of this paper contains three goals: (1) analyze the monitoring data and evaluate the loading conditions of the traffic to see if any distribution pattern could be found for live loadings; (2) assess the structural component reliability based on monitoring data from one sensor; (3) evaluate the performance for the whole system of bridge structure based on component reliability.

In the field of structural health monitoring, strain gauges are widely used in monitoring systems. They are inexpensive, easy to install, and sensitive enough to detect the potential danger of a structure. Based on the strain data history, a lot of investigations and applications have been done on fatigue damage evaluation and life prediction of bridge structures. Two traditional approaches are commonly used: (1) S-N curve method, which focus on the relationship between the constant-amplitude stress range and the number of cyclic loadings; (2) fracture mechanics, which is dedicated to explore the characteristics of crack initialization and growth.

Over the past several decades, the concepts and methods of structural reliability have developed rapidly and widely accepted. Most of the research work on reliability-based fatigue analysis has focused on steel bridges. The general approach is to formulate a mathematical model, usually the lognormal and Weibull distribution are used for load distribution. The fatigue reliability assessment of steel bridges can be performed by using the probability density function of the equivalent stress range (Kim *et al.*, 2001) and a continuous probabilistic formulation of Miner's rule (Kwon *et al.*, 2010).

Professor Dan M. Frangopol has extensive research work in the field of Bridge reliability assessment. He proposed an efficient approach to use monitoring data to evaluate structural reliability (Frangopol *et al.*, 2008). Ming Liu and Dan M. Frangopol also presented a system reliability-based approach using SHM data

(Liu *et al*, 2009). The above two papers provide a solid basis for integrating monitoring data into bridge reliability assessment, which is also adapted in this chapter.

3.2 Bridge monitoring system

The I-91 Northbound Bridge across Baldwin Avenue was built in 1964 in Meriden, Connecticut, United States. A photo of the bridge is shown in Figure 5.1. The studied bridge is a single-span eight-girder composite bridge. It has a span length of 85 feet, a width of 55 feet, a horizontal skew of 12% and a longitudinal slope of 3%. The bridge has a fixed bearing at the south abutments, and expansion bearing at the north abutments. The expansion bearing allows horizontal expansion of bridge under environmental and operational effects. According to the Connecticut Department of Transportation, the bridge carries three lanes with an annual average daily traffic of 57,000 vehicles, with 9% trucks (Christenson *et al.*, 2011).

Figure 3.1 Side view of Meriden Bridge

A bridge monitoring system had been installed in 2011 on the Meriden Bridge are for bridge health monitoring (BHM) and bridge weight in motion (BWIM) purposes. The long-term BHM includes 38 sensors consisting of 18 foil strain gages, 4 piezoelectric strain sensors, 8 piezoelectric accelerometers, 4 capacitance accelerometers, and 4 resistance temperature detectors (RTDs). As seen in the sensor layout

graph in Figure 2, the strain sensors are installed on the bearings at the bridge abutments and at the mid-span of each of the eight girders. The accelerometers are installed at quarter-span and mid-span of the bridge, and the RTDs are mounted underneath the bridge to monitor the temperature variability. The data acquisition hardware is a National Instruments (NI) cDAQ-9178 CompactDAQ chassis, which provides signal conditioning and high sampling rates 2048 Hz for the different types of sensors. A desktop located at the bridge site operates the data collection and implementation automatically, and be remotely accessed through a cellular modem. The acceleration and temperature data are collected during the last five minutes of each hour, so that each sensor acquires 24 sets of 5-minute data files every day continuously. More details about the Meriden Bridge and the structural health monitoring system have been reported by (Christenson *et al.*, 2011; Li, 2014).

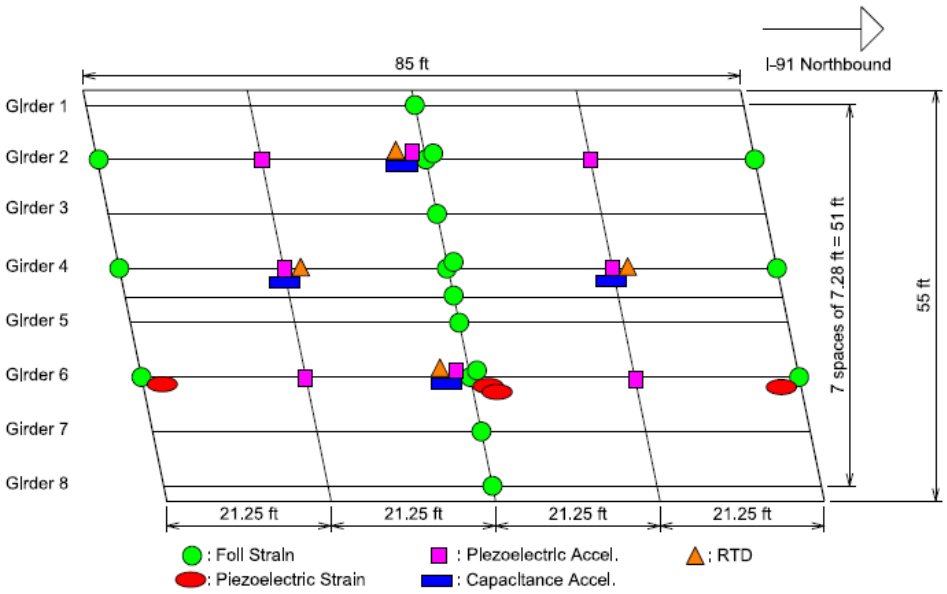

Figure 3.2 Sensor layout on Meriden Bridge

3.3 Statistical analysis for strain sensor readings

This project focuses on the monitored data from sensors on Girder 4 and Girder 6, which are located on the right lane and middle lane respectively. Sensor 1 is located on the right lane, and sensor 2 is located on the middle lane. As a first step, 24-hour continuous monitoring data was chosen on January 1, 2014. The

corresponding sensors are installed on the top flange of the bridge. In order to minimize the volume of monitoring data, only maximum live load induced by traffic are extracted and analyzed. Totally 67869 peak loadings were captured by sensor 1, and 67823 by sensor 2. For sensor 1, the mean of maximum live loading is 11.1291, and the standard deviation is 3.4248. For sensor 2, the mean value is 9.2670, and the standard deviation is 3.6387. These descriptors are listed in Table 1 below. The reason for right lane has larger strain loading than middle lane can be verified by the common sense that heavy trucks prefer right lanes for safety. And this result is supported by live loading result that about 70% heavy vehicles traffic occurred on the right lane in a two-lane bridge (Liu *et al.*, 2009)

Table 3.1 Statistical descriptors for monitoring data

	Number of Peaks	**Mean**	**Standard Deviation**
Sensor1 (Right Lane)	67869	11.1291 (μm/m)	3.4248 (μm/m)
Sensor2 (Middle Lane)	67823	9.267 (μm/m)	3.6387 (μm/m)

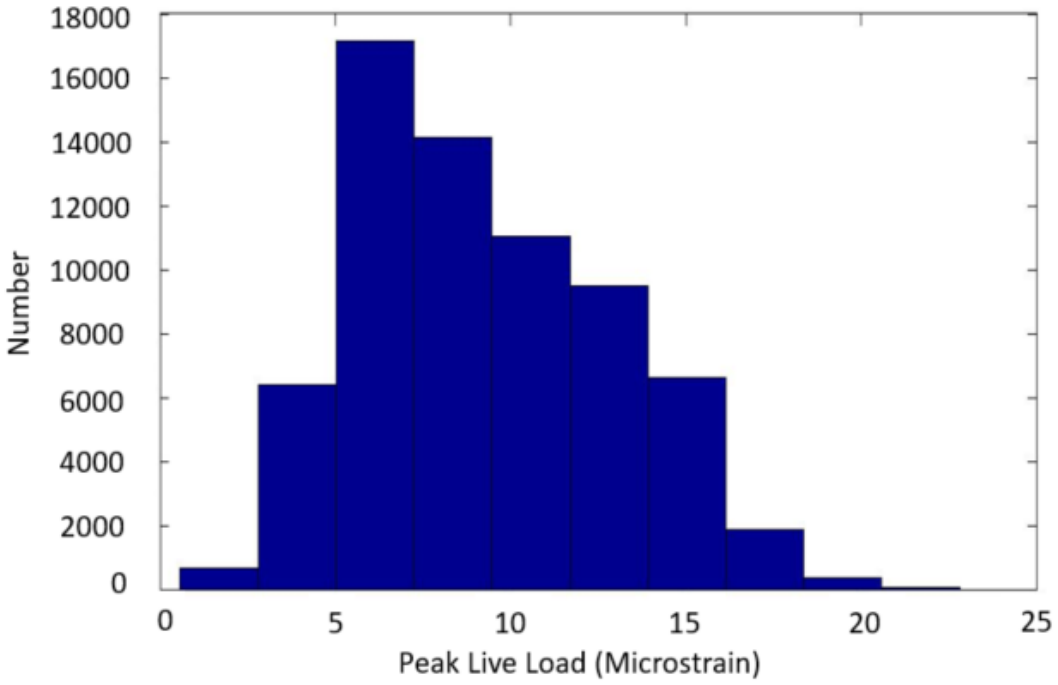

Figure 3.3 Histograms of peak live load from monitoring data on middle lane

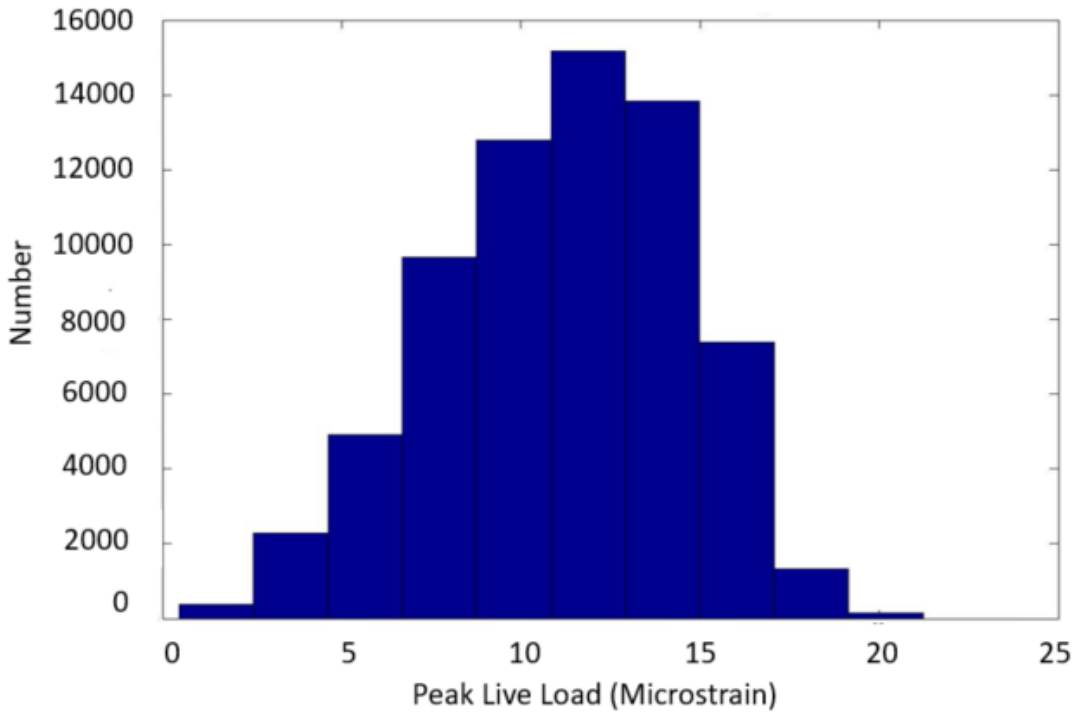

Figure 3.4 Histograms of peak live load from monitoring data on right lane

The histogram graphs of the monitoring data are shown in Figure 3.3 and 3.4. The probability distribution of monitoring data will be assessed to see if they fit a particular distribution. The probability plots of six distributions will be used for the data assessment. Its idea is to scale the x-axis of a CDF so that the result would be a straight line if the data conforms to the assumed distribution. As shown in Figure 3.5 and 3.6, probability plots of monitoring data with normal, lognormal, Weibull, Exponential, extreme value and Rayleigh distribution are compared. The result shows that normal and Weibull distribution has the best fitting for peak live loadings from monitoring data. This result could be verified through more tests on long-term monitoring data.

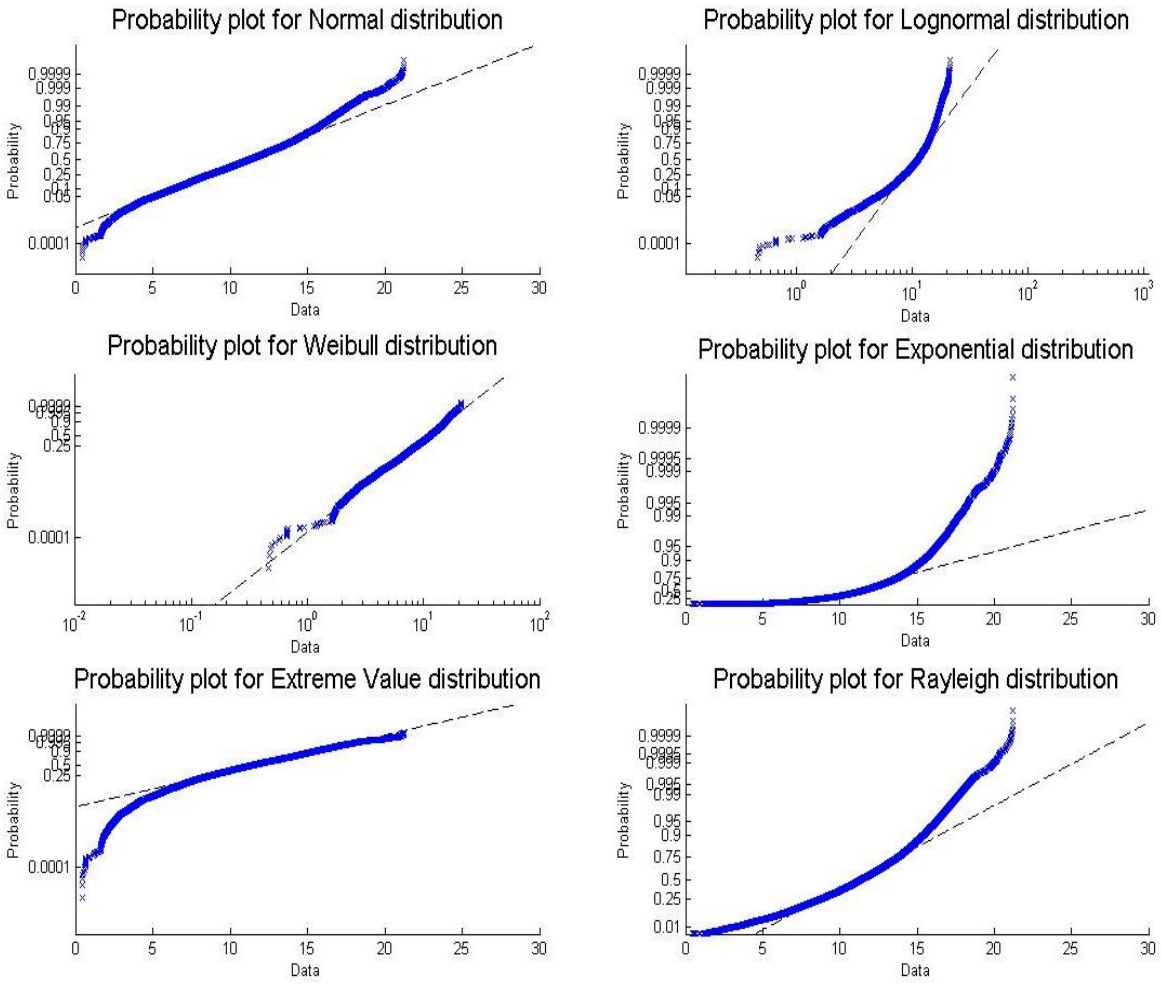

Figure 3.5 Distribution fitting test for monitoring data from right lane

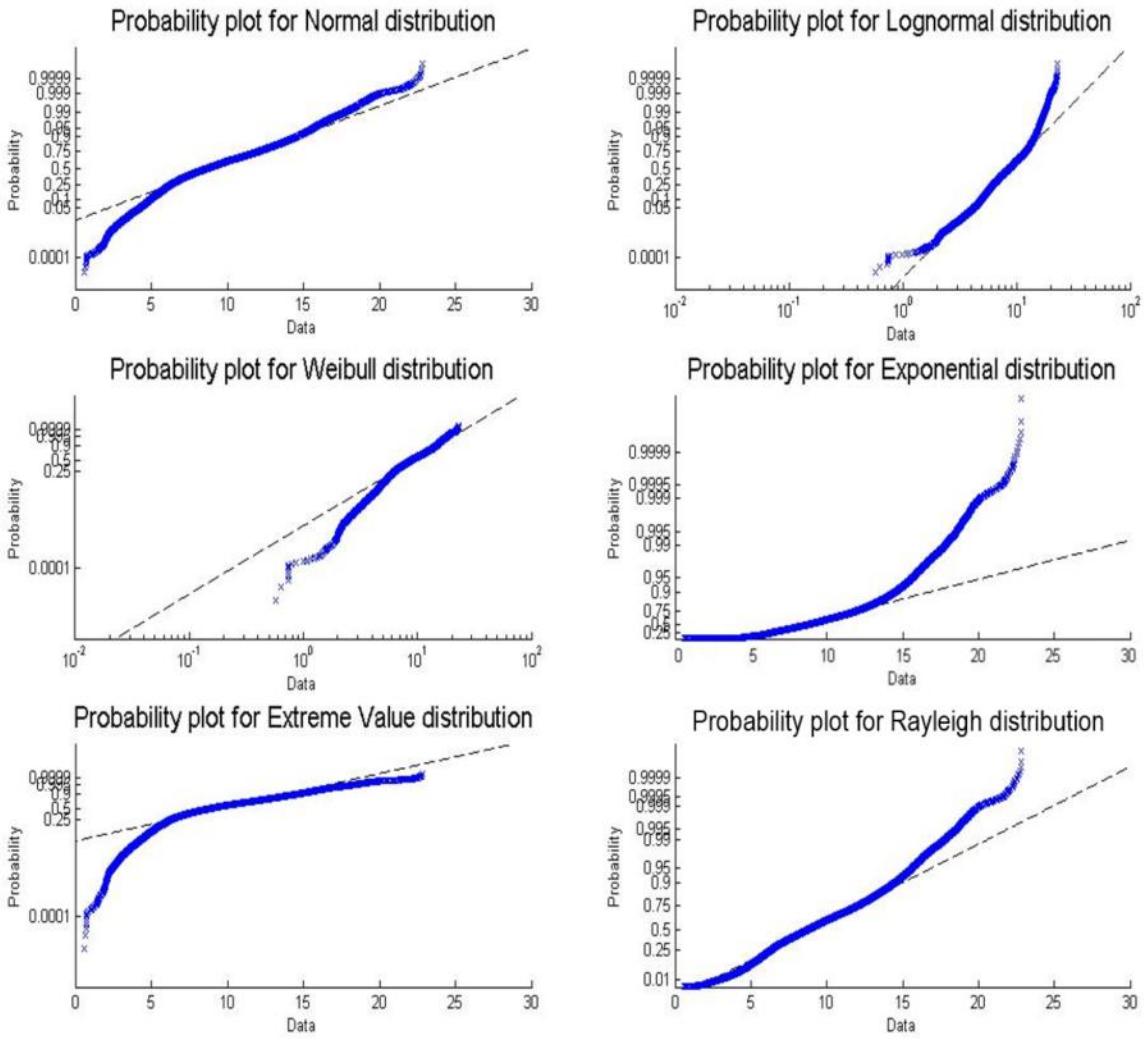

Figure 3.6 Distribution fitting test for monitoring data from middle lane

3.4 Reliability based model

3.4.1 Yield strength limit state

The First Order Reliability Method (FORM) is used to estimate the structural reliability. It has been verified that FORM method has a good approximation linear and sometimes nonlinear conditions. The design of any structure requires that its resistance R is greater than the monitored load M. This can be expressed by using the limit state function

$$g(X) = R - M > 0, \tag{3.1}$$

The reliability index is defined as

$$\beta = \frac{\mu_R - \mu_M}{\sqrt{(\sigma_R^2 + \sigma_M^2)}}, \tag{3.2}$$

where μ_R and μ_M are the mean value for resistance and monitored load effect, and σ_R and σ_M are standard deviation for them respectively. In this project, the monitored load *M* only contains the amplitude of peak values of all loadings, which is different from previous researches that consider all time history of loading. This method was implemented by using command '*findpeaks'* in Matlab.

In addition to the uncertainties in the material and loading, the uncertainty in the sensors $e_s(\%)$ can be added in the reliability index

$$\beta = \frac{\mu_R - \mu_M \times (1 + e_s)}{\sqrt{(\sigma_R^2 + \sigma_M^2)}}, \tag{3.3}$$

The resistance R and the load effect M are assumed normally distributed, thus the probability of failure can be determined as

$$P_f = \Phi(-\beta), \tag{3.4}$$

3.4.2 Reliability model for whole bridge strain monitoring system

The bridge system reliability can be assessed by the Parallel-Series combined system model, where all sensors on one structural component are represented by a parallel system model, and all structural components are represented by a series system model. In this way, the probability of failure of the whole bridge can be calculated based on probability of failure for each sensor. The equation to calculate the probability of failure for a parallel system is

$$(P_f)_{parallel} = \prod_{i=1}^{n} P_{fi}, \tag{3.5}$$

And the equation for the probability of failure of a series system is

$$(P_f)_{series} = 1 - \prod_{i=1}^{n} (1 - P_{fi}), \tag{3.6}$$

where P_{fi} represents the probability of failure for structural component at *i*th sensor location.

It is possible to focus on the probabilistic assessment on the steel yielding based on sensor data and design data of Meriden Bridge. The steel used in the top flange is M270 Grade 50 W. The nominal yield strength of this steel is 345 MPa (50 ksi). The probabilistic analysis of this kind of steel has been studied by Strauss *et al*. 2006, which yields at a mean value of 380 MPa (55.11 ksi) and a standard deviation of 28 MPa. The modulus of elasticity of 200,000 MPa (29,000 ksi) is used to transform the strain data to stress. Then the computation for reliability index β for each sensor can be completed. The reliability index for sensor 1 and sensor 2 are 13.49 and 13.50, which means they are not reliability critical components.

The reliability model for Meriden Bridge is established based on the above theory in Section 3.2. The eight girders of the bridge are within a series system, and three sensors located on Girder 2, 4, 6 and 8 are in a sub-parallel system. The plot of the system model is shown in Figure 3.7.

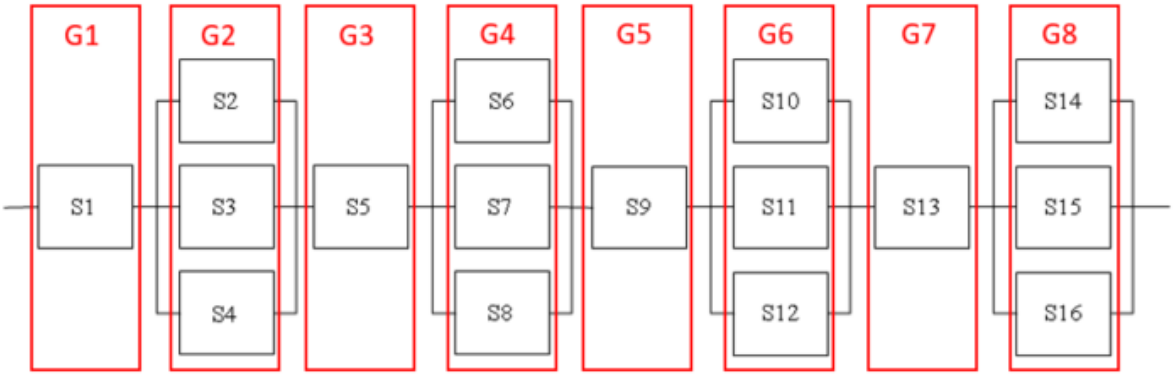

Figure 3.7 System model of the Meriden Bridge

$$(P_f)_{MeridenBridge} = 1-(1-P_{f1})(1-P_{f2}\times P_{f3}\times P_{f4})(1-P_{f5})(1-P_{f6}\times P_{f7}\times P_{f8})(1-P_{f9})$$
$$\times(1-P_{f9})(1-P_{f10}\times P_{f11}\times P_{f12})(1-P_{f13})(1-P_{f14}\times P_{f15}\times P_{f16}), \quad (3.7)$$

Table 3.2 Reliability index and probability of failure.

	Mean		Standard Deviation		Reliability Index, β	Pf
	Microstrain(μm/m)	Stress(Mpa)	Microstrain(μm/m)	Stress(Mpa)		
Sensor1 (Right Lane)	11.1291	2.22582	3.4248	0.68496	13.48789981	9.21376E-42
Sensor2 (Middle Lane)	9.267	1.8534	3.6387	0.72774	13.50067651	7.74734E-42

In this project, we assume sensor 1 can represent all the other sensors, thus the probability of failure of sensor 1 is used in the system model. The result for system probability failure we got is zero, which means the bridge is in good condition. The system model has the potential to be used when data from other sensors are used to reflect the overview of condition for the whole bridge. It also can be used in on-line monitoring, which means it can assess the reliability of bridge in real time.

3.5 Fatigue reliability assessment

This brief document presents a general procedure to predict the fatigue reliability of an in-service short-span bridge, based on in-field measurement data. Due to time constraint, the bridge deterioration effects, including crack and corrosion are not considered. In addition, the calculation process is based on only one day SHM data for only one sensor, which may overestimate or underestimate the actual bridge (or structural component) fatigue reliability. For future analysis, these two effects along with other important factors should be considered for more reliable fatigue reliability assessment.

3.5.1 One day stress time history extraction

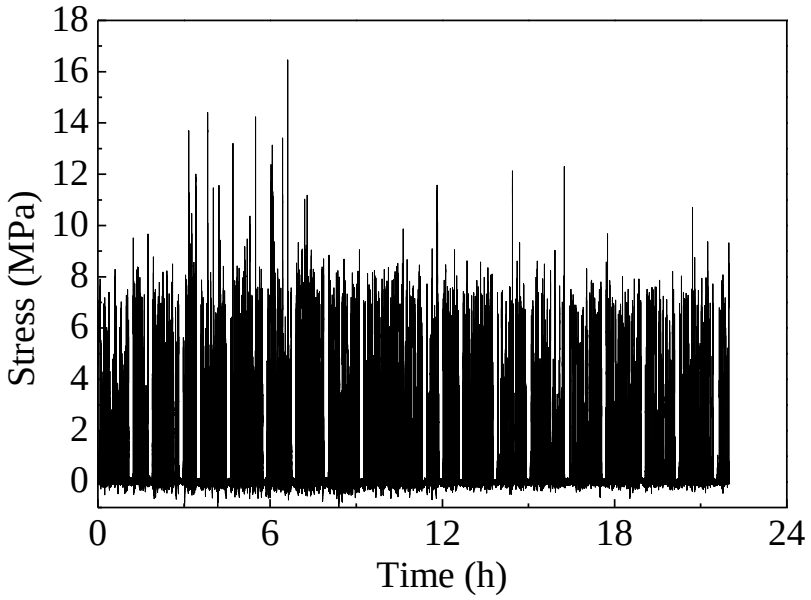

Figure 3.8 One-day stress time history (June 10th, 2015)

3.5.2 Obtain stress range and the equivalent stress

The cycle counting method, such as the rain-flow cycle-counting method, is used to process irregular stress-histories and store the data. The total number of cycles, n_{tc}, is obtained after a stress-range cut-off level is defined. Applicable cut-off levels for stress-ranges are suggested in a range from 3.45 MPa (0.5 ksi) to 33%, the constant amplitude fatigue limit (CAFL). In total, 732771 stress ranges are obtained based on one-day stress time history as shown in Figure 3.9, and 1742 effective stress ranges (i.e., $\Delta\sigma$>3.45 Mpa) are identified. The corresponding stress-range bin histogram is shown in Figure 3.9.

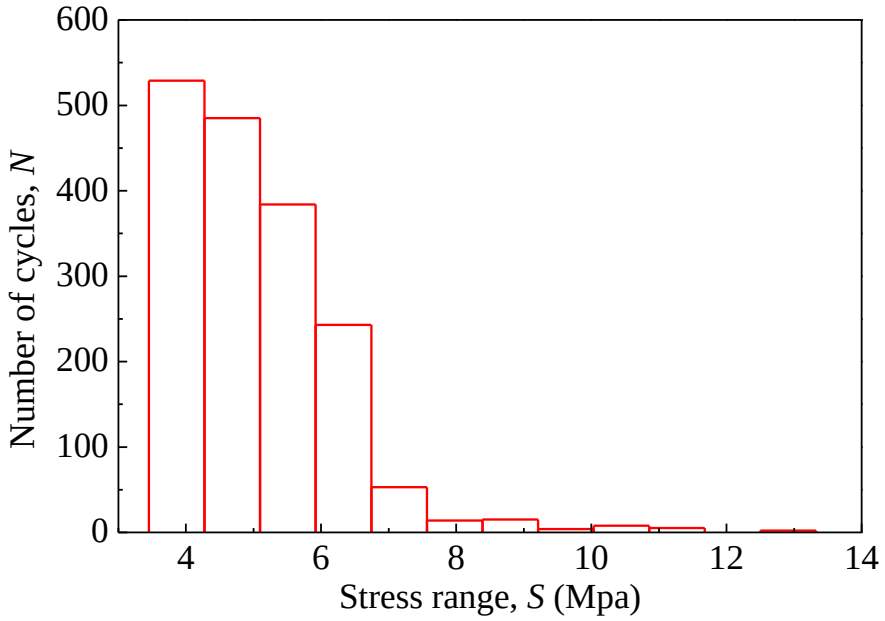

Figure 3.9 Stress-range bin histogram

The equivalent stress-ranges are defined as the constant-amplitude stress-range that can yield the same fatigue life as the variable amplitude stress-range for a structural detail. According to Miner's rule, the accumulated damage is,

$$D(t) = \sum_i \frac{n_i}{N_i} = \frac{n_{total}}{N}, \tag{3.8}$$

where n_i = number of observations in the predefined stress-range bin S_{ri}; N_i = number of cycles to failure corresponding to the predefined stress-range bin; n_{total} = total number of stress cycles of the stress range histogram; and N = number of cycles to failure under an equivalent constant amplitude loading.

The equation for N is given by

$$N = A \cdot S_{re}^{-m} \tag{3.9}$$

where material constant m represents the slope of the S-N curve; A is detail constant taken from Table 6.6.1.2.5–1 in the AASHTO LRFD bridge design specifications (AASHTO 2010); S_{re} represents the equivalent stress range.

S_{re} can be obtained through using the Miner's rule,

$$S_{re} = \left(\sum_{i=1}^{n} \frac{n_i}{n_{total}} \cdot S_{ri}^{m} \right)^{1/m} \tag{3.10}$$

Note that the Eq. (3.10) can be used to obtain the equivalent stress range based on the stress range bin histogram that is derived from Figure 3.9. The equivalent stress range is S_{re} is 5.43 Mpa in this case study. Then substitute S_{re} = 5.43 Mpa into (3.9), the N is obtained as 4.89×10^8.

3.5.3 Limit state function (LSF)

In this research, the one-day monitoring data obtained on June 10, 2015 are assumed to represent the whole year. In section 3.5.2, the number of daily average effective stress ranges is calculated as $N_{avg}^{*} = 1742$. Therefore, the total number of stress cycles in one year N_{year} can be expressed as,

$$N_{year} = 365 \times N_{avg}^{*}, \tag{3.11}$$

The remaining life of the bridge is assumed y years, thus the accumulated number of stress cycles for the future years $N(y)$, can be expressed as,

$$N(y) = N_{year} \times y = 365 \times N_{avg}^{*} \times y \tag{3.12}$$

When the fatigue damage variable D increases to 1, a fatigue failure is expected. For fatigue reliability analysis, a limit state function (LSF) is often used and defined based on the S-N approach and Minder's rule,

$$g(\mathbf{X}) = D_f - D = D_f - \left(N(y)/A\right)\cdot\left(S_{re}^{*}\right)^{m} \tag{3.13}$$

where D_f = miner's critical damage accumulation index in terms of resistance and is assumed to be deterministic for metallic materials; D = Miner's damage accumulation index; the number of cycles, $N(y)$, is a lognormal random variable with its mean value obtained from Eq. (3.13) and COV of 0.2; and the predicted effective stress range is also a lognormal random variable with its mean value obtained from Eq. (3.10), which is 5.43 Mpa in the present study, and COV of 0.2. The information for all the parameters in the LSF are provided in Table 3.3.

Table 3.3 Summary of LSF Parameters

Parameter	Distribution	Mean	COV	Description	Source
D_f	Deterministic	1	--	Critical damage accumulation index	Wirsching (1984)
[a]A	Lognormal	7.83E+10	0.34	Fatigue detail coefficient	AASHTO (2010)
[b]S_{re}	Lognormal	5.43	0.2	Predicted effective stress range	Based on SHM data
[b]N_{avg}^{*}	Lognormal	1742	0.2	Predicted average daily number of cycles	Based on SHM data

Note: [a]The value of A is assigned by the S–N category C (unit: MPa^3). [b]The predicted equivalent stress range, S_{re}, and the predicted average daily number of cycles, N_{avg}^{*}, are obtained based on 1-day SHM data, and S_{re} and N_{avg}^{*} are assigned with values such that, S_{re}=5.43 (Mpa) and N_{avg}^{*}=1742 (cycle/day).

3.5.4 Annual fatigue reliability index

The method used in this chapter was adapted from Zhang *et al.* (2012). Assuming that all the random variables (i.e., $N(y)$, A, S_{re}) are lognormal, the fatigue reliability index can then be estimated based on the LSF as follows,

$$\beta = \frac{\mu_A - \left(\mu_{N(y)} + m\cdot\mu_{S_{re}}\right)}{\sqrt{\sigma_A^2 + \sigma_{N(y)}^2 + \left(m\cdot\sigma_{S_{re}}\right)^2}} \tag{3.14}$$

where the parameters μ and σ denote the mean value and standard deviation of the corresponding lognormal random variables, respectively.

Based on Eq. (3.14), the annual fatigue reliability index is obtained and plotted in Figure 3.10. Two cases can be studied to calculate remaining life for reference. In the case of target reliability index β_{target}=1.65, which corresponds to a 5% failure probability or a 95% survival probability, the remaining life of the bridge is about 250 years. When β_{target} equals to 3.5, which corresponds to 1/5000 probability of failure in AASHTO LRFD Design Code, the remaining life is calculated around 75 years, which is very close to the designing life of a bridge.

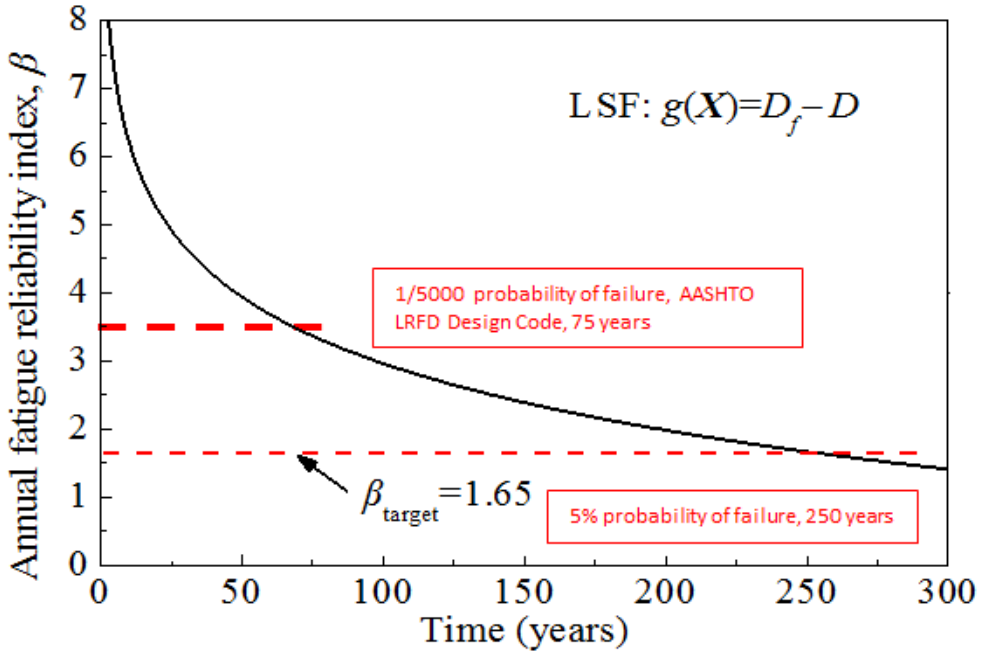

Figure 3.10 Annual fatigue reliability index plot

3.6 Summary

This paper presented two practical approaches to assess the probability of failure of bridge using strain monitoring data. The following conclusions can be drawn from this study.

(1) Two efficient approaches to assess the reliability for bridge structure using strain monitoring data. One is based on yield strength limit state, and the other is based on fatigue limit state.

(2) The yield strength based model considers the yield strength and only requires statistical parameters of yield strength and loading. The sensor error is also included in the reliability index equation. A parallel-series combined system is presented in order to assess the bridge reliability based on multi-sensor monitoring systems.

(3) Fatigue reliability based method can calculate structural probability of failures in future years based on fatigue theory and Miner's rule. The accumulated damage is obtained based on monitoring strain data to calculate the fatigue reliability index.

CHAPTER 4 STRUCTURAL PARAMETER IDENTIFICATION FOR MR DAMPER EQUIPPED STRUCTURES

4.1 Introduction

The Magneto-rheological (MR) dampers have been widely used in many civil engineering structures due to its advantages including mechanical simplicity, high dynamic range, low power requirements, large force capacity, and robustness. However, research about structural parameter identification methods for MR damper equipped structures is limited. This paper aims to develop a real-time structural damage detection method for MR damper controlled structures. A novel state-space model of MR damper controlled structure is first built by combining the structural dynamic equation of motion and MR damper's hyperbolic tangent model. In this way, the state parameters of both the structure and MR damper are included in the extended state vector of the new state-space model. Extended Kalman filter is then used to provide predictions for state variables based on the measurement data. The two techniques are combined to identify parameters and track the changes of both structure and MR damper in real time. The proposed method is tested using simulation response data of a three-floor linear building structure equipped with one MR damper under earthquake excitation. The testing results show that the adaptive extended Kalman filter based approach is capable to estimate structural parameters, so that more insights and understanding of the structural damage can be obtained. The developed method also demonstrates high parameter identification accuracy and light computation, as well as the potential to implement in a structural health monitoring system.

Applications of control devices used in civil engineering have received great interests in the past decades. Structural control devices can protect civil structures from natural or disaster loadings such as earthquake, waves and winds. Through this energy dissipating mechanism, the structural damage and failure can be effectively reduced and prevented. On the other hand, structural health monitoring is also important to determine the status of the structure and detect the damage when it occurs. Structural health

monitoring can be used to identify the existence, location and severity of structural damage, and help to estimate the remaining service life. Many model-based structural parameter identification methods require prior knowledge of the equations for structural dynamic model. However, for a typical structural control device equipped structure, the structure control device also changes the structural dynamic model, which makes it unrepresentative of the current condition of the structure and add difficulty for applying existing model-based methods. In the view that control devices are installed in more and more civil structures, current structural parameter identification methods need to be modified to adapt the control device-equipped structures. In this paper, the authors aim to develop an efficient structural parameter identification method which can incorporate both health monitoring and control systems for civil engineering structures.

Among many innovative structural control devices, the magneto-rheological (MR) fluid damper is a promising device in structural control. Changing the current inputs and settings of the damper can result in significant difference in the force response of the damper and structure. MR dampers exhibit highly nonlinear hysteretic dynamic behaviors due to magnetic and friction forces, which make them difficult to model and control. Various mathematical models have been developed to represent the highly nonlinear dynamic behavior of MR dampers, including hyperbolic tangent model (Gavin 2001; Gamota and Filisko, 1991; Bass and Christenson, 2007), Bouc-Wen model (Bouc 1971; Wen 1976; Spencer *et al.* 1997), viscous plus Dahl model (Dahl 1968, 1976; Bouc 1971; Aguirre *et al.* 2012), Algebraic model (Choi *et al.* 2001, Song *et al.* 2005; Ruangrassamee *et al.* 2006), LuGre friction model (Jimenez and Alvarez-Icaze, 2005) and Bingham model (Stanway *et al.* 1985, 1987). In order to estimate corresponding values of the parameters in the above models, a considerable amount of approaches have been developed, including resursive least square (RLS) method (Jimenez and Alvarez-Icaze, 2005), artificial neural network (ANN) method (Chang and Roschke, 1998), neuro-fuzzy method (Atray and Roschke, 2004) and recurrent neural network (RNN) method (Wang and Liao, 2005). All the above literatures are helpful to understand dynamic models of MR damper and the integrating MR damper into structural dynamic model.

Many structural parameter identification methods have been developed in order to estimate system parameters based on the measurements of structural response data directly, including extended Kalman

filter (EKF) (Hoshiya *et al.* 1984; Mariani and Corigliano, 2005), unscented Kalman filter (UKF) (Mariani and Ghisi, 2007; Wu and Smyth, 2007) and Particle filter (Charzi and Smyth, 2009; Eftekhar Azam *et al.* 2012). In these Kalman filter-based methods, the dynamic structures are modeled in the state space formulation including state equations and measurement equations. These methods are attractive in view of the recursive feature of Kalman filter such that they can estimate structural parameters straightly, and provide detailed information and understanding about the existence, location, and severity of the structural damage. In the EKF, the state distribution is approximately by a Gaussian random variable, which is then propagated through the first-order linearization of a nonlinear system. The unscented Kalman filter (UKF) differs from the EKF in the manner of representing Gaussian random variables. The UKF uses an unscented transform to generate a minimal set of carefully chosen sample points to present the state distribution. These sample points capture the means and covariance of the Gaussian random variables, and when propagated through the nonlinear system, captures the posterior mean and covariance accurately to the 2^{nd} order for any nonlinearity. The particle filters can deal with nonlinear systems with non-Gaussian posterior distribution of the state. The concept of the method is that the approximation of the posterior distribution of the state is done through the generation of a large number of samples (weighted particles), using Monte Carlo Methods. The basic drawback is the fact that depending on the problem a large number of samples may be required thus making the particle filter analysis computationally expensive. The UKF and particle filter may estimate more accurately than the EKF for highly nonlinear systems, however, the EKF is widely used in state estimation and structural parameter estimation for civil engineering problems due to its straightforward implementation, high updating frequency, fast convergence speed, and low computational costs (Yang *et al.* 2006 2007; Zhou *et al.* 2008; Soyoz *et al.* 2008; Liu *et al.* 2009; Lei *et al.* 2012; Yin *et al.* 2013; Jin *et al.* 2016a), and EKF is also adopted in this paper.

Recently, a novel MR damper parameter identification method using EKF has been developed by authors (Jin *et al.* 2015, 2016b). In this paper, the EKK based method is further improved with more rigorous derivations and discussion on testing results. This paper proposes a new method to combine hyperbolic tangent model and EFK to identify structural parameters in real time. In Section 2, the

methodology about hyperbolic tangent model for MR damper is reviewed. Section 3 described EFK-based method for structural parameter estimation. Section 4 summarized how EKF and hyperbolic tangent model are combined for real-time parameter identification in this paper. Subsequently in Section 5, application of the proposed EKF based method will be presented for a 3-degree-of-freedom (3DOF) linear structure equipped with a MR damper. Finally, testing results discussion and the benefits of developed damage detection method will be highlighted.

4.2 Hyperbolic tangent model for MR damper

The hyperbolic tangent model was proposed by Gavin to provide damper force prediction for an 8 KN Electro-Rheological fluid damper (Gavin, 2001). Gavin's model is a simplified version of a model proposed by (Gamota and Filisko, 1991). The hyperbolic tangent model used in this research is based on the model proposed by (Bass and Christenson, 2007). The schematic of this hyperbolic tangent model is shown in Figure 4.1.

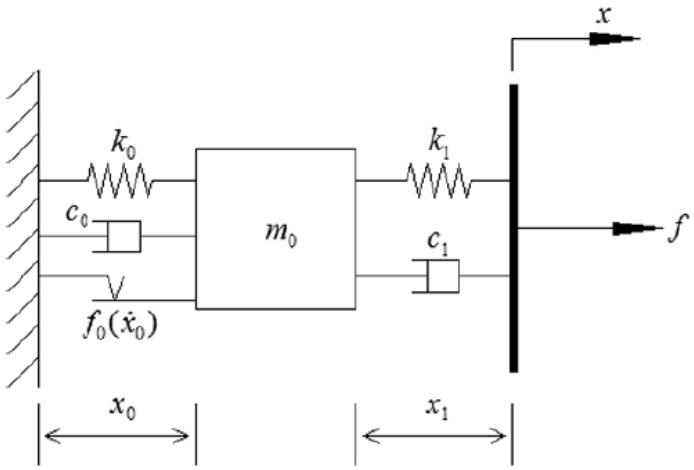

Figure 4.1 Schematic of the MR damper hyperbolic tangent model

In the hyperbolic tangent model, MR damper can be represented by two sets of spring-dashpot elements connected by an inertial mass element. The inertial mass element resists motion by means of a Coulomb friction element. All parameters in MR damper can be represented as pre-identified functions of current. The dynamics of the system and force output can be described in state space form as,

$$\begin{bmatrix} \dot{x}_0 \\ \ddot{x}_0 \end{bmatrix} = \begin{bmatrix} 0 & 1 \\ (-k_0 - k_1)/m_0 & (-c_0 - c_1)/m_0 \end{bmatrix} \begin{bmatrix} x_0 \\ \dot{x}_0 \end{bmatrix} + \begin{bmatrix} 0 & 0 \\ k_1/m_0 & c_1/m_0 \end{bmatrix} \begin{bmatrix} x \\ \dot{x} \end{bmatrix}$$

$$+ \begin{bmatrix} 0 \\ 1/m_0 \end{bmatrix} \times f_0 \tanh(\dot{x}_0 / V_{ref}) \tag{4.1}$$

$$f = \begin{bmatrix} -k_1 & -c_1 \end{bmatrix} \begin{bmatrix} x_0 \\ \dot{x}_0 \end{bmatrix} + \begin{bmatrix} k_1 & c_1 \end{bmatrix} \begin{bmatrix} x \\ \dot{x} \end{bmatrix} \tag{4.2}$$

where x_0 and $\dot{x}_0$ are the displacement and velocity of the inertial mass relative to a fixed end, x_1 and $\dot{x}_1$ are the displacement and velocity of the damper piston end relative to the inertial mass. The k_1 and c_1 model the pre-yield visco-elastic behavior, and k_0 and c_0 model the post-yield visco-elastic behavior. The m_0 represents the inertia of both fluid and the moving piston. In the Coulomb friction function term, f_0 is the yield force and V_{ref} is a reference velocity.

The hyperbolic tangent model contains seven parameters (k_0, k_1, c_0, c_1, m_0, f_0, V_{ref}), each of them can be expressed through a function of current. The functions of these parameters with current used in this study are shown in Table I. More details about how these parameters are determined can be found in (Bass and Christenson, 2007).

Table 4.1 Parameters in the hyperbolic tangent model.

Parameters as a function of damper current, i (A)	**Units**
$k_0 = (0.10i^4 - 1.00i^3 + 1.30i^2 + 2.30i + 6.20) \times 10^{-4}$	kN mm^{-1}
$k_1 = -2.43i^4 + 23.76i^3 - 80.70i^2 + 110.62i + 55.08$	kN mm^{-1}
$c_0 = (-0.98i^4 + 9.33i^3 - 29.96i^2 + 35.80i + 12.64) \times 10^{-2}$	kN s mm^{-1}
$c_1 = (-0.62i^4 - 6.73i^3 + 29.96i^2 - 46.06i + 35.67) \times 10^{-2}$	kN s mm^{-1}
$m_0 = (0.16i^4 - 1.62i^3 + 5.48i^2 - 7.05i + 4.85) \times 10^{-3}$	kg
$f_0 = 1.52i^4 - 10.27i^3 + 2.79i^2 + 94.56i + 6.19$	kN
$V_{\text{ref}} = -0.12i^4 + 1.36i^3 - 6.19i^2 + 13.12i + 0.76$	mm s^{-1}

4.3 EKF-based structural parameter identification

4.3.1 Kalman filter and extended Kalman filter

The Kalman filter (KF) provides a recursive solution for linear dynamic systems that can be represented in state-space formulation. Each updated estimate of the state is computed from the previous estimate and new input data only, instead of all previous data points. Thus, the KF is less demanding in storage space and computationally more efficient. The state equation and measurement equation of KF are given by:

$$x_{k+1} = F_k x_k + w_k , \tag{4.3}$$

$$y_k = H_k x_k + v_k , \tag{4.4}$$

where x_k is the state vector, and y_k is the measurement vector. The process noise w_k and observation noise v_k are independent, zero-mean, Gaussian processes with covariance matrix Q_k and R_k, respectively. The matrices F, H, Q and R are assumed known and possibly time-varying.

The KF consists of two steps: time update and measurement update. In time update, the state and covariance propagations are implemented as follows:

$$\hat{x}_{k+1|k} = F_k \hat{x}_{k|k} , \tag{4.5}$$

$$P_{k+1|k} = F_k P_{k|k} F_k ' + Q_k , \tag{4.6}$$

$$\hat{y}_{k+1|k} = H_k \hat{x}_{k+1|k} , \tag{4.7}$$

where the prior state $\hat{x}_{k|k}$ and state covariance matrix $P_{k|k}$ are propagated to $\hat{x}_{k+1|k}$ and $P_{k+1|k}$, respectively. The $\hat{x}_{k+1|k}$ is then used to generate the estimated measurement $\hat{y}_{k+1|k}$ through H_k.

In the measurement-update step, the filter gain W_k, the posterior state $\hat{x}_{k+1|k+1}$, and the state covariance $P_{k+1|k+1}$ are produced as follows:

$$S_{k+1} = H_{k+1} P_{k+1|k} H_{k+1}' + R_{k+1}, \tag{4.8}$$

$$W_{k+1} = P_{k+1|k} H_{k+1}' S_{k+1}^{-1}, \tag{4.9}$$

$$\hat{x}_{k+1|k+1} = \hat{x}_{k+1|k} + W_{k+1}(y_k - \hat{y}_{k+1|k}), \tag{4.10}$$

$$P_{k+1|k+1} = P_{k+1|k} - W_{k+1} S_{k+1} W_{k+1}', \tag{4.11}$$

where S_{k+1} is the innovation covariance matrix. Note that the roots of the diagonal elements of $P_{k+1|k+1}$ are the standard deviation of each state variable in the state vector.

The EKF approach applies the standard KF to nonlinear systems by continually updating a linearization around the previous state estimate through first-order Taylor series expansion. The linearized state matrix F_k is taken as the partial derivative of nonlinear function $f(x_k, u_k, k)$ with respect to x at $\hat{x}_{k|k}$, i.e. a Jacobian matrix, while the linearized measurement matrix H_k is obtained as the partial derivative of nonlinear function $h(x_k, u_k, k)$ with respect to x at $\hat{x}_{k+1|k}$, and are given by:

$$F_k = \left. \frac{\partial f(x_k, u_k, k)}{\partial x} \right|_{x=\hat{x}_{k|k}}, \tag{4.12}$$

$$H_k = \left. \frac{\partial h(x_k, u_k, k)}{\partial x} \right|_{x=\hat{x}_{k+1|k}}. \tag{4.13}$$

The recursions of time update and measurement update for EKF follow equations (4.5)-(4.11) used in the standard KF.

Given the initial values of state vector x_0, the initial state covariance matrix P_0, the process noise covariance matrix Q_0, and the measurement noise covariance matrix R_0, the EKF procedure can be recursively implemented to estimate the structural parameters based on the measurement data of the dynamic system. Due to the nature of the recursion method, these structural parameters can be updated at each time step, which makes real-time structural damage detection possible. More details on KF and EKF can be found in Welch and Bishop (2002).

4.3.2 Extended Kalman filter for linear structures

The equation of motion for an m-DOF linear structure can be represented as,

$$M\ddot{q}(t) + C\dot{q}(t) + Kq(t) = \eta u(t) \tag{4.14}$$

where M, C and K represent ($m \times m$) mass matrix, damping matrix and stiffness matrix, respectively; $q(t)$ is the ($m \times 1$) displacement vector; $\dot{q}(t)$ is the velocity vector; $\ddot{q}(t)$ is the ($m \times 1$) is the acceleration vector; $u(t)$ is the ($m \times 1$) excitation force vector; and η is the ($m \times m$) excitation influence matrix.

As discussed in Section 4.3.1, KF-based approaches give a simple and efficient way to estimate the state and parameters in any system models. For structural dynamic systems, the states (e.g., displacement and velocity) and parameters (e.g., stiffness and damping) are often required to be identified simultaneously. Therefore, even though the structural model is linear, due to the nonlinear coupling feature between the structural states and parameters, EKF will be used. The state vector for structure model is thus formed as:

$$x'(t) = \begin{bmatrix} x(t) \\ \alpha \end{bmatrix} = \begin{bmatrix} q(t) \\ \dot{q}(t) \\ \alpha \end{bmatrix} \tag{4.15}$$

where $x(t)$ is the state of structural dynamic system including displacement $q(t)$ and velocity $\dot{q}(t)$, and α is the parameter vector to be estimated. The continuous state equation becomes:

$$\dot{x}'(t) = \begin{bmatrix} \dot{x}(t) \\ \dot{\alpha} \end{bmatrix} = \begin{bmatrix} \dot{q}(t) \\ \ddot{q}(t) \\ \dot{k} \\ \dot{c} \end{bmatrix} = \begin{bmatrix} \dot{q}(t) \\ M^{-1}\left[\eta u(t) - (C\dot{q}(t) - Kq(t))\right] \\ 0 \\ 0 \end{bmatrix} \equiv f(x'(t), u(t), t), \tag{4.16}$$

and the continuous measurement equation becomes:

$$y(t) = h(x'(t), u(t), t). \tag{4.17}$$

By discretizing and linearizing at time t_k (k = 1,2,…) using first-order Taylor series expansion, the discrete-time space model is formulated as:

$$x'_{k+1} = F_k x'_k + w_k, \tag{4.18}$$

$$y_k = H_k x'_k + v_k, \tag{4.19}$$

where

$$F_k = \frac{\partial f(x'_k, u_k, k)}{\partial x'}\Big|_{x'=x'_k}$$
$$= \begin{bmatrix} [0] & I & [0] & \cdots & [0] \\ -M^{-1}K & -M^{-1}C & -M^{-1}\dfrac{\partial K}{\partial \alpha_1}q(k) - M^{-1}\dfrac{\partial C}{\alpha_1}\dot{q}(k) & \cdots & -M^{-1}\dfrac{\partial K}{\partial \alpha_\alpha}q(k) - M^{-1}\dfrac{\partial C}{\alpha_\alpha}\dot{q}(k) \\ [0] & [0] & [0] & \cdots & [0] \end{bmatrix}$$

, (4.20)

When the measurement is the acceleration $\ddot{q}(t)$, the measurement matrix H_k has the form

$$H_k = \frac{\partial h(x'_k, u_k, k)}{\partial x'}\Big|_{x'=x'_k}$$
$$= \begin{bmatrix} -M^{-1}K & -M^{-1}C & -M^{-1}\dfrac{\partial K}{\partial \alpha}q(k) - M^{-1}\dfrac{\partial C}{\partial \alpha}\dot{q}(k) \end{bmatrix}. \tag{4.21}$$

The EKF recursion process follows the equations (4.5)-(4.11) as shown in Section 4.3.1. The selection of initial state, initial state covariance matrix, process noise and measurement covariance matrices will be

discussed in Section 4.4.

4.4 EKF-based parameter identification method for MR damper equipped structures

In order to use extended Kalman filter to estimate structural parameters for MR damper equipped structures, a synchronized state space model need to be formed to represent the whole system including both structure and MR damper. In order to form the model, parameters from both structure and damper are added in the new state vector.

The state vector now becomes

$$x'(t) = \begin{bmatrix} q \\ \dot{q} \\ \alpha \end{bmatrix} = \begin{bmatrix} q \\ \dot{q} \\ x_0 \\ \dot{x}_0 \\ kk \\ cc \\ k_1 \\ k_0 \\ c_1 \\ c_0 \\ m_0 \\ f_0 \\ V_{ref} \end{bmatrix}, \tag{4.22}$$

which include the state vector contains displacement and velocity of structure and inertial mass of damper (q, $\dot{q}$, x_0, $\dot{x}_0$), structural parameters (stiffness parameter *kk*, damping parameter *cc*) and parameters in hyperbolic tangent damper model (k_1, k_0, c_0, c_1, m_0, f_0, V_{ref}).

The continuous state equation is thus obtained as follows

$$\dot{x}'(t) = \begin{bmatrix} \dot{q} \\ \ddot{q} \\ \dot{\alpha} \end{bmatrix} = \begin{bmatrix} \dot{q}(t) \\ M^{-1}\left[\eta u(t) - (Cx(t) + Kz(t))\right] \\ 0 \end{bmatrix} = f(x'(t), u(t), t) \tag{4.23}$$

.

The hyperbolic MR damper model (Eq. 1 and 2) and structural dynamic equation of motion (Eq. 14) are combined to form the new state-space model, as shown in Eq. 24 and 25.

$$\begin{bmatrix} \dot{x} \\ \ddot{x} \\ \dot{x}_0 \\ \ddot{x}_0 \end{bmatrix} = \begin{bmatrix} 0 & I & 0 & 0 \\ -M^{-1}K + M^{-1}GG^T k_1 & -M^{-1}C + M^{-1}GG^T c_1 & -M^{-1}GG^T k_1 & -M^{-1}GG^T c_1 \\ 0 & 0 & 0 & 1 \\ (k_1/m_0)\times G^T & (c_1/m_0)\times G^T & (-k_1-k_0)/m_0 & (-k_1-k_0)/m_0 \end{bmatrix} \begin{bmatrix} x \\ \dot{x} \\ x_0 \\ \dot{x}_0 \end{bmatrix}$$

$$+ \begin{bmatrix} 0 \\ M^{-1} \\ 0 \\ 0 \end{bmatrix} u + \begin{bmatrix} 0 \\ 0 \\ 0 \\ 1/m_0 \end{bmatrix} \times f_0 \tanh(\dot{x}_0 / V_{ref}) \tag{4.24}$$

$$\begin{bmatrix} \ddot{x} \\ f \end{bmatrix} = \begin{bmatrix} -M^{-1}K - M^{-1}GG^T k_1 & -M^{-1}C - M^{-1}GG^T c_1 & M^{-1}GG^T k_1 & M^{-1}GG^T c_1 \\ k_1 & c_1 & -k_1 & -c_1 \end{bmatrix} \begin{bmatrix} x \\ \dot{x} \\ x_0 \\ \dot{x}_0 \end{bmatrix}$$

$$+ \begin{bmatrix} M^{-1} \\ 0 \end{bmatrix} u \tag{4.25}$$

The measurements are the accelerations of each floor and damper force ($\ddot{x}$, f). The new state-space model contains all structural parameters and MR damper parameters, in this way, all these parameters can be updated using EKF at the same time in each step.

4.5 Numerical validation

The developed EKF based MR damper parameter identification method is tested using numerical simulations of dynamic structural systems excited by El Centro earthquake ground motion. The numerical testing is performed using Simulink in Matlab. The testing structure is a three story one bay steel frame building, with total weight of 596 kN. As shown in Figure 4.2, the structure is a linear, in-plane, three degree-of-freedom model with an MR damper installed at the first story. The MR damper is controlled by a constant 2A current. The time history data of acceleration for each floor, MR damper force and ground acceleration are obtained from simulation tests, and then are fed into EKF algorithms to estimate the states

and parameters of structure and MR damper. To achieve the goal of structural parameter identification, this method is expected to demonstrate the capacity to identify stiffness for each floor.

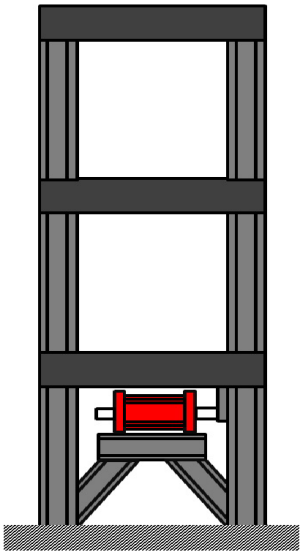

Figure 4.2 Three story building structure with MR damper

Consider a 3DOF linear shear frame structure subject to an earthquake excitation. The equation of motion for the 3DOF linear structure can be represented as,

$$M\ddot{x} + C\dot{x} + Kx = Gf - ML\ddot{x}_g, \tag{4.26}$$

where $x = [x_1; x_2; x_3]^T$, $\dot{x} = [\dot{x}_1; \dot{x}_2; \dot{x}_3]^T$, $\ddot{x} = [\ddot{x}_1; \ddot{x}_2; \ddot{x}_3]^T$ are the displacement, velocity and acceleration vector, respectively. f is the MR damper force, $G = [-1; 0; 0]^T$ is the influence vectors for MR damper force. $L = [1; 1; 1]^T$ is the ground excitation matrix, and $\ddot{x}_g$ is the acceleration of ground excitation. The mass matrix M, stiffness matrix K and damping matrix C, are as:

$$M = \begin{bmatrix} m_1 & 0 & 0 \\ 0 & m_2 & 0 \\ 0 & 0 & m_3 \end{bmatrix}, \tag{4.27}$$

$$K = \begin{bmatrix} kk_1 + kk_2 & -kk_2 & 0 \\ -kk_2 & kk_2 + kk_3 & -kk_3 \\ 0 & -kk_3 & kk_3 \end{bmatrix}, \tag{4.28}$$

$$C = \begin{bmatrix} cc_1 + cc_2 & -cc_2 & 0 \\ -cc_2 & cc_2 + cc_3 & -cc_3 \\ 0 & -cc_3 & cc_3 \end{bmatrix}, \tag{4.29}$$

where mass $m_1 = m_2 = m_3 = 20.253\times10^{-3}$ $kN\cdot s^2/mm$, stiffness $kk_1 = 9.933$ kN/mm, $kk_2 = 5.662$ kN/mm, $kk_3 = 5.662$ kN/mm, and damping $cc_1 = 7.243\times10^{-3}$ $kN\cdot s/mm$, $cc_2 = 2.069\times10^{-3}$ $kN\cdot s/mm$, $cc_3 = 2.069\times10^{-3}$ $kN\cdot s/mm$.

The N-S component of the El Centro earthquake recorded at the Imperial Valley Irrigation District substation in California of May 18, 1940 is used as excitation input, as shown in Figure 2. The peak ground acceleration (PGA) is set to 2g as ground motion in the testing. The sampling frequency is 50 Hz for all measured signals. The accelerations of each floor $\ddot{x}_i$ (i = 1, 2, 3) and the ground excitation $\ddot{x}_g$ are assumed as known measurements, and used as inputs in EKF estimation. The extended state vector is defined as,

$$x' = \left[x_1; x_2; x_3; \dot{x}_1; \dot{x}_2; \dot{x}_3; kk_1; kk_2; kk_3; cc_1; cc_2; cc_3; k_1; k_0; c_1; c_0; m_0;\ f_0; V_{ref}\right]^T. \tag{4.30}$$

The initial values for parameters in EKF are defined as follows. The initial state vector is defined as [0; 0; 0; 0; 0; 0; 4; 5; 5; 0.002; 0.002; 0.002; 100; 0.2; 0.05; 0.02; 150; 10]^T. The corresponding initial error covariance matrix of the extended state vector is a 21×21 diagonal matrix as $P_0 = 10^{-4}\times$diag{1; 1; 1; 1; 1; 1; 1; 1; 100; 100; 100; 100; 100; 100; 100; 100; 100; 100; 100; 100; 100}. The covariance matrix of the process noise w_k is $Q_0 = 10^{-5}\mathbf{I}_{21}$, in which $\mathbf{I}_{21}$ is 21×21 identity matrix. The covariance matrix of the measurement noise v_k is selected as $R_0 = 10^{-3}\mathbf{I}_4$. In this paper, the state covariance matrix and noise covariance matrices are selected based on the experience and extensive testing.

Based on the EKF and the measurements of the response data, the estimations for all state variables can be obtained. As shown in Figure 4, the EKF estimations for acceleration, velocity and displacement response of first floor are presented as blue solid curves. For comparison, the simulated measurements for the above responses are plotted as red dashed curves. Both the blue solid curves and red dashed curves almost coincide, indicating that the EKF algorithm has a good tracking capability to update the states based on new measurements.

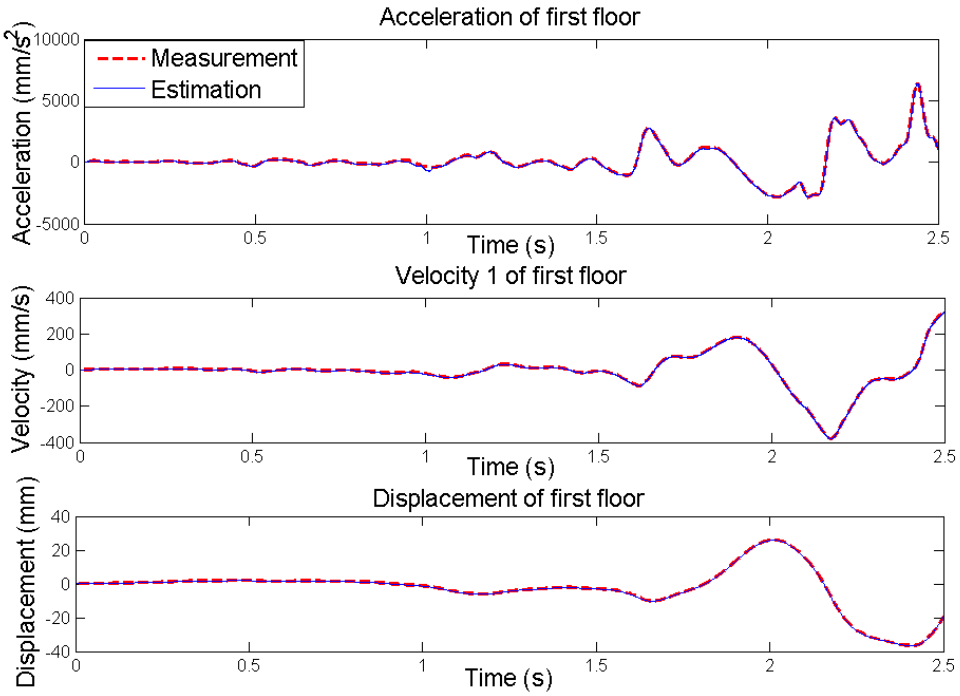

Figure 4.3 Simulation comparison: response of first floor

In Figure 5, the EKF estimation results for the output force of MR damper is plotted in blue solid lines, while the actual measurement of the damper force in the simulation is plotted in red dashed curves. The testing result for MR damper force demonstrate that EKF method has a good tracking capability for MR damper output, even under large-peak external loadings during an earthquake event.

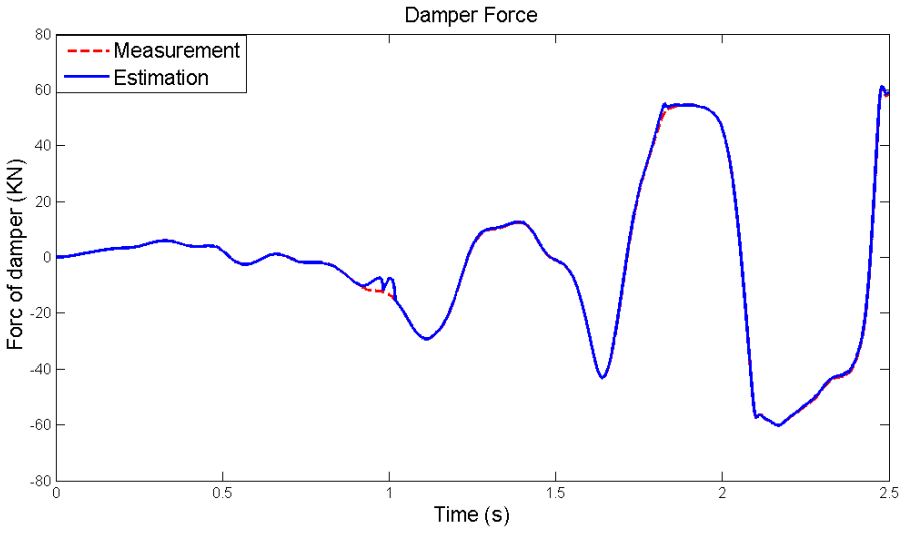

Figure 4.4 Simulation comparison: damper force time history

The testing results for stiffness estimation for three floors are plotted in Figure 6. The EKF estimation for stiffness parameter of each floor are presented in blue solid curves, while the actual values of the same structural parameters used in the simulation are plotted in red dashed lines. For all three floors, both the blue solid curves and red dashed lines almost coincide, indicating that EKF algorithm has an excellent capability to provide high quality estimations for structural parameters for MR damper-equipped structures.

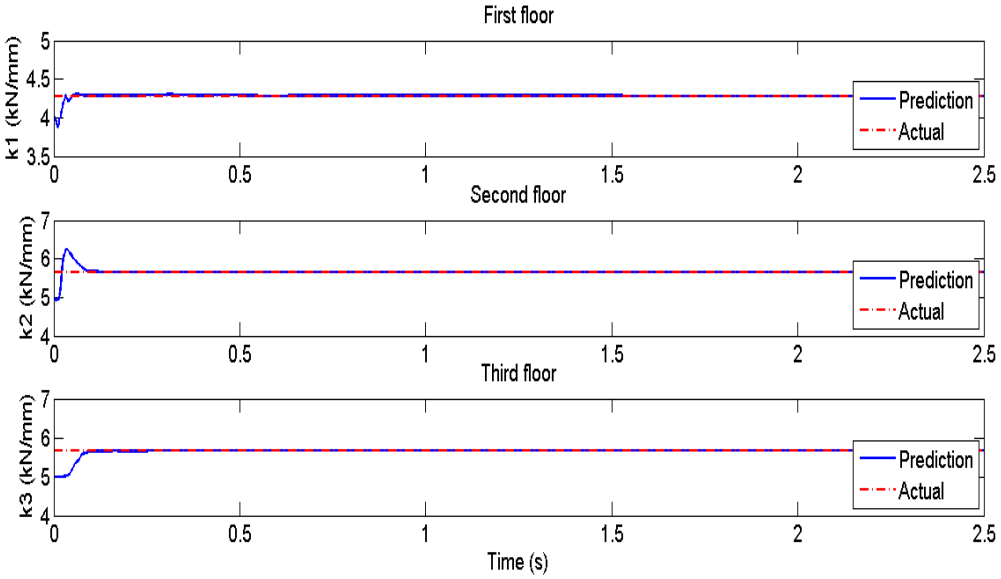

Figure 4.5 Simulation comparison: stiffness of each floor

Moreover, the recursion process of EKF on each time step only involves the new measurement and the calculation of state covariance matrix, therefore the developed method is computationally efficient.

4.6 Summary

In this paper, a novel structural parameter identification method based on extended Kalman filter is developed for linear structures equipped with MR damper devices. In order to incorporate the MR damper into the structural dynamic model, a new state-space model is established by combining hyperbolic tangent model and equation of motion of structural dynamic system. To estimate the structural variables and parameters, EKF is used to update the states based on new measurement in each time step. Based on measurements of accelerations of three stories and damper force, the EKF algorithm can produce real-time

estimation for the structural parameters and state variables. The EKF based method is tested using simulated data of a three stories linear building with MR damper under earthquake excitations, and numerical results demonstrate high estimation accuracy and light computation of this presented method. The developed EKF based method can be easily replicated to other types of structures equipped with MR dampers. And the developed EKF-based method has a good potential to be implemented in real-time SHM systems for in-service MR damper equipped structures.

CHAPTER 5 REAL-TIME STRUCTURAL DAMAGE DETECTION FOR BUILDING STRUCTURES

(Part of this chapter was published as Chenhao Jin, Shinae Jang and Xiaorong Sun "An integrated real-time structural damage detection method based on extended Kalman filter and dynamic statistical process control", *Advances in Structural Engineering*, Published online July 5, 2016, doi: 10.1177/1369433216658484)

5.1 Introduction

Real-time structural parameter identification and damage detection are of great significance for structural health monitoring systems. The extended Kalman filter has been implemented in many structural damage detection methods due to its capability to estimate structural parameters based on online measurement data. Current research assumes constant structural parameters and uses static statistical process control for damage detection. However, structural parameters are typically slow-changing due to variations such as environmental and operational effects. Hence, false alarms may easily be triggered when the data points falling outside of the static statistical process control range due to the environmental and operational effects. In order to overcome this problem, this article presents a novel real-time structural damage detection method by integrating extended Kalman filter and dynamic statistical process control. Based on historical measurements of damage-sensitive parameters in the state-space model, extended Kalman filter is used to provide real-time estimations of these parameters as well as standard derivations in each time step, which are then used to update the control limits for dynamic statistical process control to detect any abnormality in the selected parameters. The numerical validation is performed on both linear and nonlinear structures, considering different damage scenarios. The simulation results demonstrate high detection accuracy rate and light computational costs of the developed extended Kalman filter–dynamic statistical process control damage detection method and the potential for implementation in structural health monitoring systems for in-service civil structures.

Maintaining civil engineering structures in good conditions through structural health monitoring (SHM) has become an increasingly viable option in recent decades. The goal of SHM is to determine the status of the structure, detect damage, and implement characterization strategies for engineering structures (Yan *et al.* 2007). Some extreme events, such as earthquake, typhoon, and blast, can cause structural damages and lead to structural failure rapidly. During these events, real-time reliable information regarding the condition and the integrity of the structure is invaluable for infrastructure owners and first responders (e.g., policemen, fire fighters, rescuers, etc.) to make rapid decisions (Dyke *et al.* 2010). Improving the capabilities of real-time performance evaluation and damage detection for structural health monitoring systems are extremely valuable.

Many structural parameter identification methods have been developed in order to estimate system parameters based on the measurements of structural response data directly, including extended Kalman filter (EKF) (Hoshiya *et al.* 1984; Mariani and Corigliano, 2005), unscented Kalman filter (UKF) (Mariani and Ghisi, 2007; Wu and Smyth, 2007) and Particle filter (Charzi and Smyth, 2009; Eftekhar Azam *et al.* 2012). In these Kalman filter-based methods, the dynamic structures are modeled in the state space formulation including state equations and measurement equations. These methods are attractive in view of the recursive feature of Kalman filter such that they can estimate structural parameters straightly, and provide detailed information and understanding about the existence, location, and severity of the structural damage. In the EKF, the state distribution is approximately by a Gaussian random variable, which is then propagated through the first-order linearization of a nonlinear system. The unscented Kalman filter (UKF) differs from the EKF in the manner of representing Gaussian random variables. The UKF uses an unscented transform to generate a minimal set of carefully chosen sample points to present the state distribution. These sample points capture the means and covariance of the Gaussian random variables, and when propagated through the nonlinear system, captures the posterior mean and covariance accurately to the 2nd order for any nonlinearity. The particle filters can deal with nonlinear systems with non-Gaussian posterior distribution of the state. The concept of the method is that the approximation of the posterior distribution of the state is done through the generation of a large number of samples (weighted particles), using Monte

Carlo Methods. The basic drawback is the fact that depending on the problem a large number of samples may be required thus making the particle filter analysis computationally expensive. The UKF and particle filter may estimate more accurately than the EKF for highly nonlinear systems, however, the EKF is widely used in state estimation and structural parameter estimation for civil engineering problems due to its straightforward implementation, high updating frequency, fast convergence speed, and low computational costs (Yang *et al.* 2006 2007; Zhou *et al.* 2008; Soyoz et al. 2008; Liu *et al.* 2009; Lei *et al.* 2012; Yin *et al.* 2013), and EKF is also adopted in this chapter.

In the above studies, the structural parameters are assumed constant values throughout time. In this case, if the identified values of structural parameters deviate from their constant values, then the structural damage is identified. However, this assumption does not consider the influence of varying environmental and operational conditions, which can cause structural parameters to fluctuate and differ from their constant values even when no damage has occurred. The effects of environmental and operational conditions on the variance of structural parameters have been found and reported in many long-term structural monitoring projects (Peeters et al. 2001; Sohn 2007; Cross et al. 2013; Reynders et al. 2014; Spiridonakos et al. 2014). Thus the performance and reliability of current EKF-based methods for structural damage detection, especially for in-service large-scale civil structures, are in urgent needs to be improved.

Statistical process control (SPC) has been widely used to monitor and control processes due to its advantages of early detection and prevention capability. The SPC attempts to differentiate additional sources of variation from natural sources in a process by using control limits. When the process data deviate from their normal range and trigger the control limits, the excessive variation of data indicates the presence of faults or damage in the system. SPC has been applied to many solve damage detection problems in the field of SHM, especially in long-term bridge monitoring research projects (Sohn et al. 2000; Fugate et al. 2001; Kullaa et al. 2003; Deraemaeker et al. 2008; Zapico-Valle et al. 2011; Magalhaes et al. 2012). The above studies all used static SPC methods, in which the control limits are fixed constant values calculated from statistical indicators of historical data. However, the range of control limits might not be able to adjust to the changing trends of structural parameters due to environmental and operational variations, which may

trigger false alarms when data points are falling outside static control limits but the structure has not been damaged.

To overcome all the above limitations, dynamic statistical process control (DSPC) method can be used to adjust control limits continuously and provide adaptive changing boundaries in real time. In order to establish the dynamic control limits for the target parameters, the values of the mean and standard deviation are required to be updated in each time step. The Kalman filter provides an ideal approach to establish dynamic control limits for its state variables for engineering damage detection problems (Sun et al. 2012). In each time step, the Kalman filter not only updates estimation values for state variables, but also generates a state covariance matrix, which stores variance of each state variable in the diagonal elements. Therefore, the combination of EKF and DSPC can achieve both online parameter estimation and dynamic control limits formulation, which has potential to be used for real-time structural damage detection.

Recently, a novel structural damage detection method combining EKF and DSPC has been developed by authors (Jin et al. 2015a, 2015b). In this paper, the EKF-DSPC is further improved with more rigorous derivations and testing scenarios. Moreover, the entire paper has been extended with more discussion and insights on the initialization of the state and covariance matrix, noise covariance matrices, and the estimate processes on different structural models. This paper aims to develop a real-time EKF-DSPC based structural damage detection method considering variation effects that an in-service structure may encounter during operation. Numerical tests are performed to validate the effectiveness of the EKF-DSPC method for identify structural parameters and detect the occurrence of damage, including a three-story linear structure and a two-story nonlinear hysteric structure, with multiple common damage scenarios considered. The testing results show that proposed method has a good performance to identify structural parameters and detect damage with high accuracy and with low computational costs. In Section 5.2, the methodology about EKF-based structural parameter identification is reviewed. Section 5.3 describes the theory of dynamic statistical process control, and summarizes how the two methods are combined for real-time damage detection in this paper. Subsequently in Section 5.4, application of the proposed EKF-DSPC method will be presented for a 3-degree-of-freedom (3DOF) linear structure and a 2DOF nonlinear hysteretic dynamic system, considering

various damage scenarios. Finally, testing results discussion and the benefits of developed damage detection method will be highlighted.

5.2 EKF-based structural parameter identification

5.2.1 Kalman filter and extended Kalman filter

The Kalman filter (KF) provides a recursive solution for linear dynamic systems that can be represented in state-space formulation. Each updated estimate of the state is computed from the previous estimate and new input data only, instead of all previous data points. Thus, the KF is less demanding in storage space and computationally more efficient. The state equation and measurement equation of KF are given by:

$$x_{k+1} = F_k x_k + w_k , \tag{5.1}$$

$$y_k = H_k x_k + v_k , \tag{5.2}$$

where x_k is the state vector, and y_k is the measurement vector. The process noise w_k and observation noise v_k are independent, zero-mean, Gaussian processes with covariance matrix Q_k and R_k, respectively. The matrices F, H, Q and R are assumed known and possibly time-varying.

The KF consists of two steps: time update and measurement update. In time update, the state and covariance propagations are implemented as follows:

$$\hat{x}_{k+1|k} = F_k \hat{x}_{k|k} , \tag{5.3}$$

$$P_{k+1|k} = F_k P_{k|k} F_k ' + Q_k , \tag{5.4}$$

$$\hat{y}_{k+1|k} = H_k \hat{x}_{k+1|k} , \tag{5.5}$$

where the prior state $\hat{x}_{k|k}$ and state covariance matrix $P_{k|k}$ are propagated to $\hat{x}_{k+1|k}$ and $P_{k+1|k}$, respectively. The $\hat{x}_{k+1|k}$ is then used to generate the estimated measurement $\hat{y}_{k+1|k}$ through H_k.

In the measurement-update step, the filter gain W_k, the posterior state $\hat{x}_{k+1|k+1}$, and the state covariance $P_{k+1|k+1}$ are produced as follows:

$$S_{k+1} = H_{k+1} P_{k+1|k} H_{k+1}' + R_{k+1}, \tag{5.6}$$

$$W_{k+1} = P_{k+1|k} H_{k+1}' S_{k+1}^{-1}, \tag{5.7}$$

$$\hat{x}_{k+1|k+1} = \hat{x}_{k+1|k} + W_{k+1}(y_k - \hat{y}_{k+1|k}), \tag{5.8}$$

$$P_{k+1|k+1} = P_{k+1|k} - W_{k+1} S_{k+1} W_{k+1}', \tag{5.9}$$

where S_{k+1} is the innovation covariance matrix. Note that the roots of the diagonal elements of $P_{k+1|k+1}$ are the standard deviation of each state variable in the state vector.

The EKF approach applies the standard KF to nonlinear systems by continually updating a linearization around the previous state estimate through first-order Taylor series expansion. The linearized state matrix F_k is taken as the partial derivative of nonlinear function $f(x_k, u_k, k)$ with respect to x at $\hat{x}_{k|k}$, i.e. a Jacobian matrix, while the linearized measurement matrix H_k is obtained as the partial derivative of nonlinear function $h(x_k, u_k, k)$ with respect to x at $\hat{x}_{k+1|k}$, and are given by:

$$F_k = \left. \frac{\partial f(x_k, u_k, k)}{\partial x} \right|_{x=\hat{x}_{k|k}}, \tag{5.10}$$

$$H_k = \left. \frac{\partial h(x_k, u_k, k)}{\partial x} \right|_{x=\hat{x}_{k+1|k}}. \tag{5.11}$$

The recursions of time update and measurement update for EKF follow equations (5.3)-(5.9) used in the standard KF.

Given the initial values of state vector x_0, the initial state covariance matrix P_0, the process noise covariance matrix Q_0, and the measurement noise covariance matrix R_0, the EKF procedure can be recursively implemented to estimate the structural parameters based on the measurement data of the dynamic system. Due to the nature of the recursion method, these structural parameters can be updated at each time step, which makes real-time structural damage detection possible. More details on KF and EKF can be found in Welch and Bishop (2002).

5.2.2 Extended Kalman filter for linear structures

The equation of motion for an m-DOF linear structure can be represented as,

$$M\ddot{q}(t) + C\dot{q}(t) + Kq(t) = \eta u(t) \tag{5.12}$$

where M, C and K represent ($m \times m$) mass matrix, damping matrix and stiffness matrix, respectively; $q(t)$ is the ($m \times 1$) displacement vector; $\dot{q}(t)$ is the velocity vector; $\ddot{q}(t)$ is the ($m \times 1$) is the acceleration vector; $u(t)$ is the ($m \times 1$) excitation force vector; and η is the ($m \times m$) excitation influence matrix.

As discussed in Section 2.1, KF-based approaches give a simple and efficient way to estimate the state and parameters in any system models. For structural dynamic systems, the states (e.g., displacement and velocity) and parameters (e.g., stiffness and damping) are often required to be identified simultaneously. Therefore, even though the structural model is linear, due to the nonlinear coupling feature between the structural states and parameters, EKF will be used. The state vector for structure model is thus formed as:

$$x'(t) = \begin{bmatrix} x(t) \\ \alpha \end{bmatrix} = \begin{bmatrix} q(t) \\ \dot{q}(t) \\ \alpha \end{bmatrix} \tag{5.13}$$

where $x(t)$ is the state of structural dynamic system including displacement $q(t)$ and velocity $\dot{q}(t)$, and α is the parameter vector to be estimated. The continuous state equation becomes:

$$\dot{x}'(t) = \begin{bmatrix} \dot{x}(t) \\ \dot{\alpha} \end{bmatrix} = \begin{bmatrix} \dot{q}(t) \\ \ddot{q}(t) \\ \dot{k} \\ \dot{c} \end{bmatrix} = \begin{bmatrix} \dot{q}(t) \\ M^{-1}\left[\eta u(t) - (C\dot{q}(t) - Kq(t))\right] \\ 0 \\ 0 \end{bmatrix} \equiv f(x'(t), u(t), t) \tag{5.14}$$

and the continuous measurement equation becomes:

$$y(t) = h(x'(t), u(t), t) \tag{5.15}$$

By discretizing and linearizing at time t_k (k = 1,2,…) using first-order Taylor series expansion, the discrete-time space model is formulated as:

$$x'_{k+1} = F_k x'_k + w_k \tag{5.16}$$

$$y_k = H_k x'_k + v_k , \tag{5.17}$$

where

$$F_k = \frac{\partial f\left(x'_k, u_k, k\right)}{\partial x'}\Big|_{x'=x'_k}$$

$$= \begin{bmatrix} [0] & I & [0] & \cdots & [0] \\ -M^{-1}K & -M^{-1}C & -M^{-1}\dfrac{\partial K}{\partial \alpha_1}q(k) - M^{-1}\dfrac{\partial C}{\alpha_1}\dot{q}(k) & \cdots & -M^{-1}\dfrac{\partial K}{\partial \alpha_\alpha}q(k) - M^{-1}\dfrac{\partial C}{\alpha_\alpha}\dot{q}(k) \\ [0] & [0] & [0] & \cdots & [0] \end{bmatrix}$$

, (5.18)

When the measurement is the acceleration $\ddot{q}(t)$, the measurement matrix Hk has the form

$$H_k = \frac{\partial h\left(x'_k, u_k, k\right)}{\partial x'}\Big|_{x'=x'_k}$$

$$= \begin{bmatrix} -M^{-1}K & -M^{-1}C & -M^{-1}\dfrac{\partial K}{\partial \alpha}q(k) - M^{-1}\dfrac{\partial C}{\partial \alpha}\dot{q}(k) \end{bmatrix}. \tag{5.19}$$

The EKF recursion process follows the equations (5.3)-(5.9) as shown in Section 5.2.1. The selection of initial state, initial state covariance matrix, process noise and measurement covariance matrices will be discussed in Section 5.4.

5.2.3 Extended Kalman filter for nonlinear hysteretic structure

The equation of motion of a nonlinear hysteretic structure subject to ground excitation can be written as

$$M\ddot{q}(t) + C\dot{q}(t) + r(t) = f(t), \tag{5.20}$$

where M represents mass matrix, C represents damping matrix; $q(t)$, $\dot{q}(t)$ and $\ddot{q}(t)$ are the displacement, velocity and acceleration vector, respectively; $r(t)$ is the restoring force matrix, and $f(t)$ is the excitation force matrix.

The excitation force matrix is expressed as:

$$f(t) = \eta u(t), \tag{5.21}$$

where η is the excitation influence matrix, $u(t)$ is excitation force.

The restoring force is expressed as:

$$r(t) = KZ(t) \tag{5.22}$$

where K represent stiffness matrix, $Z(t)$ is the non-observable hysteretic component vector, which can be defined by Bouc-Wen model (Bouc, 1967; Wen, 1976, 1989; Nayyerloo, 2011; Constantinou and Tadjbakhsh, 1986; Ismail et al., 2009).

The hysteretic component vector is expressed as

$$Z(t) = \begin{bmatrix} z_1(t) & \cdots & z_i(t) \end{bmatrix}^T, \tag{5.23}$$

$$\dot{z}_i = \dot{q}_i - \beta_i \left|\dot{q}_i\right| \left|z_i\right|^{\alpha_i - 1} z_i - \gamma_i \dot{q}_i \left|z_i\right|^{\alpha_i}, \tag{5.24}$$

where i represents i^{th} DOF; $\dot{q}(t)$ and z_i are the velocity and hysteretic component of i^{th} DOF; α_i, β_i, γ_i are the hysteretic parameters of the Bouc-Wen model; β_i and γ_i control the size and shape of the hysteretic loop; β_i is fatness parameter; γ_i is loop pinching parameter; the power factor α_i determines the sharpness of the curve from elastic to the post-elastic force-deflection behavior.

When extended Kalman filter is applied to this model, the state vector now becomes

$$x'(t) = \begin{bmatrix} q(t) \\ \dot{q}(t) \\ z(t) \\ k \\ c \\ \alpha \\ \beta \\ \gamma \end{bmatrix}. \tag{5.25}$$

The continuous state equation is thus obtained as follows

$$\dot{x}'(t)=\begin{bmatrix}\dot{q}(t)\\ \ddot{q}(t)\\ \dot{z}(t)\\ \dot{k}\\ \dot{c}\\ \dot{\alpha}\\ \dot{\beta}\\ \dot{\gamma}\end{bmatrix}=\begin{bmatrix}\dot{q}(t)\\ M^{-1}\left[\eta u(t)-(C\dot{q}(t)+Kz(t))\right]\\ \dot{q}_i-\beta_i|\dot{q}_i||z_i|^{\alpha_i-1}z_i-\gamma_i\dot{q}_i|z_i|^{\alpha_i}\\ 0\\ 0\\ 0\\ 0\\ 0\end{bmatrix}=f(x'(t),u(t),t). \tag{5.26}$$

Since the measurement is typically the acceleration, the continuous measurement equation becomes

$$y(t)=M^{-1}\left[\eta u(t)-(C\dot{q}(t)+Kz(t))\right]=h(x'(t),u(t),t). \tag{5.27}$$

The discretization and linearization follow the same manner as for linear structures shown in Section 5.2.2. With the formulation in the state-space model, the recursive estimation process follows the standard EKF.

5.3 Dynamic statistical process control (DSPC)

The structural parameters for in-service civil structures can be viewed as slow changing variables, driven by various environmental and operational effects (e.g., temperature, ground and traffic loadings, system noise, etc.). In previous parameter identification researches, structural parameters were usually treated as constant values, however, on-site long-term monitoring shows that these structural parameters have significant variances under the above effects (Sohn 2007), which may cause false alarm problems. Enabling online monitoring system to detect structural damage and maintain a low false alarm rate is a significantly important issue in SHM.

SPC can be used to distinguish the abnormal variance from the normal variance of a process. If a structure is in good health without any structural damage, the structural parameters should jump and fall insignificantly within the SPC control limits. However, when the structural damage occurs, the key parameter is more likely to jump outside the range of the control limits, thus the potential damage can be detected. Traditional static SPC uses constant values as upper and lower boundaries of control limits, which can be represented as,

$$[\mu - n \times \sigma, \mu + n \times \sigma], \tag{5.28}$$

where μ is the mean, σ is the standard deviation of the estimated state, and n is a pre-defined integer number to set the confidence level for control limits.

In equation (25), the values of μ and σ are obtained from historical measurements when the structure is operating in good condition. Nevertheless, this approach may not be effective due to the following reasons. If μ and σ are calculated too conservatively, e.g., large σ, a large range of SPC control limits may make it difficult to capture any occurrence of damage; If μ and σ are calculated too risky, e.g., a small σ, the narrow range of SPC control limits may not be able to update and adjust to varying environmental and operational conditions, thus lead to false alarms.

To address the above issues, DSPC is adopted in this paper to replace the traditional static SPC. Instead of using the pre-defined fixed control limits based on the historical data, the real-time structural damage detection requirements call for an approach to enable the control boundaries to update and adjust to the changing trend of the state parameters. The recursive property of Kalman filter and the standard deviation obtained from covariance matrix provide a good solution to update the parameters of DSPC. At each time step, EKF not only estimates the state variables, but also generates state covariance matrix P_k, whose diagonal elements store the variance value of each state variable. The averaged estimated state variables over the past j points are used as the updated mean values, and the standard deviations are averaged using the same manner. In this approach, the control limits of DSPC can be updated in real time only based on new measurements.

The EKF assumes a Gaussian random variable to estimate the state. Typically, "three-sigma Gaussian rule" is widely used in industry to cover the 99.7% probability of all values lying within three standard deviations of the mean in a normal process, which can be empirically treated as "near certainty" (Wheeler et al. 1992; Pukelsheim 1994; Wiborg et al. 2014). This means that by default, the EKF holds that at every step the confidence interval in the estimate equals to the mean ±3·times standard deviation. The "three-

sigma Gaussian rule" will be followed in this paper to set *n* equal to 3, and the range of three-sigma control limits of DSPC is thus described as,

$$[\bar{\mu}_{\alpha_i,k}-3\bar{\sigma}_{\alpha_i,k},\bar{\mu}_{\alpha_i,k}+3\bar{\sigma}_{\alpha_i,k}], \tag{5.29}$$

where $\bar{\mu}_{\alpha_i,k}$ and $\bar{\sigma}_{\alpha_i,k}$ are the averaged mean and averaged standard deviation of the state α_i at time *k*, respectively. This novel integration of EKF and DSPC is very simple but efficient since the standard deviations are obtained as the byproducts of Kalman filter and the damage can be detected online once the estimates exceed the control limits.

The flow chart for the proposed EKF-DSPC structural damage detection method in this paper is depicted in Figure 5.1. As the flow chart shows, starting from a set of initiation for state variables and covariance matrices, the EKF recursively estimates and updates the state variables based on new measurements. Then in each time step, the DSPC is integrated with EKF to identify the abnormal changes of state variables based on the presented control rules. In this approach, real-time structural damage detection can be achieved with high accuracy and short time.

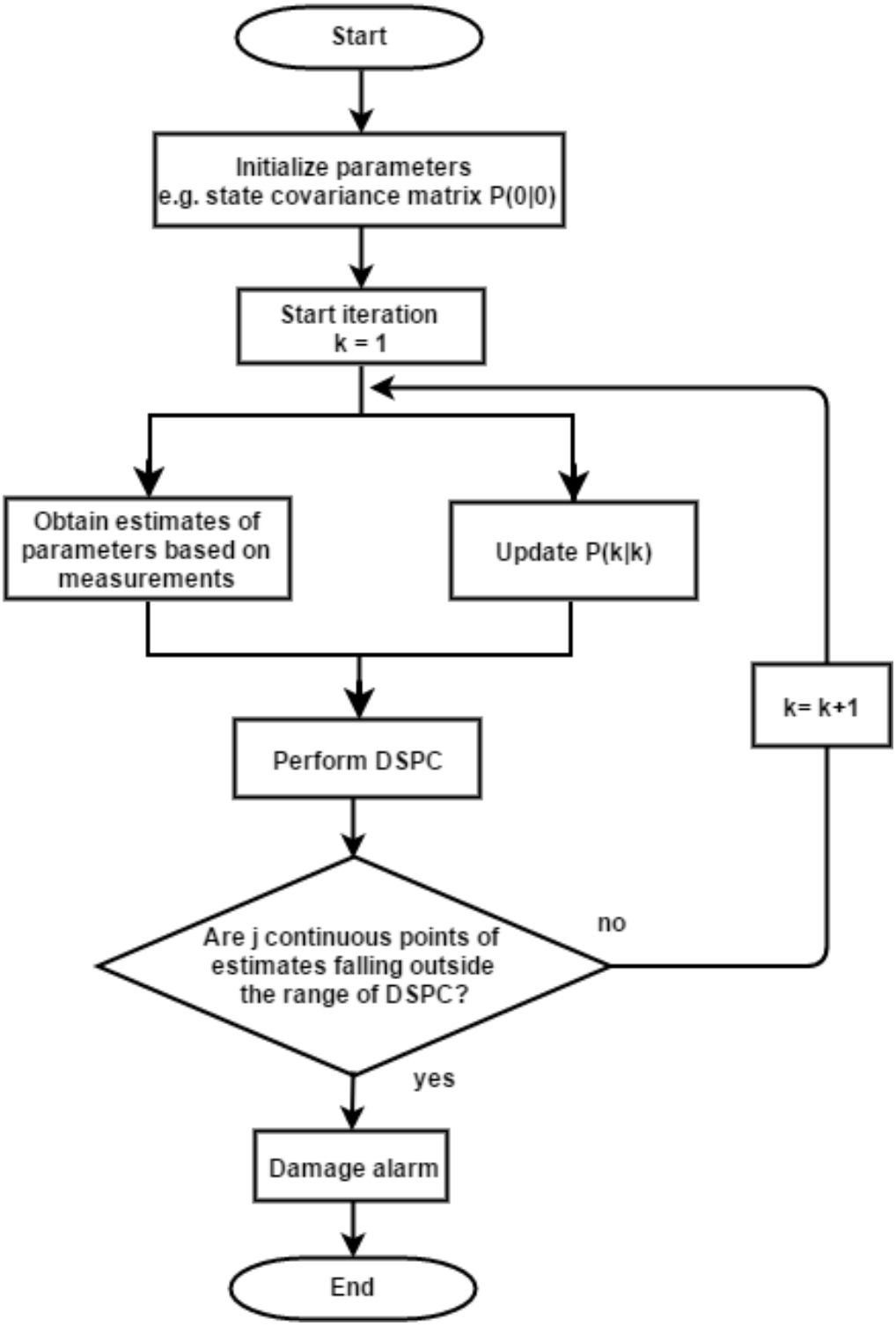

Figure 5.1 Flow chart of EKF-DSPC damage detection method

5.4 Numerical Validation

The developed EKF-DSPC structural damage detection method is tested using numerical simulations of buildings excited by El Centro earthquake ground motion. Both linear and nonlinear structures in different damage scenarios are considered. Simulated acceleration for each story of the structure and the ground excitation are fed into the EKF algorithm to estimate the structural parameters. At the same time, the DSPC is utilized for real-time damage detection purposes. The numerical testing demonstrates the capacity of the developed method can identify the structural parameter online and trigger alarm warnings with high accuracy within rapid time.

5.4.1 Three-story linear structure

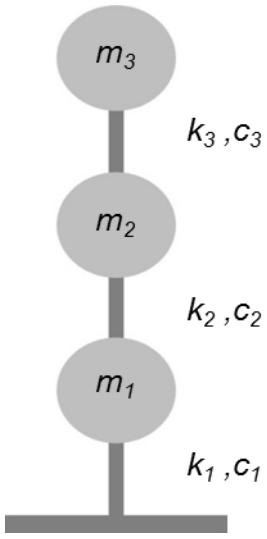

Figure 5.2 Three story linear structure

Consider a three-story linear building structure subject to an earthquake excitation. The equation of motion for the three-story linear structure can be represented as,

$$M\ddot{x} + C\dot{x} + Kx = -ML\ddot{x}_g \tag{5.30}$$

where $x = [x_1; x_2; x_3]^T$ is the relative displacement of each story, $\dot{x} = [\dot{x}_1; \dot{x}_2; \dot{x}_3]^T$, $\ddot{x} = [\ddot{x}_1; \ddot{x}_2; \ddot{x}_3]^T$ are the relative velocity and acceleration of each story, $\ddot{x}_g$ is the acceleration of ground excitation, and L is the ground excitation matrix. The mass matrix M, stiffness matrix K, and damping matrix C are defined as:

$$M = \begin{bmatrix} m_1 & 0 & 0 \\ 0 & m_2 & 0 \\ 0 & 0 & m_3 \end{bmatrix}, \tag{5.31}$$

$$K = \begin{bmatrix} k_1 + k_2 & -k_2 & 0 \\ -k_2 & k_2 + k_3 & -k_3 \\ 0 & -k_3 & k_3 \end{bmatrix}, \tag{5.32}$$

$$C = \begin{bmatrix} c_1 + c_2 & -c_2 & 0 \\ -c_2 & c_2 + c_3 & -c_3 \\ 0 & -c_3 & c_3 \end{bmatrix}, \tag{5.33}$$

where mass $m_1 = m_2 = m_3 = 1$ kg, stiffness $k_1 = k_2 = k_3 = 12$ kN/m, and damping $c_1 = c_2 = c_3 = 0.6$ kN s/m.

The N-S component of the El Centro earthquake recorded at the Imperial Valley Irrigation District substation in California of May 18, 1940 is used in this paper, as shown in Figure 5.3. The peak ground acceleration (PGA) is set to 2g as ground motion in the testing. The sampling frequency is 50 Hz for all measured signals. The relative accelerations of each floor $\ddot{x}_i$ (i = 1, 2, 3) and the ground excitation $\ddot{x}_g$ are assumed as known measurements, and used as inputs in EKF estimation. The unknown parameters to be identified are stiffness and damping of all floors, i.e., k_i and c_i (i = 1, 2, 3), thus the extended state vector is defined as,

$$x' = \left[x_1; x_2; x_3; \dot{x}_1; \dot{x}_2; \dot{x}_3; k_1; k_2; k_3; c_1; c_2; c_3\right]^T. \tag{5.34}$$

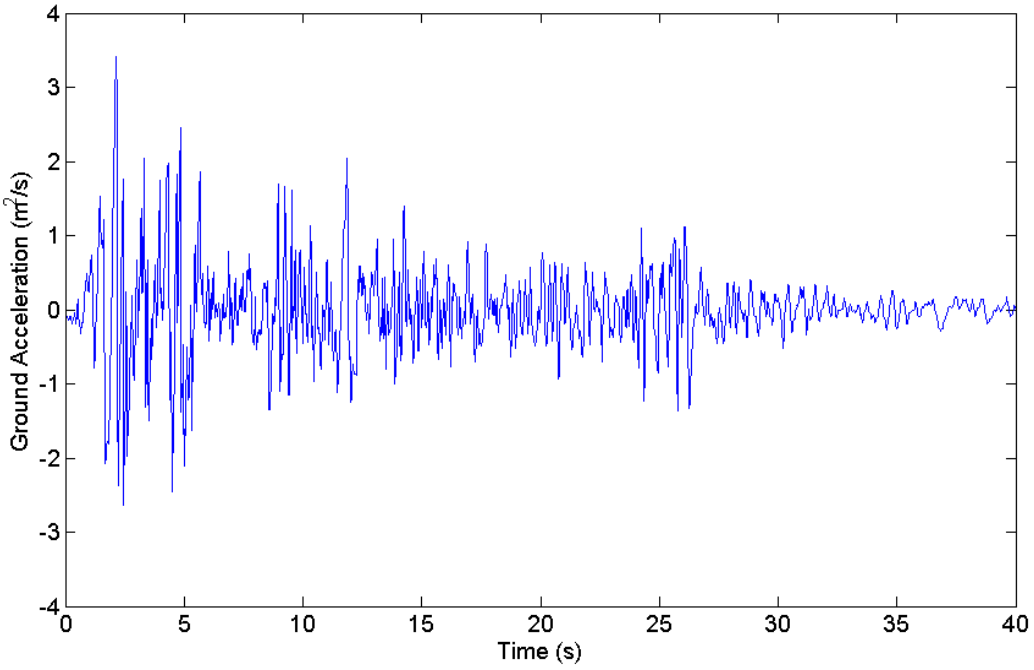

Figure 5.3 Ground acceleration record of El Centro Earthquake

The initial values for parameters in EKF are defined as follows. The initial values for stiffness k_i and damping c_i are k_{i0} = 15 kN/m and c_{i0} = 0.1 kN s/m (i = 1, 2, 3), and the initial values for displacement x_i and velocity $\dot{x}_i$ are zero, i.e., x_{i0} = 0 and $\dot{x}_{i0}$ = 0 (i = 1, 2, 3). Thus the initial state vector is defined as [0; 0; 0; 0; 0; 0; 15; 15; 15; 0.1; 0.1; 0.1]^T. The corresponding initial error covariance matrix of the extended state vector is a 12×12 diagonal matrix as P_0 = diag{1; 1; 1; 1; 1; 1; 10^5; 10^5; 10^5; 10^5; 10^5; 10^5}. The covariance matrix of the process noise w_k is $Q_0 = 10^{-6}\mathbf{I}_9$, in which $\mathbf{I}_9$ is 9×9 identify matrix. The covariance matrix of the measurement noise v_k is selected as $R_0 = 10^{-6}$diag{1; 1; 1; 1; 1; 1; 10^2; 10^2; 10^2; 1; 1; 1}. In all testing cases of the three-story linear structure, the same above initial parameters will be used.

Based on EKF and the measurements of the response data, the estimations for all state variables can be obtained. As shown in Figure 5.4, the EKF estimations of displacements for all three floors are presented as red dashed curves. For comparison, the simulated results of displacements for all three floors are plotted as blue solid curves. Moreover, as shown in Figure 5.5 and Figure 5.6, the EKF estimation results for stiffness and damping of each floor are plotted in red dashed curves, while the actual values of the same

structural parameters used in the simulation are plotted in blue solid lines. In Figures 5.4, 5.5 and 5.6, both the solid curves and dashed curves almost coincide, indicating that the EKF algorithm has an excellent tracking capability to provide high-quality estimations for structural parameters.

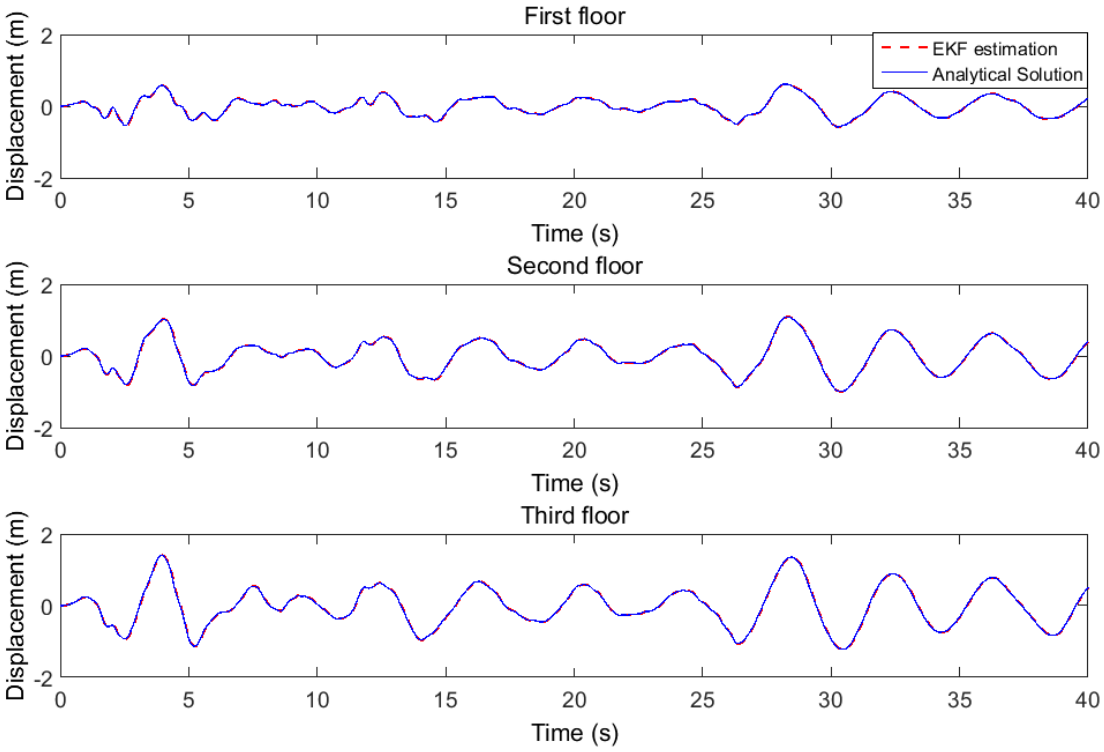

Figure 5.4 Comparisons of displacement between EKF estimation and measurement

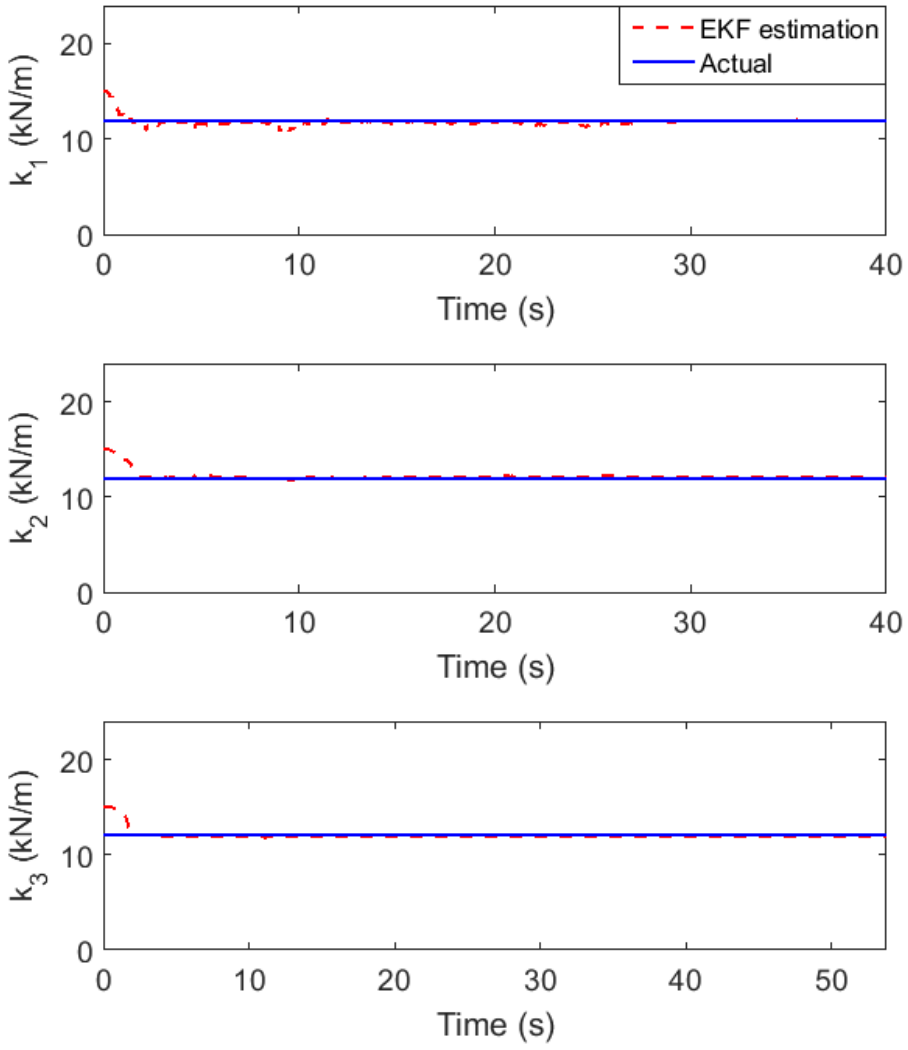

Figure 5.5 Performance of EKF estimation for stiffness parameters in linear structure

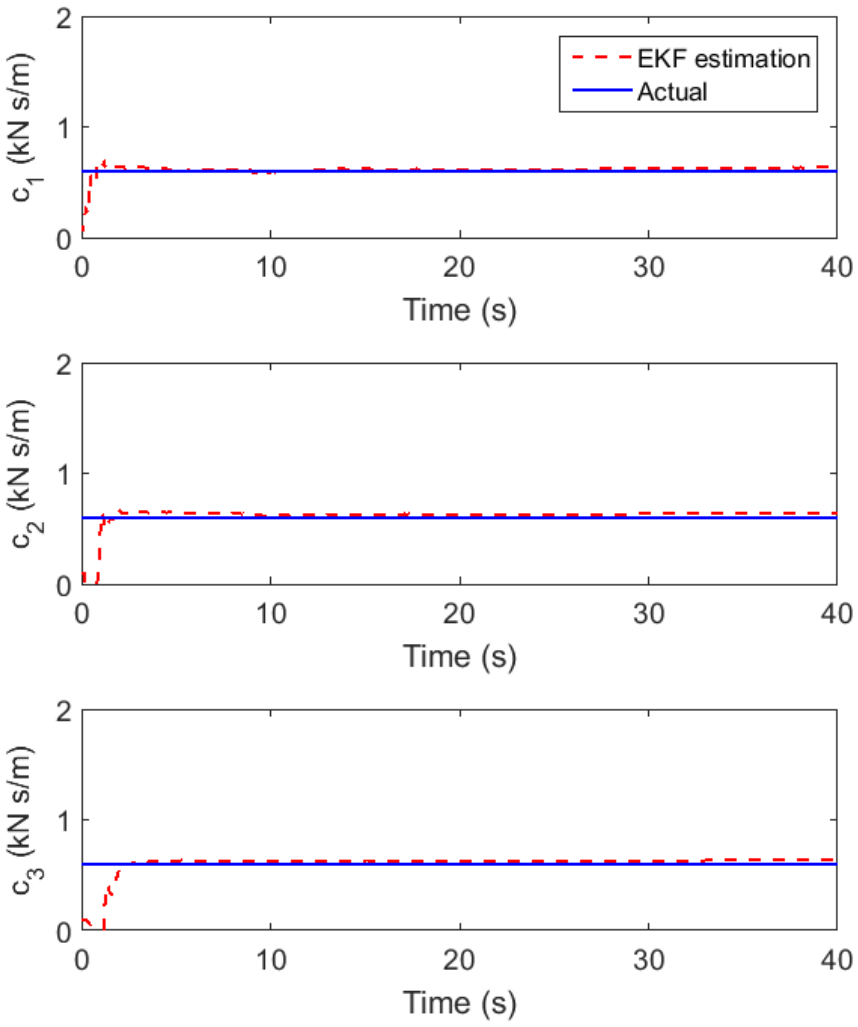

Figure 5.6 Performance of EKF estimation for damping parameters in linear structure

In order to verify the capability and accuracy of the EKF-DSPC based damage detection method, different structural damage scenarios are considered in the numerical validation. Two damage cases are presented for the linear structure: (1) damage only on structural stiffness; (2) damage on both stiffness and damping at the same time.

Case 1: k_1 is reduced abruptly from 12 to 6 kN/m at t = 20 s. The parameter estimation and damage detection performance for all 6 parameters based on the developed EKF-DSPC method is depicted in Figure 5.7 and 5.8. The testing results indicate that the EKF estimation of identified parameters (blue solid curves) and actual values (black dashed curves) almost coincide. When the damage occurs on k_1 at t = 20 s, the

sudden drop from 12 to 6 kN/s is captured by EKF rapidly. The effectiveness of DSPC to detect damage on k_1 is verified in Figure 5.9, which is the zoomed-in process during 19 to 25 s. The DSPC detects the damage successfully when the EKF estimation of k_1 jumps outside of the control range of DSPC while the estimation for other identified parameters fall inside DSPC when no structural damage appears. The testing results for damage Case 1 demonstrate that EKF-DSPC method has an excellent tracking capability for the structural parameters during damage events, leading to the online detection of damage on stiffness parameter with high confidence.

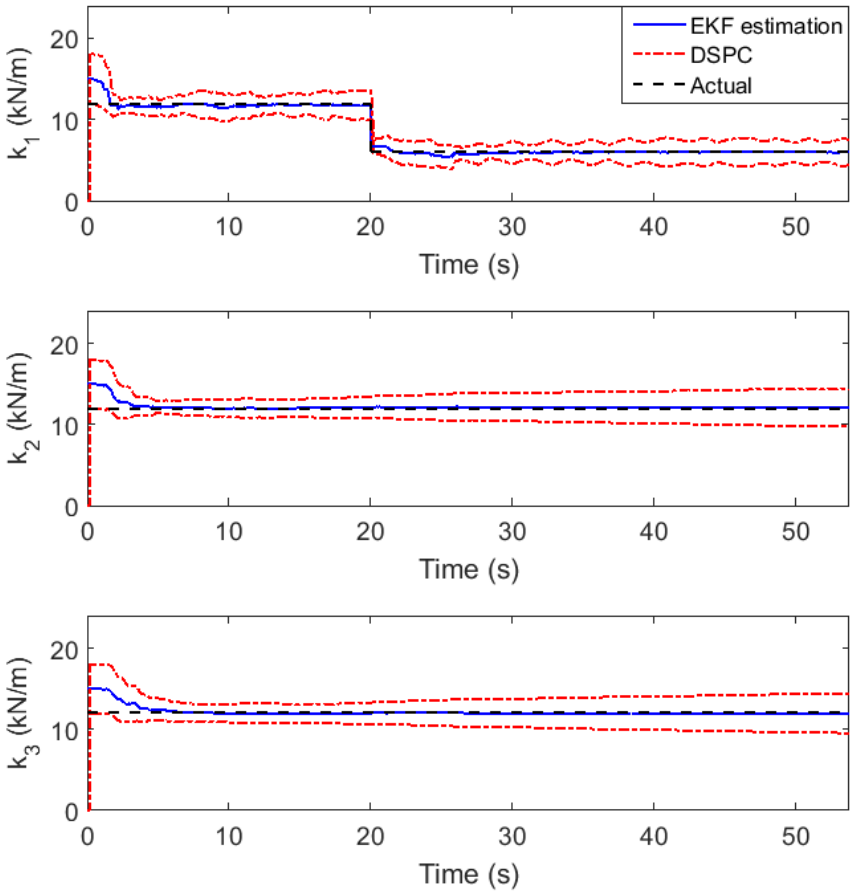

Figure 5.7 Performance of EKF-DSPC for stiffness parameters in Case 1

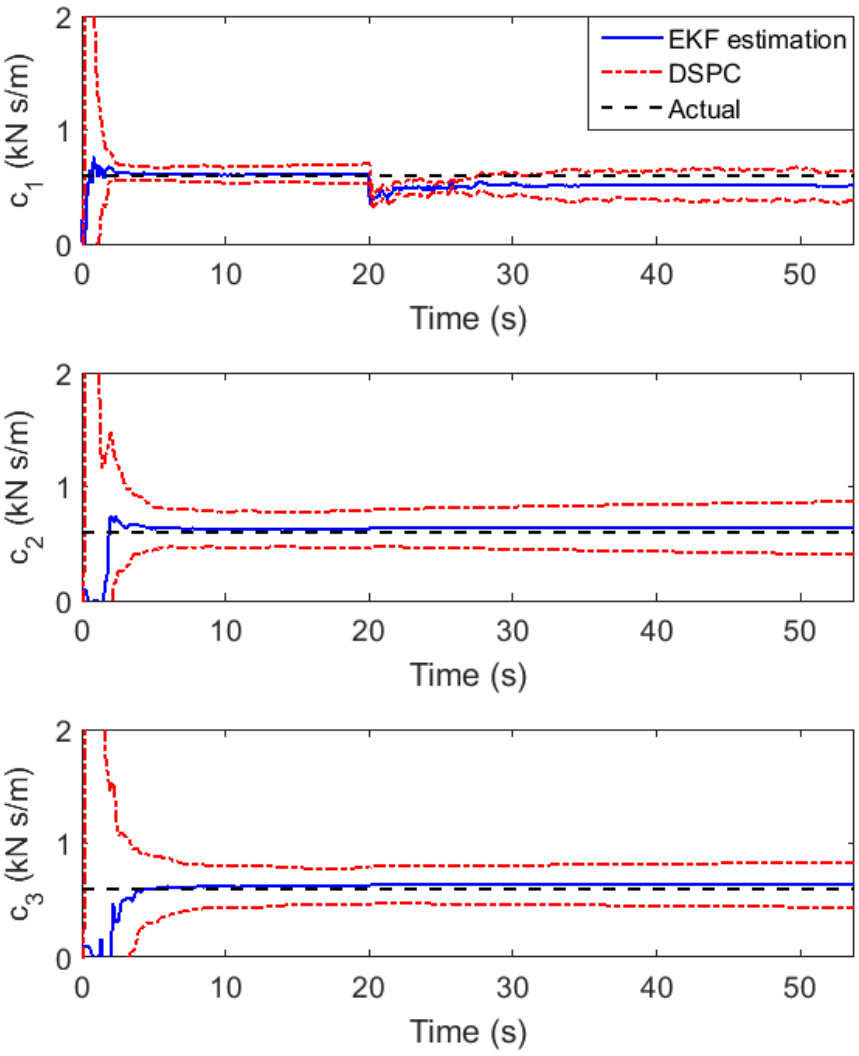

Figure 5.8 Performance of EKF-DSPC for damping parameters in Case 1

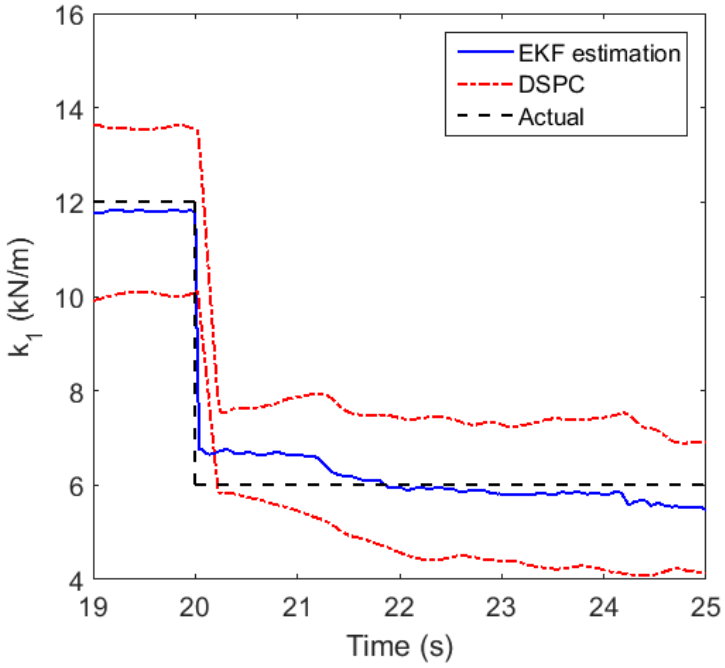

Figure 5.9 Performance of EKF-DSPC method for k_1 in Case 1

Case 2: Parameters k_1 and c_1 are reduced abruptly at t = 20 s, from 12 to 6 kN/m and 0.6 to 0.4 kN s/m, respectively. Parameter estimation for all stiffness and damping parameters identified by EKF-DSPC are presented in Figure 5.10 and 5.11. And the details of damage detection for k_1 and c_1 during 19 to 25 s are presented in Figure 5.12 and 5.13. The EKF estimation of both k_1 and c_1 jump outside of the DSPC ranges at t = 20 s, thus simultaneous damage on both stiffness and damping in linear structure are also detected by EKF-DSPC method successfully.

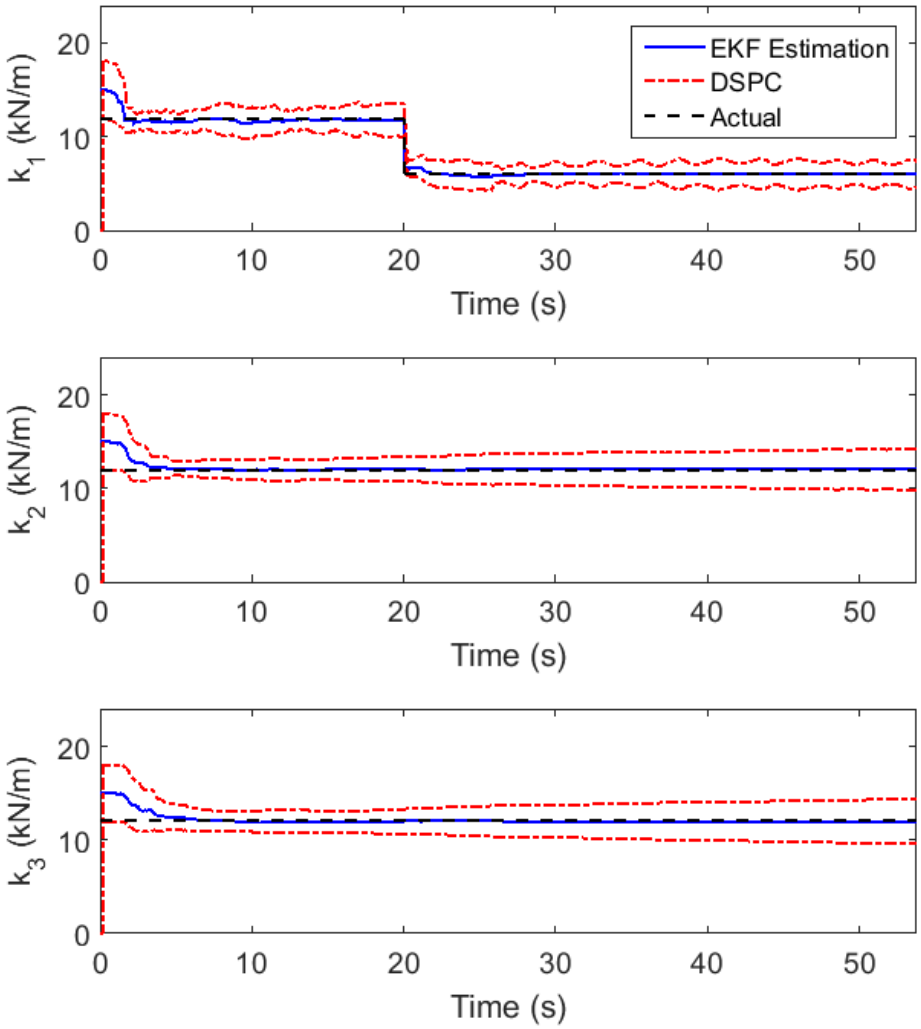

Figure 5.10 Performance of EKF-DSPC for stiffness parameters in Case 2

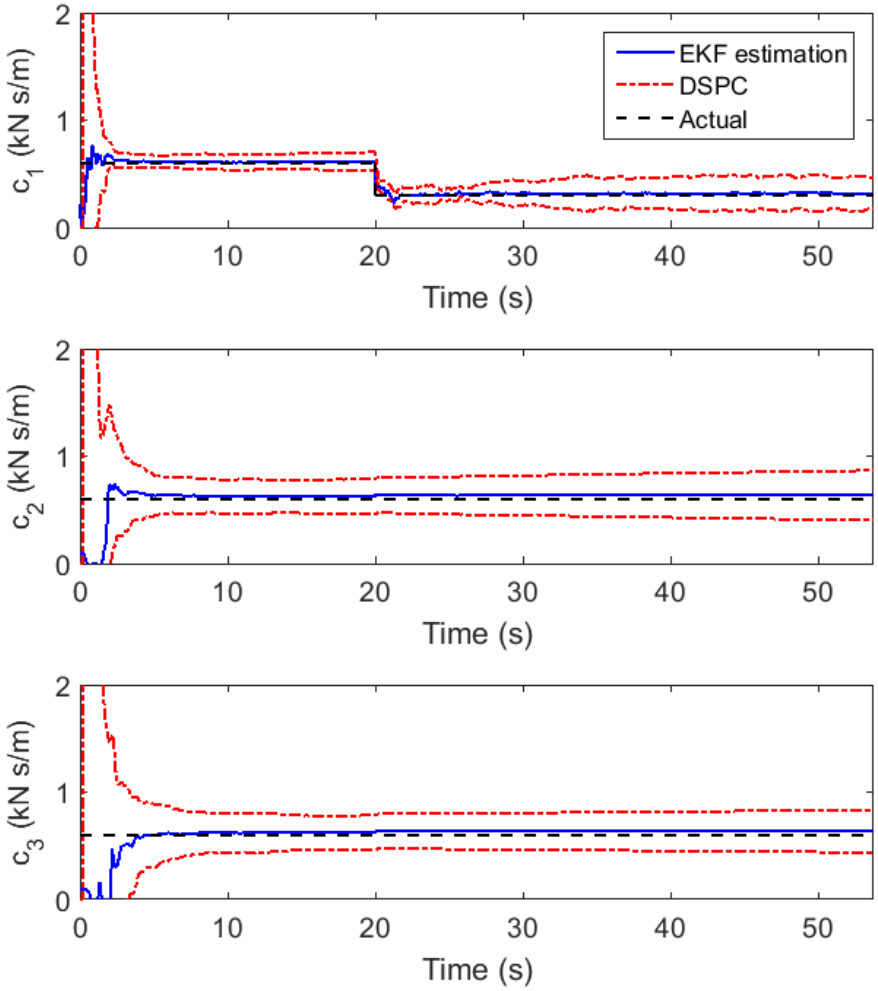

Figure 5.11 Performance of EKF-DSPC for damping parameters in Case 2

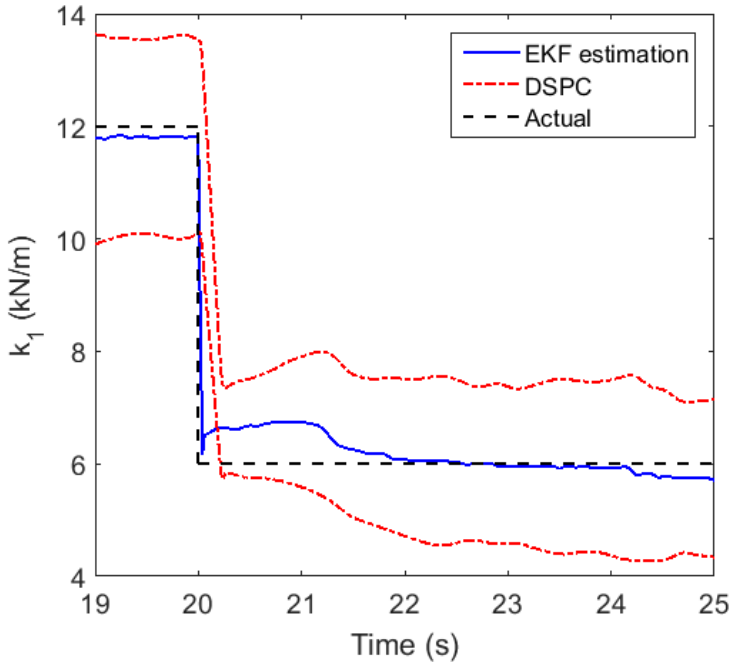

Figure 5.12 Performance of EKF-DSPC method for k_1 in Case 2

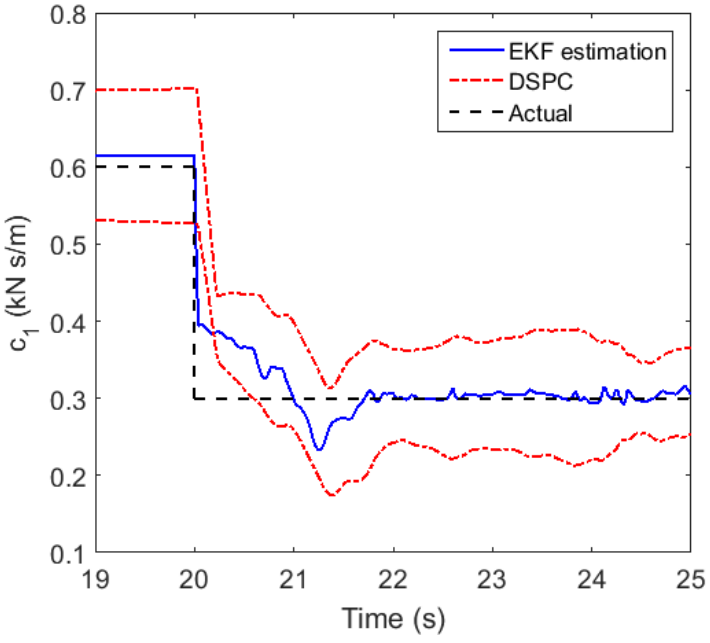

Figure 5.13 Performance of EKF-DSPC method for c_1 in Case 2

5.4.2 Two-story nonlinear hysteretic structure

Civil structures generally exhibit nonlinear hysteretic behavior under damage events. A numerical study is performed to validate the performance of the EKF-DSPC based damage detection method for a nonlinear hysteretic model. The goal is to estimate the structure's parameters and identify the damage by considering the hysteretic behavior exhibited by the structure during an earthquake.

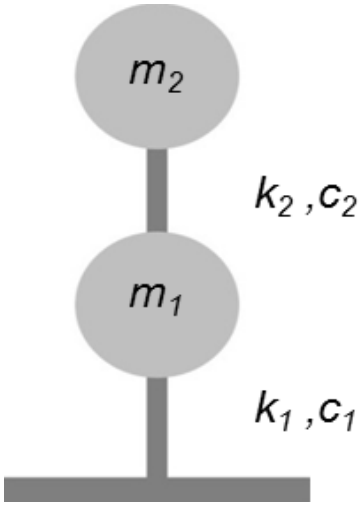

Figure 5.14 Two story nonlinear hysteretic structure

Consider a two-story nonlinear hysteretic building structure (as shown in Figure 5.14), which can be represented by the equations of motion as described in,

$$\begin{bmatrix} m_1 & 0 \\ 0 & m_2 \end{bmatrix}\begin{bmatrix} \ddot{x}_1 \\ \ddot{x}_2 \end{bmatrix}+\begin{bmatrix} c_1+c_2 & -c_2 \\ -c_2 & c_2 \end{bmatrix}\begin{bmatrix} \dot{x}_1 \\ \dot{x}_2 \end{bmatrix}+\begin{bmatrix} k_1+k_2 & -k_2 \\ -k_2 & k_2 \end{bmatrix}\begin{bmatrix} z_1 \\ z_2 \end{bmatrix}=-\begin{bmatrix} m_1 \\ m_2 \end{bmatrix}\ddot{x}_0, \tag{5.35}$$

in which z_1 and z_2 are the hysteretic components defined by Bouc-Wen model (Bouc, 1967; Wen, 1976, 1989) as,

$$\dot{z}_i = \dot{x}_i - \beta_i|\dot{x}_i||z_i|^{\alpha-1} z_i - \gamma_i \dot{x}_i |z_i|^{\alpha} \quad (i = 1, 2), \tag{5.36}$$

where the mass coefficients $m_1 = m_2 = 1$ kg, the stiffness coefficients $k_1 = k_2 = 15$ kN/m, damping coefficients $c_1 = c_2 = 1$ kN s/m. For the hysteretic parameters, the abruptness parameter $\alpha = 2$, hysteric loop fatness parameter $\beta_1 = \beta_2 = 2$, and loop pinching parameters $\gamma_1 = \gamma_2 = 1$.

The El Centro Earthquake with peak ground acceleration (PGA) equals to 5g is used as the ground excitation in the numerical testing. The sampling time is 40 seconds, and the sampling frequency is 100 Hz for all measured signals. The fourth order Runge-Kutta method (Jameson *et al.* 1981) is used to implement the analytical solution to obtain the dynamic responses of the nonlinear hysteretic structure. The measurements of absolute acceleration of each floor $\ddot{x}_1$, $\ddot{x}_2$ and the ground excitation $\ddot{x}_0$ will be used in the EKF-DSPC method to perform system identification and damage detection. The unknown parameters to be identified are stiffness k_i, damping c_i, restoring force z_i and hysteretic parameters β_i and γ_i ($i = 1, 2$). These unknown parameters are appended to the state vector to form the new state vector as,

$$x = \left[x_1; x_2; \dot{x}_1; \dot{x}_2; z_1; z_2; k_1; k_2; c_1; c_2; \beta_1; \beta_2; \gamma_1; \gamma_2\right]^T. \tag{5.37}$$

The initial values for parameters in EKF are defined as follows. The initial values for stiffness k_i and damping c_i are $k_{i0} = 20$ kN/m and $c_{i0} = 0.5$ kN s/m ($i = 1, 2$), the initial values for hysteretic parameters β_i and γ_i are $\beta_{i0} = 1.5$ and $\gamma_{i0} = 0.5$ ($i = 1, 2$). And the initial values for displacement x_i, velocity $\dot{x}_i$ and restoring force z_i are zero, i.e., $x_{i0} = 0$, $\dot{x}_{i0} = 0$ and $Z_{i0} = 0$ ($i = 1, 2$). Thus the initial state vector is defined as [0; 0; 0; 0; 0; 0; 20; 20; 0.5; 0.5; 1.5; 1.5; 0.5; 0.5]^T. The initial error covariance matrix of the extended state vector is a 14×14 diagonal matrix $P_0 = \text{diag}\{1; 1; 1; 1; 1; 1; 10^5; 10^5; 10^5; 10^5; 10^5; 10^5; 10^5; 10^5\}$. The covariance matrix of the process noise w_k is selected as $Q_0 = 10^{-6}\text{diag}\{1; 1; 1; 1; 1; 1; 10^2; 10^2; 1; 1; 1; 1; 1; 1\}$. The covariance matrix of the measurement noise v_k is selected as $R_0 = 10^{-6}\mathbf{I}_2$. In all testing cases of the two-story nonlinear hysteretic structure, the same above initial parameters will be used.

Before any structural damage is introduced, the EFK estimation for all state variables for the nonlinear structure are obtained, and verified by comparing with analytical solutions. The comparison of hysteresis loops (relative displacement versus restoring force) between EKF estimation and analytical solution for two floors are presented in Figure 5.15 and 5.16. The comparison of time history of hysteretic component z

between EKF estimation and analytical solution for each floor are presented in Figure 5.17 and 5.18. Moreover, the EKF estimations for four structural parameters for each floor are presented in Figure 5.19 and 5.20. In the two figures, the curves of EKF estimation all coincide with the curves of exact values, which indicate the accuracy of EKF to be used for parameter estimation for nonlinear structures.

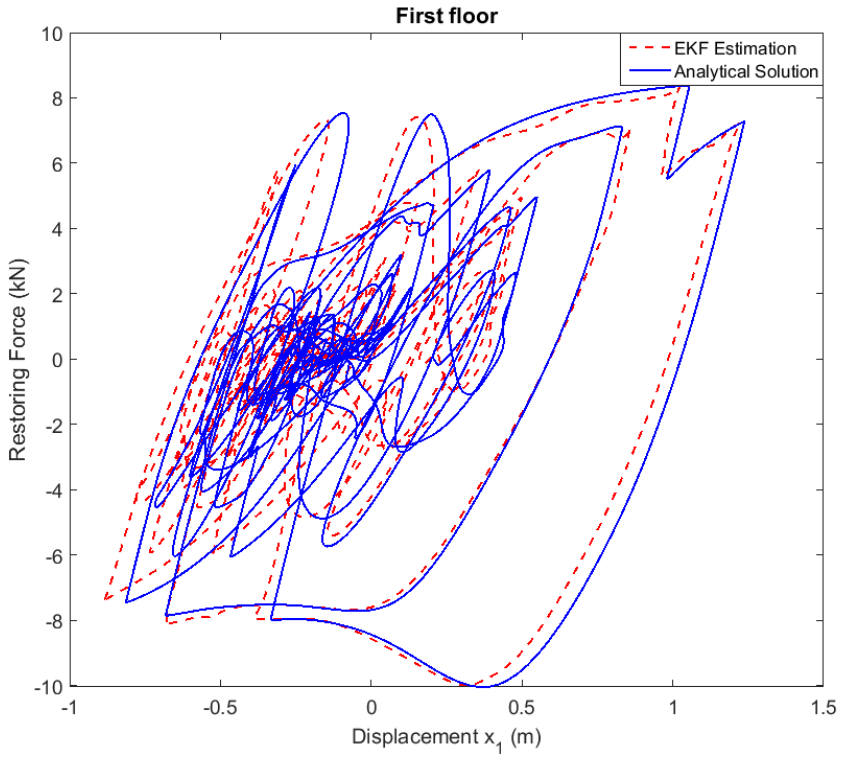

Figure 5.15 Comparison of hysteresis loops between EKF estimation and analytical solution for the first floor

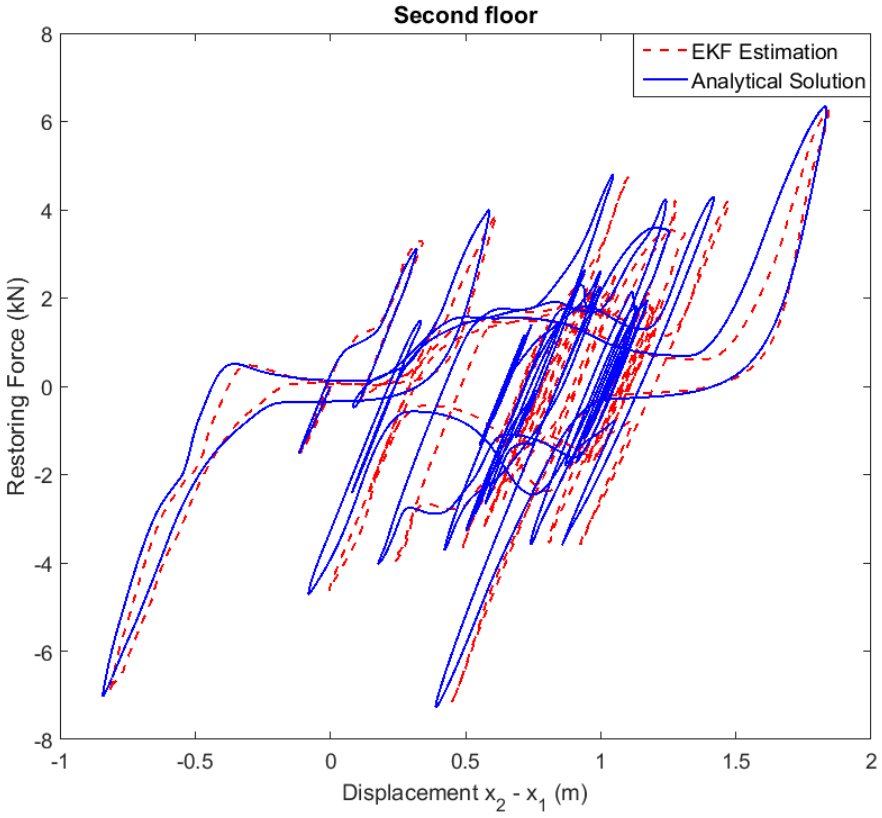

Figure 5.16 Comparison of hysteresis loops between EKF estimation and analytical solution for the second floor

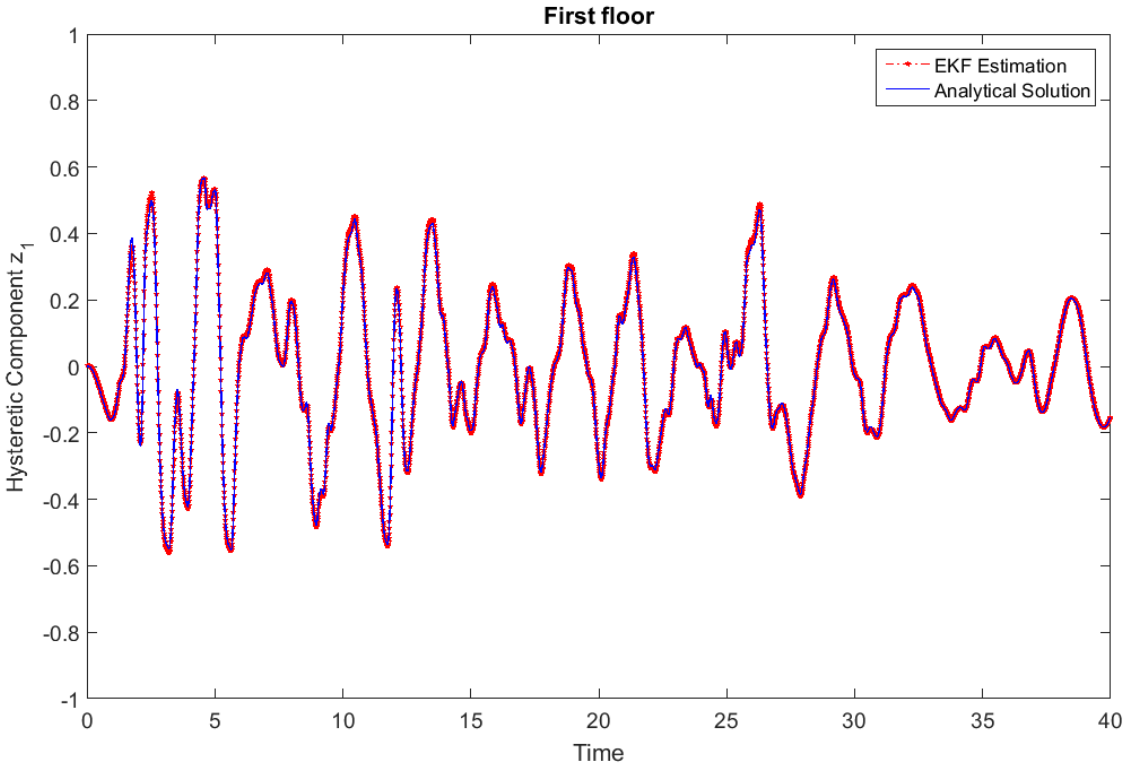

Figure 5.17 Comparison of hysteretic component z_1 time history between EKF estimation and analytical solution for the first floor

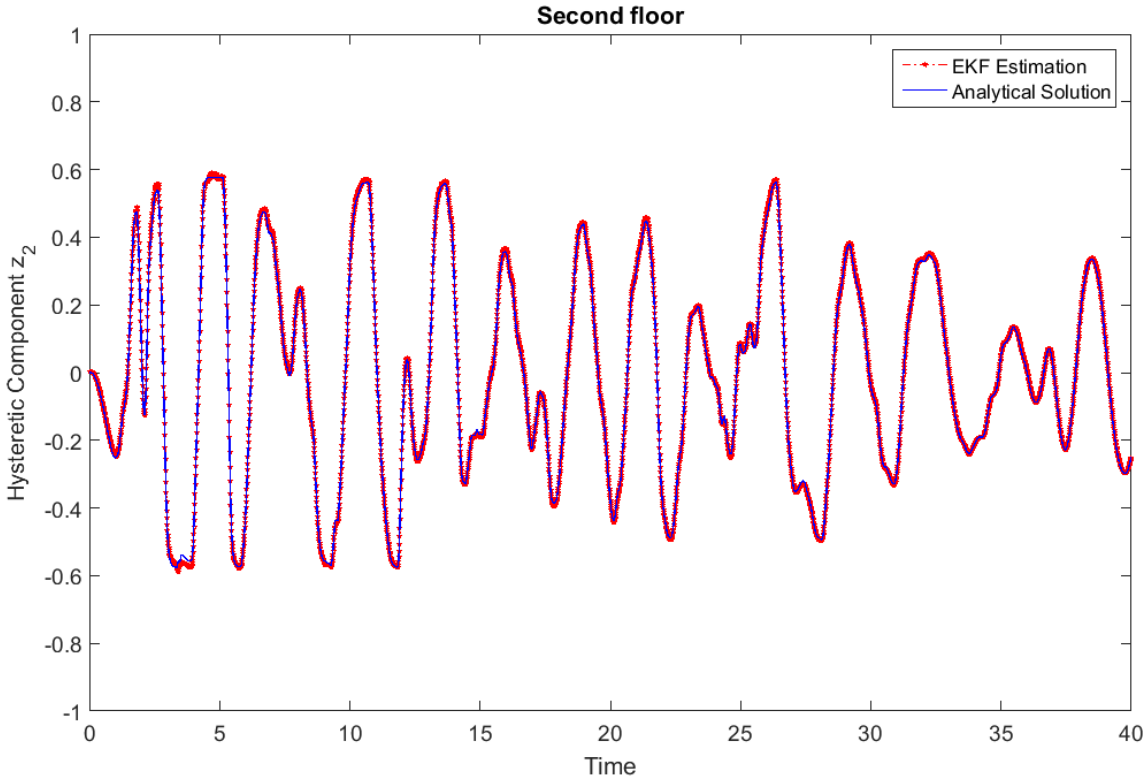

Figure 5.18 Comparison of hysteretic component z_2 time history between EKF estimation and analytical solution for the second floor

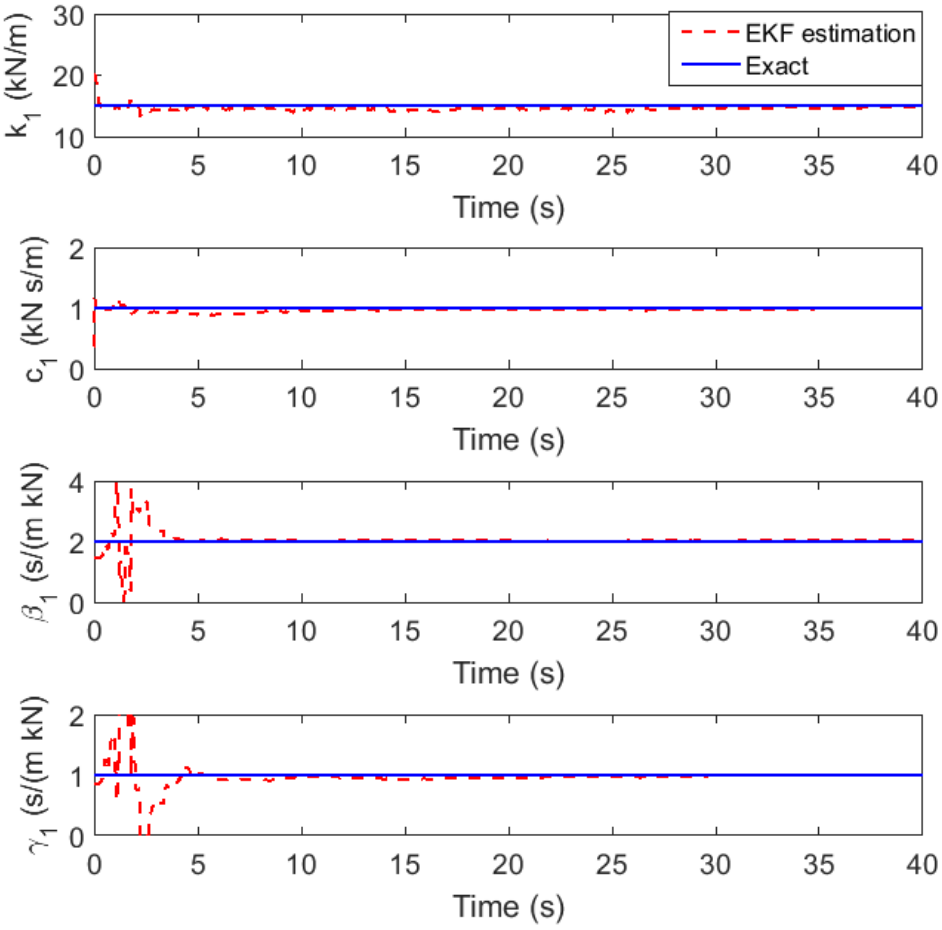

Figure 5.19 Performance of EKF estimation for nonlinear hysteretic parameters in first floor

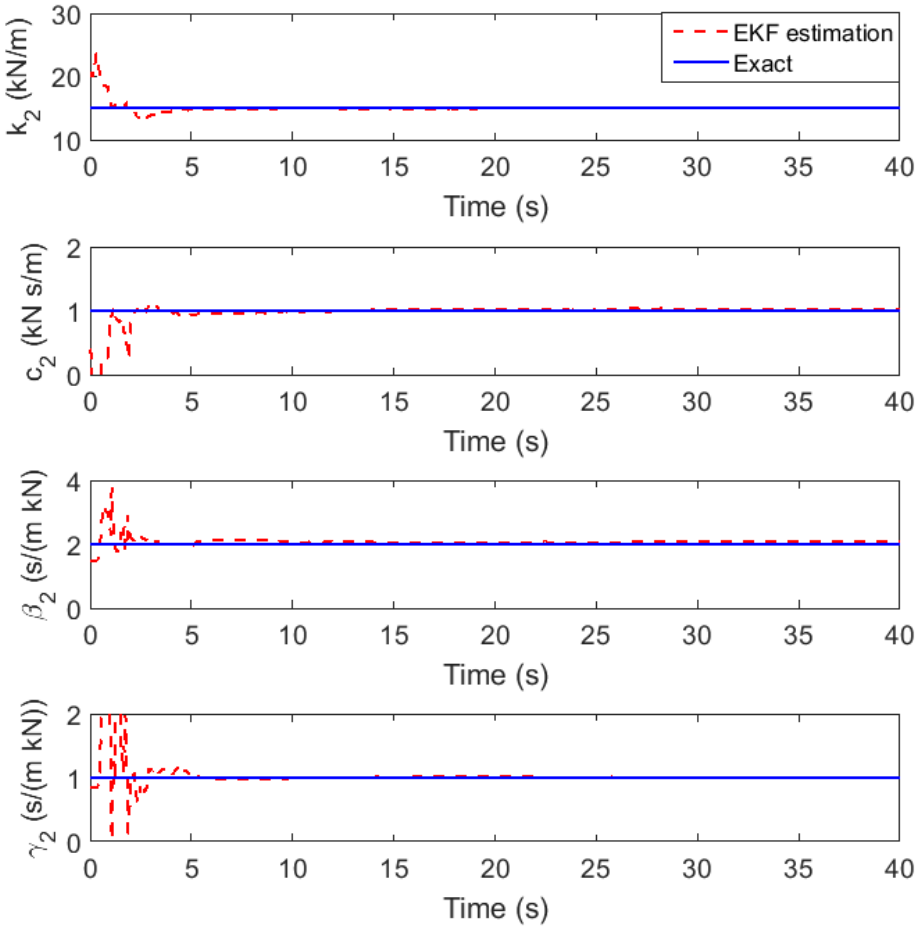

Figure 5.20 Performance of EKF estimation for nonlinear hysteretic parameters in second floor

Two structural damage scenarios are considered in the numerical validation for the nonlinear hysteretic structure: (1) damage only on structural stiffness; (2) damage on both stiffness and damping at the same time, as presented in following Case 3 and 4, respectively.

Case 3: k_1 is reduced abruptly from 15 to 10 kN/m at t = 20 s. The parameter estimation and damage detection performance based on EKF-DSPC method is depicted in Figure 5.21 and 5.22. And the details of damage detection for k_1 during 18 to 23 s are presented in Figure 5.23. The EKF estimation of k_1 jump outside of the DSPC ranges at t = 20 s, thus the damage on stiffness in nonlinear structure is also detected by EKF-DSPC method successfully.

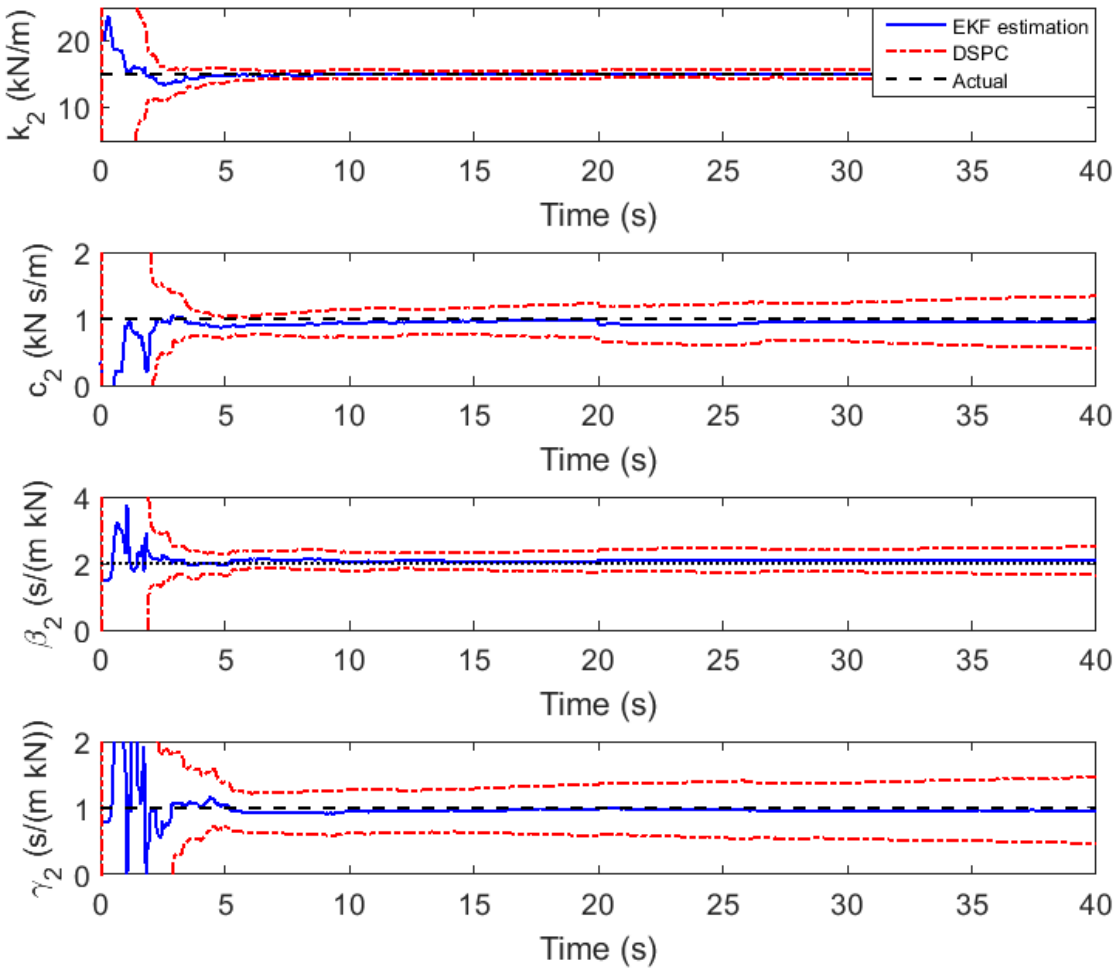

Figure 5.21 Performance of EKF-DSPC for first floor in Case 3

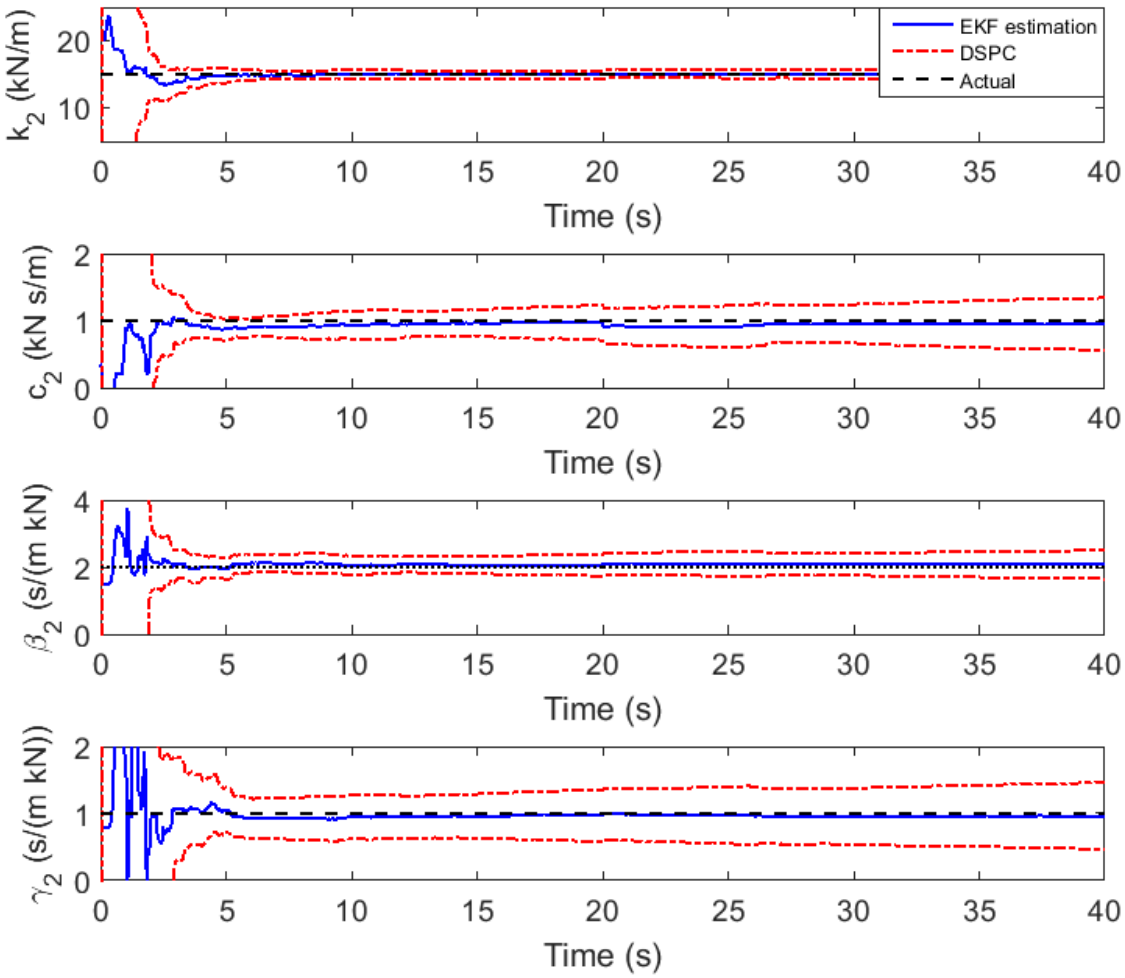

Figure 5.22 Performance of EKF-DSPC for second floor in Case 3

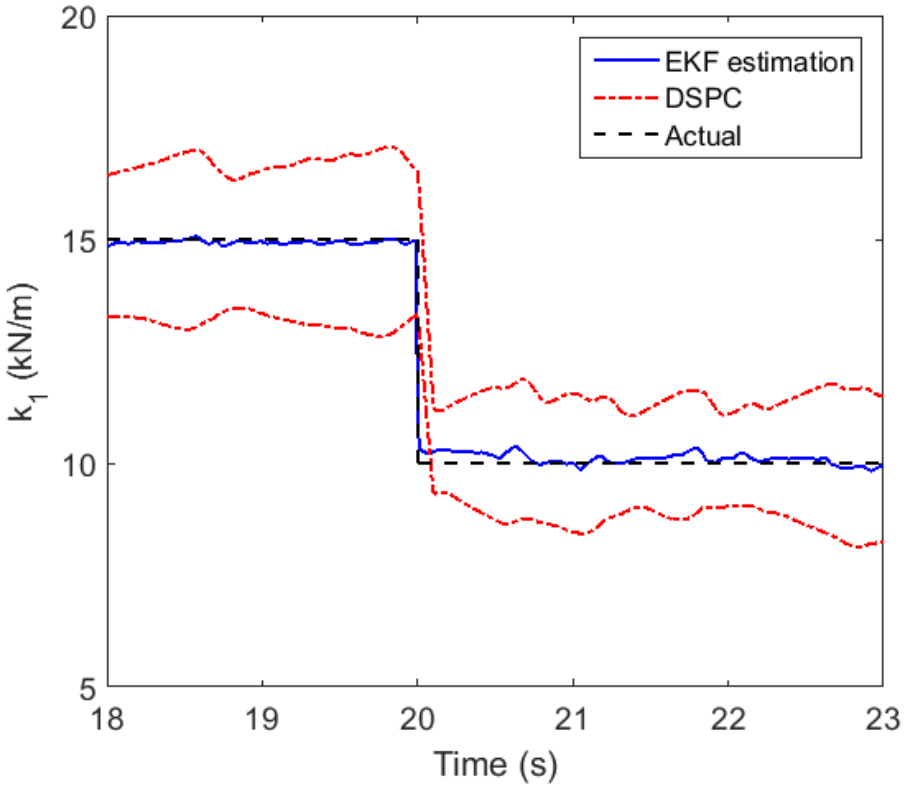

Figure 5.23 Performance of EKF-DSPC method for k_1 in Case 3

Case 4: Parameters k_1 and c_1 are reduced abruptly from 15 to 10 kN/m and 1 to 0.5 kN s/m at t = 20 s, respectively. Parameter estimation and the details of the damage detection by EKF-DSPC are presented in Figure 5.24 to 5.27. As can be observed, when the damage occurs on k_1 and c_1 concurrently at t = 20 s, the sudden drop of both parameters can be captured by EKF within rapid time. The effectiveness of DSPC is verified by the fact that at t = 20 s, only parameters k_1 and c_1 run out of the DSPC ranges while other parameters are still within the DSPC range.

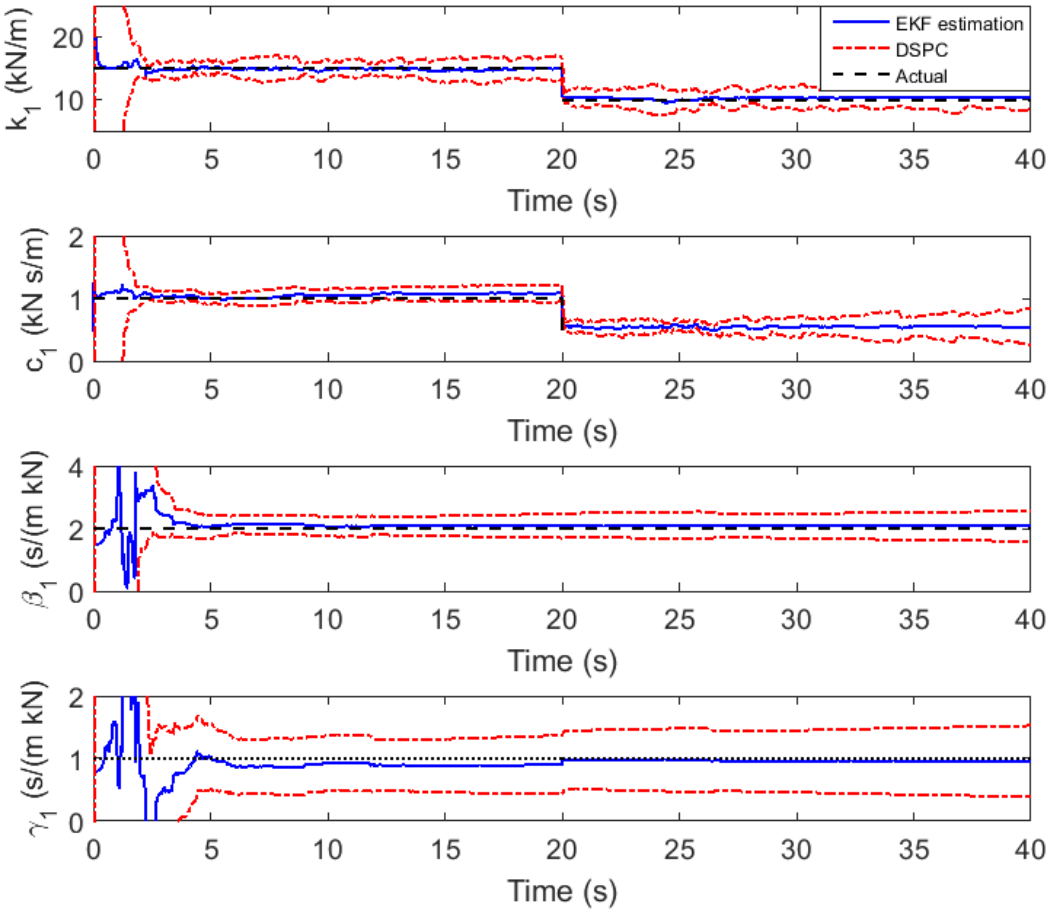

Figure 5.24 Performance of EKF-DSPC for first floor in Case 4

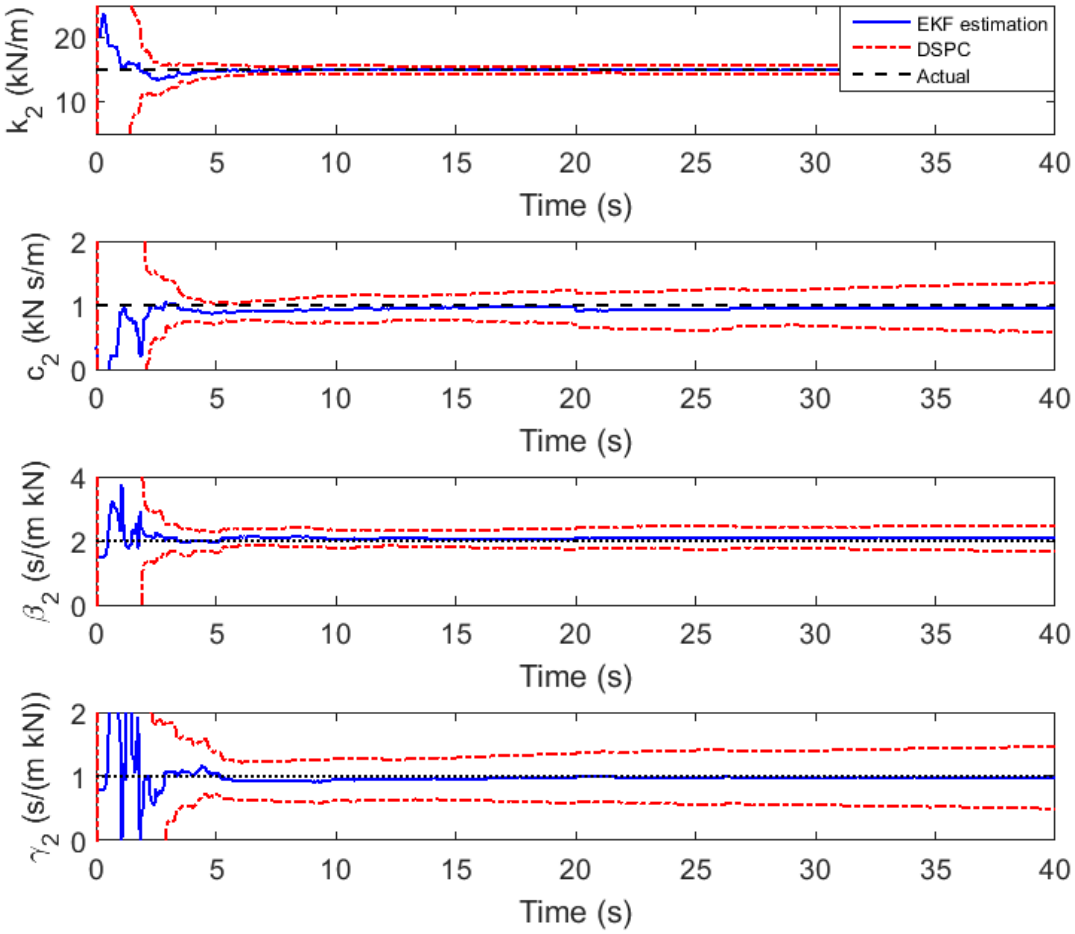

Figure 5.25 Performance of EKF-DSPC for second floor in Case 4

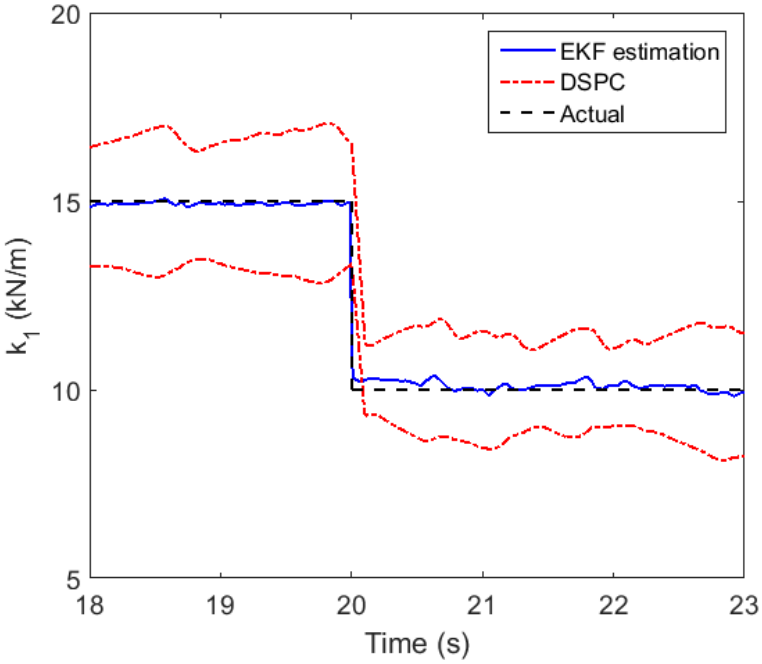

Figure 5.26 Performance of EKF-DSPC method for k_1 in Case 4

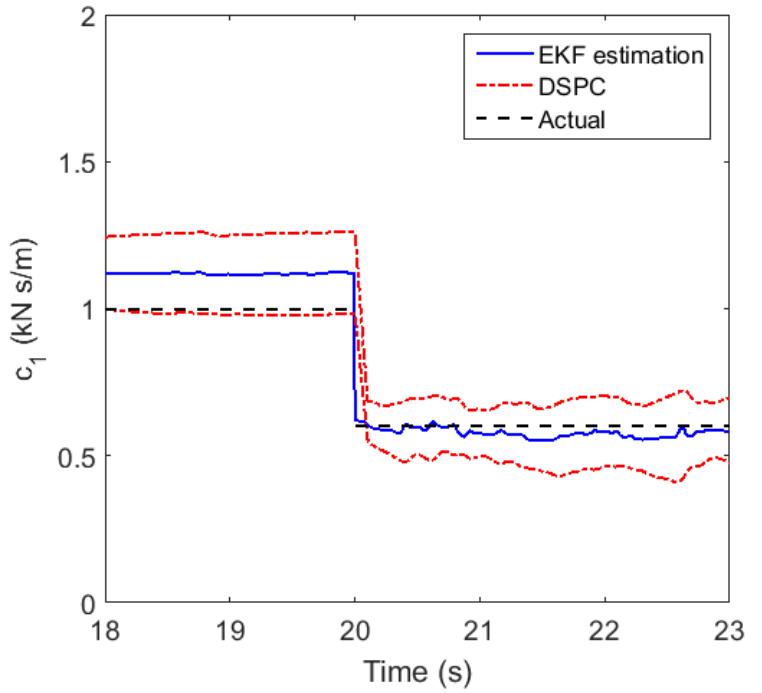

Figure 5.27 Performance of EKF-DSPC method for c_1 in Case 4

5.5 Summary

In this chapter, a real-time structural damage detection method for civil structures is developed based on the combination of EKF and DSPC. Based on measurements of damage-sensitive parameters involved in the state-space model of structural dynamic systems, the EKF algorithm produces real-time estimation means and standard deviations for the identified structural parameters to form the dynamic control limits to detect any abnormality in the selected parameters. The developed EKF-DSPC damage detection method is validated using simulation response data of a three-story linear structure and a two-story nonlinear hysteretic structure under earthquake excitation considering different damage scenarios, and the testing results demonstrate fast convergence rate, high damage detection accuracy and light computational costs. The EKF-DSPC method can be easily replicated in other structural damage detection problems for both linear and nonlinear structures. Moreover, since the EFK is a well-developed methodology that does not require large computation, and DPSC is capable to handle system variations caused by operational and environmental effects, the EKF-DSPC method has a good potential to be implemented in real-time SHM systems for in-service civil structures.

CHAPTER 6 REAL-TIME STRUCTURAL DAMAGE DETECTION FOR A HIGHWAY BRDIGE

(Part of this chapter has been published as Chenhao Jin, Shinae Jang, Xiaorong Sun, Jingcheng Li and Richard Christenson (2016) "Damage detection of a highway bridge under severe temperature changes using extended Kalman filter trained neural network", *Journal of Civil Structural Health Monitoring*, 6 (3), 545-560.)

6.1 Introduction

Detecting structural damage in civil engineering structures has become an increasingly viable option for efficient maintenance and management of infrastructures. Vibration-based damage detection methods have been widely used for structural health monitoring (SHM). However, those methods may not be effective when modal properties have significant variance under environmental effects, especially severe temperature changes. In this paper, an extended Kalman filter-based artificial neural network (EKFNN) method is developed to eliminate the temperature effects and detect damage for structures equipped with long-term monitoring systems. Based on the vibration acceleration and temperature data obtained from an in-service highway bridge located in Connecticut, United States, the correlations between natural frequencies and temperature are analyzed to select proper input variables for the neural network model. Weights of the neural network are estimated by extended Kalman filter, which is also used to derive the confidence intervals of the natural frequencies to detect the damage. A year-long monitoring data are fed into the developed neural network for the training purpose. In order to assess the changes of natural frequencies in real structural damages, structural damage scenarios are simulated in the finite element model. Numerical testing results show that the temperature-induced changes in natural frequencies have been considered prior to the establishment of the threshold in the damage warning system, and the simulated damages have been successfully captured. The advantages of EKFNN method are presented through

comparing with benchmark multiple linear regressions method, showing the potential of this method for structural health monitoring of highway bridge structures.

Detecting structural damage in civil engineering structures has become an increasingly viable option for efficient maintenance and management of infrastructures. Vibration-based damage detection methods have been widely used for structural health monitoring (SHM). However, those methods may not be effective when modal properties have significant variance under environmental effects, especially severe temperature changes. In this chapter, an extended Kalman filter-based artificial neural network (EKFNN) method is developed to eliminate the temperature effects and detect damage for structures equipped with long-term monitoring systems. Based on the vibration acceleration and temperature data obtained from an in-service highway bridge located in Connecticut, United States, the correlations between natural frequencies and temperature are analyzed to select proper input variables for the neural network model. Weights of the neural network are estimated by extended Kalman filter, which is also used to derive the confidence intervals of the natural frequencies to detect the damage. A year-long monitoring data are fed into the developed neural network for the training purpose. In order to assess the changes of natural frequencies in real structural damages, structural damage scenarios are simulated in the finite element model. Numerical testing results show that the temperature-induced changes in natural frequencies have been considered prior to the establishment of the threshold in the damage warning system, and the simulated damages have been successfully captured. The advantages of EKFNN method are presented through comparing with benchmark multiple linear regressions method, showing the potential of this method for structural health monitoring of highway bridge structures.

In reality, the modal parameters of civil structures are affected by many operational and environmental factors including temperature, traffic loading, wind speed, etc. Among these factors, temperature is the dominant factor affecting the modal parameters of the bridge under normal condition. From long-term monitoring data, the temperature effect on modal properties of structures has been intensively investigated (Xia *et al.*, 2012; Liu and Dewolf, 2007; Sohn, 2007; Soyoz and Feng, 2009; Cao *et al.*, 2011). For example, the natural frequencies of Alamosa Canyon Bridge were discovered to vary 5% during a 24-hour period

(Cornwell *et al.*, 1999), and the natural frequencies of Z-24 Bridge were found to fluctuate 14%-18% in one-year period (Peeters and Roeck, 2001). The freezing effect is also found on the relationship between natural frequencies and temperature when the temperature is below freezing point (0ºC or 32ºF) (Gonzales *et al.*, 2013; Li, 2014). If the temperature effect is not considered and eliminated in structural damage detection, false alarm problems may arise and thus limit the application of structural health monitoring in in-service structures. It is critical to study the influence of temperature effect on modal parameters for in-service bridges through long-term monitoring, and develop effective structural damage detection method which can eliminate the temperature effect and detect structural damage for in-service structures under normal operations.

To reach this goal, several methods have been developed, including statistical regression models and artificial neural networks. Linear regression model assumes a linear function to describe relationships between modal parameter and affecting factors. The coefficients of the function are estimated based on historical data, and the adequacy of the model is then verified by analyzing model residuals. Peeters presented a dynamic linear regression analysis method based on an Autoregressive and Exogenous model to filter out temperature effects on natural frequencies for the Z-24 Bridge (Peeters *et al.*, 2001). Ding and Li presented a polynomial regression model to fit frequency-temperature relations for Runyang Suspension Bridge (Ding and Li, 2001). However, the disadvantage of regression analysis is that many real-world phenomena are not simply represented as a single equation with sure estimators, especially when the regression functions do not contain all potential independent variables.

Artificial neural networks (NNs) have been widely used in structural damage detection because of their strong capability to approximate the nonlinear functions between inputs and outputs through learning from historical data. Sohn *et al.* developed an auto-associative neural network (AANN)-based method considering environmental and operational conditions for structural damage detection, which selected linear regression model parameters as input and output (Sohn *et al.*, 2002). Zhou *et al.* developed a back propagation neural network (BPNN)-based approach which picked normalized modal frequency as input, and generated novelty index as output to detect damage (Zhou *et al.*, 2010 2011). Xu *et al.* used BPNN-

based approach to predict damage magnitude based on modal energy-based damage index for Crowchild Bridge (Xu and Humar, 2006). Mata developed a neural network model which picked environmental factors as input and displacement as output to analyze behavior for a concrete dam (Mata, 2011). These papers focused on the estimation of the relationship between environmental factors and modal properties, and shared insights on input parameters selection for neural network models. However, based on the authors' best knowledge, none of them used the historical data to predict the natural frequency. Moreover, using AANN or BPNN might suffer from slow convergence in view of the nature of first order learning algorithm. In addition, the confidence intervals of the predictions were not given, which means the quality of damage detection was hard to evaluate.

To overcome the above difficulties, a neural network model trained by extended Kalman filter (EKFNN) for structural damage detection is developed in this chapter. The uniqueness of EKFNN include: (1) chooses time-lagged natural frequencies and temperature values are key inputs to predict the natural frequency in the next time step; (2) uses extended Kalman filter to train the neural network which converges faster and provides better solutions as compared with traditional widely used back prorogation algorithm; (3) provides high confidence levels for the predictions through extend Kalman filter training process. The main structure of this paper is presented as follows. In Section 6.2, in order to select independent input variables in the damage detection model, the correlation analysis for natural frequency and temperature are performed based on one-year measurement data. In Section 6.3, the methodology utilizing extended Kalman filter to train the weights of artificial neural network model is presented. To obtain the simulated natural frequencies data for damaged structure, the natural frequency reduction ratios under two common structural damage scenarios are simulated in finite element analysis in Section 6.4. In the numerical testing in Section 6.5, the monitoring data are used for training and validation, and the simulation damage data are applied for testing to validate whether the damage can be captured. In Section 6.6, the advantages of EKFNN method are presented by comparing with the benchmark approach based on multiple linear regressions.

6.2 Temperature effects on natural frequencies

The vibration and temperature data measured from Meriden Bridge during March 2013 to May 2014 were used for this research. In total, 4177 sets of five-minute hourly data files were measured. Though the measurement was interrupted occasionally due to power outage on bridge sites, the recorded measurement covered all 4 seasons with a full range of temperatures, which are sufficient for statistical analysis of the temperature effects on natural frequencies, training and testing the artificial neural network model for damage detection purposes. To select proper input variables for the neural network model, long-term monitoring data have been analyzed to set up a statistical model of natural frequencies under temperature changes in section 6.2.1. Based on the correlation analysis results of target variables, input variables for neural network model are selected in 6.2.2.

6.2.1 Freezing effects on natural frequencies

The long-term temperature trend depicted in Figure 6.1 illustrates the significant temperature change in New England region, recording the highest of 94.57 °F (34.76 °C) in August 2013 and the lowest of 3.52 °F (-15.82 °C) in February 2014. The natural frequencies of the first seven modes for Meriden Bridge were calculated and plotted in Figure 6.2, which shows that all seven natural frequencies have the same tendency to decrease in the summer from June to August 2013, and increase in the winter from December 2013 to February 2014. The measured temperature data have large fluctuations during December 2013 to March 2014 because of severe weather conditions, which also provides abundant data sets to study the correlation between natural frequencies and temperatures.

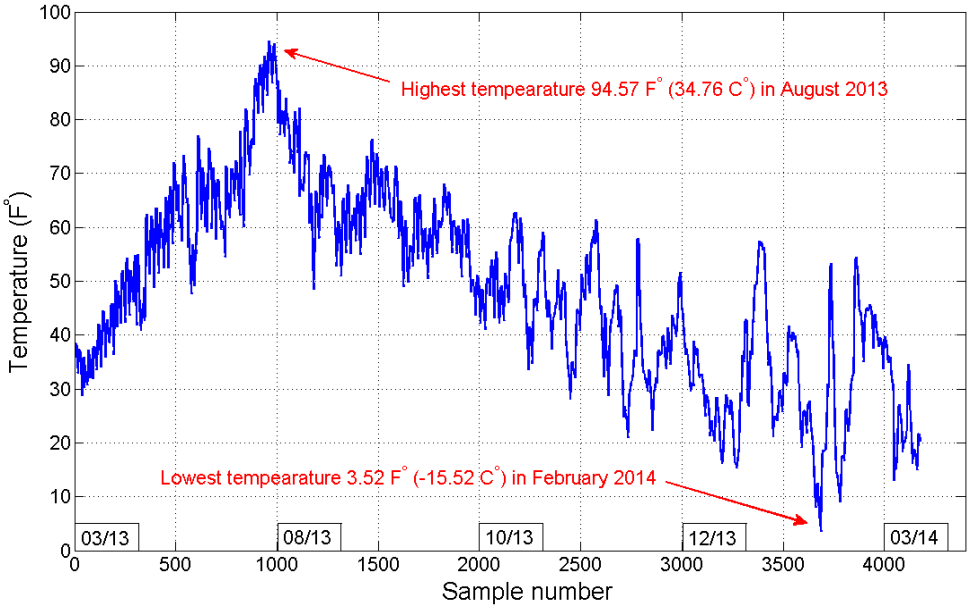

Figure 6.1 Measured temperatures from the bridge sensors during the collection period

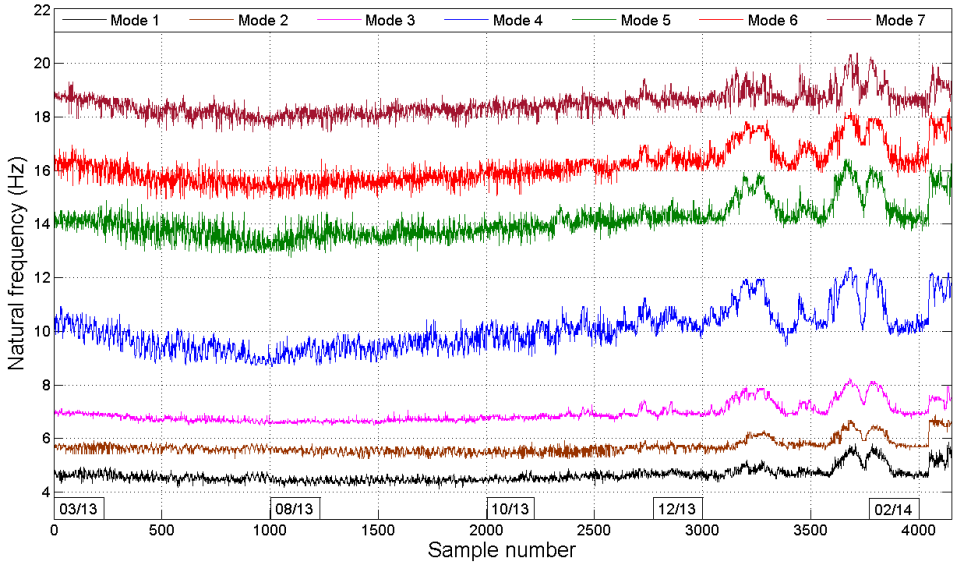

Figure 6.2 First seven natural frequencies during the collection period

In order to study the temperature effects on natural frequencies, the relationships between frequencies and temperatures for the first seven modes are plotted in Figure 6.3. Negative correlations between

temperature and the natural frequencies are clearly observed, i.e., the natural frequencies decrease when temperature increases, and vice versa. In addition, the freezing effect can be observed that the changes in the natural frequencies are more sensitive to temperatures below freezing point (32ºF, 0ºC) than above. This phenomenon is mainly resulted from three reasons: first, the stiffness of concrete and steel increases when temperature decreases; Secondly, the freezing of accumulated dust and moisture adds fixity at the girder support; thirdly, the asphalt surface layer of the deck becomes very stiffness below freezing point (Sohn, 2007). Considering the differences in temperature-natural frequency correlations below and above freezing point, both bi-linear and quadratic regression models were used to approximate the temperature-natural frequency relationship (Li, 2014). Thus, the freezing effect on natural frequencies is a significant factor, which must be considered in the damage detection for bridge structures under severe temperature changes. Therefore, a season index indicating the temperature status above or below the freezing point is included as an input factor of the NN model.

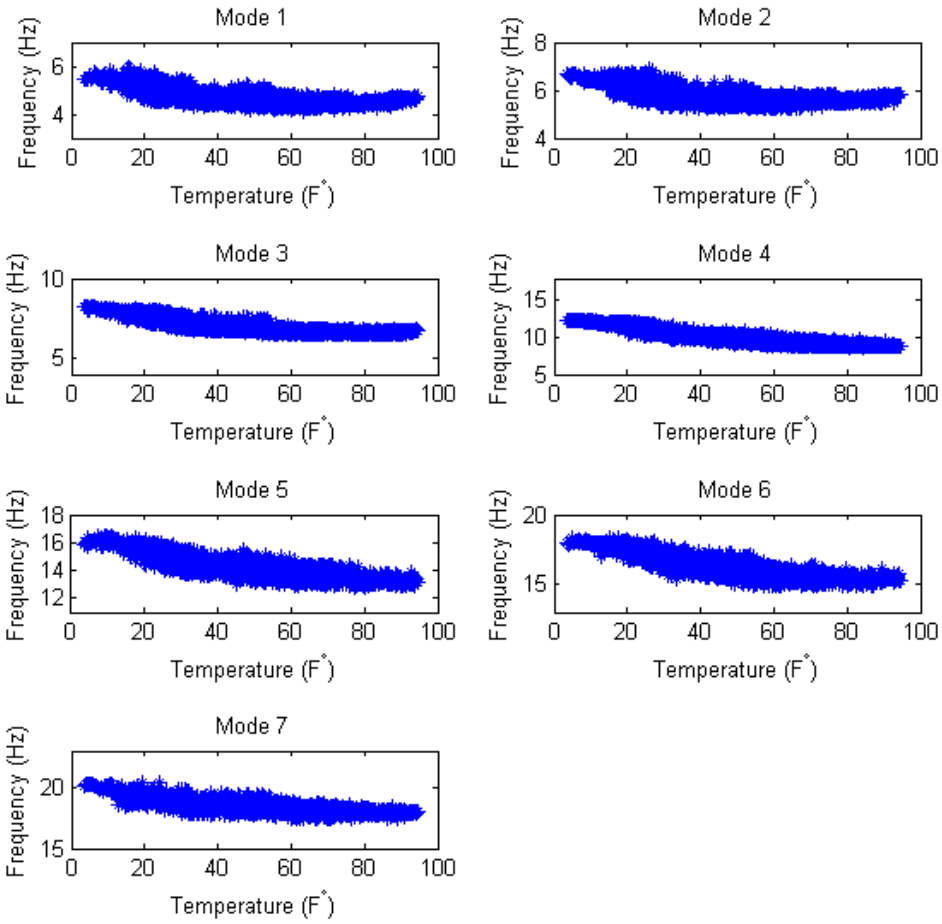

Figure 6.3 Seven identified natural frequencies versus temperature (Li, 2014)

6.2.2 Input parameter selection using auto and cross-correlations

Typically, more temperature and natural frequencies data could achieve a more accurate damage detection result. However, more input variables could result in adding computational complexity. Therefore, the optimal number of input parameters to be fed into NNs should be carefully determined. To reach this goal, the auto-correlation of the natural frequency and the cross-correlation between the natural frequency and temperature are investigated. Since all seven natural frequencies have similar features with the temperature changes, for simplicity, only the first natural frequency is used to develop the NN model for damage detection in this paper.

The auto-correlation function (ACF) of the natural frequency can evaluate the linear predictability or linear relationship of a time series by its own time lags as:

$$\rho_f(k) = \frac{\sum_{i=1}^{N-k}(f_i - \bar{f})(f_{i+k} - \bar{f})}{\sum_{i=1}^{N}(f_i - \bar{f})^2}, \tag{6.1}$$

where f_i is the natural frequency at time i, N is the number of samples, k is the time lag, and $\rho_f(k)$ is the ACF coefficient of $\{f_i\}$ at lag k. The plot of ACF coefficients for the first natural frequency with time lag from 0 to 10 hours is shown in Figure 6.4. When the time lag is equal to zero, ACF equals to 1 because it is the correlation with its own. The ACFs for other time lags are lower than 1 and decreasing as the time lag increases. Although the ACF coefficient decreases slightly as the time-lag value increases, the ACF coefficients between t-th natural frequency (f_t) and the lagged natural frequency by k-th hours (f_{t-k}) are very high (> 0.8). In time series analysis, the most correlated lagged points are used to predict the value in the next time step. Three time-lagged natural frequency and temperature data are chosen as inputs for neural network because these values all have high correlations with the prediction point, i.e. using f_{t-1}, f_{t-2} and f_{t-3} to estimate f_t. Another advantage of using limited input data is to reduce the complexity of neural network and simplify the calculation process.

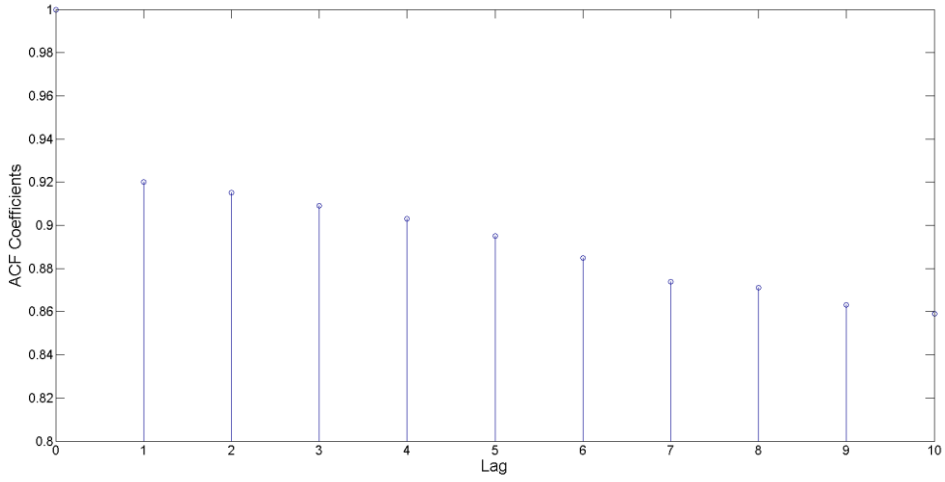

Figure 6.4 Auto-correlation coefficient of the first natural frequency against time lag

Similar to ACF, the cross-correlation function (CCF) measures the similarity between two time-series as a function of the time lag of one series relative to the other series. The CCF coefficients between natural frequency and temperature are calculated by Equation 6.2:

$$\rho_{f,T}(k) = \frac{\sum_{i=1}^{N-k}(T_i - \bar{T})(f_{i+k} - \bar{f})}{\sqrt{\sum_{i=1}^{N}(T_i - \bar{T})\sum_{i=1}^{N}(f_i - \bar{f})}}, \tag{6.2}$$

where f_i is the natural frequency at time i, T_i is the temperature at time i, N is the number of samples, k is the time lag, and $\rho_{f,T}(k)$ is the CCF coefficient of $\{f_i\}$ and $\{T_i\}$ at lag k. As can be seen from Figure 6.5, the negative correlation coefficients between the natural frequency and temperature at time lags have consistent negative values. To keep simplicity and be consistent with ACF, the identical number of the time-lag value, 3, has been selected for the temperature factor in the model, i.e., using T_{t-1}, T_{t-2}, T_{t-3} to predict f_t.

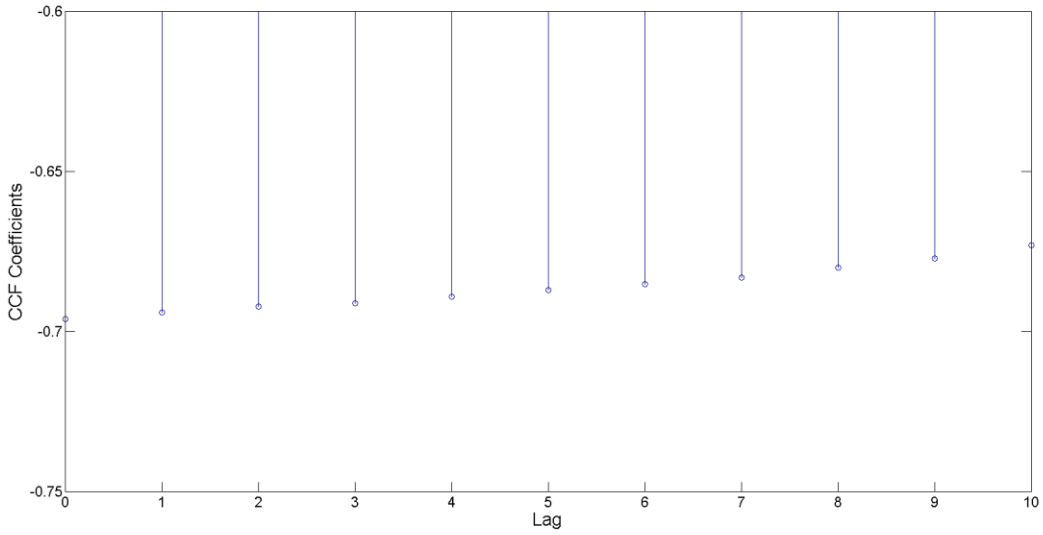

Figure 6.5 Cross-correlation coefficients between the first natural frequency and temperature against time lag

6.3 Extended Kalman filter-based artificial neural network (EKFNN)

6.3.1 Neural network model

Neural networks (NNs), as statistical learning models imitating biological neural networks, have been widely used in real practice because of their strong capability to approximate the nonlinear functions between input and output through learning a large number of samples. The basis of a neuron model (two-layer network) is shown in Figure 6.6. An artificial neuron is a unit which can achieve its unique learning process by performing simple mathematical operations on its inputs. Equations 6.3 and 6.4 are the main steps for calculation of a neuron model:

$$v_k = \sum_{j=1}^{m} x_j w_{kj} + b_k \,, \tag{6.3}$$

$$y_k = f(v_k) \,. \tag{6.4}$$

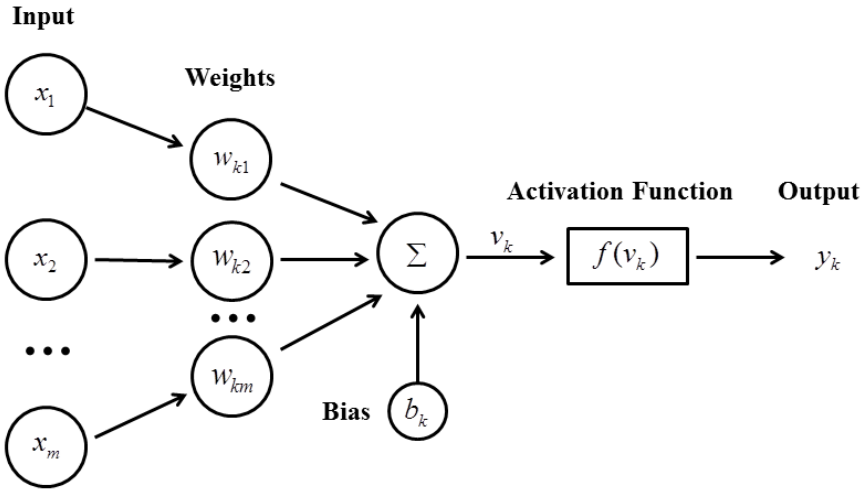

Figure 6.6 Neuron model

In this project, the NN structure is represented by a feed-forward three-layer perceptron as shown in Figure 6.7. The inputs are fed into the input layer, got multiplied by interconnection weights, and then passed from the input layer to the hidden layer. Within the hidden layer, the data obtained from previous step are summed and then processed by a nonlinear activation function (usually the hyperbolic tangent).

Finally, the data are multiplied by interconnection weights, and processed within the output layer to produce the neural network output.

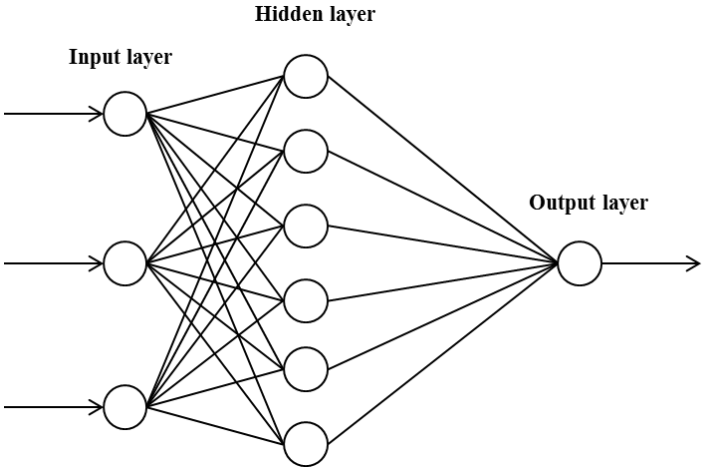

Figure 6.7 Structure of ANN with one hidden layer

Based on the temperature effects on natural frequencies discussed in the previous section, the input-output schematic of the artificial neural network model is depicted as shown in Figure 6.8. The time-lagged natural frequencies (f_{t-1}, f_{t-2}, f_{t-3}), time-lagged temperature (T_{t-1}, T_{t-2}, T_{t-3}), and season index are selected as the inputs of NNs to predict the natural frequency at the next time step. The season index is introduced as one binary input in the damage detection model to consider freezing effects, i.e., it equals to 1 when T_{t-1} is above the freezing point and 0 otherwise.

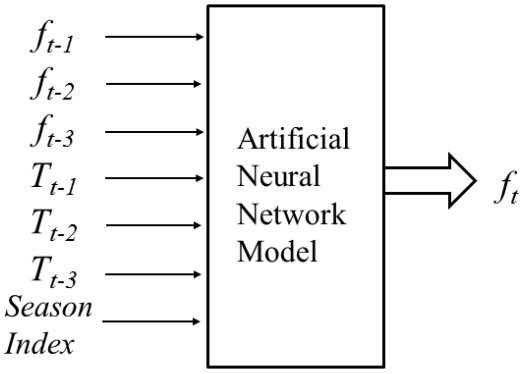

Figure 6.8 Input-output schematic of the artificial neural network

6.3.2 Extended Kalman filter for network model learning

The NN is trained by adjusting its weights (bias included) of the network using a set of input–output observations (u, y), where u is an input vector, and y is the corresponding output vector. After the NN is well trained, it predicts the output given any new inputs. The common training algorithm for NN is back propagation (BP), which looks for the minimum of the error function in weight space using the first-order steepest decent method. However, the traditional BP suffers from slow convergence, and may not be effective for predicting non-stationary processes like natural frequency. Extended Kalman filter, as a second-order algorithm, is a widely-developed method for recursive state estimation in nonlinear dynamic systems. Since NN learning procedure can be considered as a nonlinear estimation problem where the weights are to be estimated, EKF can then be used to train the NN by treating weights of the network as the state $w(t)$ of a nonlinear dynamic system. Moreover, EKF provides the estimation of state covariance matrix and innovation covariance matrix, which can be used to derive the confidence intervals of the predictions. Thus, the weights of the NN are estimated by EKF as described by state equation in Equation 6.5 and measurement equation in Equation 6.6:

$$w(t+1) = w(t) + \varepsilon(t), \tag{6.5}$$

$$y(t) = h(w(t), u(t)) + v(t), \tag{6.6}$$

where $\varepsilon(k)$ and $v(k)$ are the process noises and observation noises, respectively. The key steps of EKF in the NN weight training are summarized in Equation 6.7 to 6.12.

The time-update equations are defined as:

$$\hat{w}(k) = w(k), \tag{6.7}$$

$$\hat{y}(k) = h\left(\hat{w}(k), u(k)\right). \tag{6.8}$$

The measurement-update equations are defined as:

$$S(k+1) = H(k+1)P(t)H(k+1)^T + R(k+1), \tag{6.9}$$

$$K(k+1) = P(k)H(k+1)^T S(k+1)^{-1}, \tag{6.10}$$

$$P(k+1) = P(k) - K(k+1)H(k+1)P(k), \tag{6.11}$$

$$\hat{w}(k+1) = \hat{w}(k) + K(k+1)\big(y(k) - \hat{y}(k)\big), \tag{6.12}$$

where $K(k)$ is the Kalman gain, $H(k)$ is the partial derivative of $h\big(\hat{x}(t), u(t)\big)$ with respect to $w(t)$ at the estimated weights, i.e., a Jacobian matrix, and $P(t)$ is the weight covariance matrix. The variance of output (predicted natural frequency) can be obtained from the diagonal elements of the innovation covariance matrix $S(t+1)$, and the confidence intervals can then be derived by adding a certain number of standard deviations from the prediction. In this paper, two-sigma ranges are used with the normal assumption of the prediction errors to guarantee the 95% prediction intervals. The schematic chart of using EKF as neural network learning algorithm is shown in Figure 6.9. The flow chart of EKF trained artificial neural network is shown in Figure 6.10.

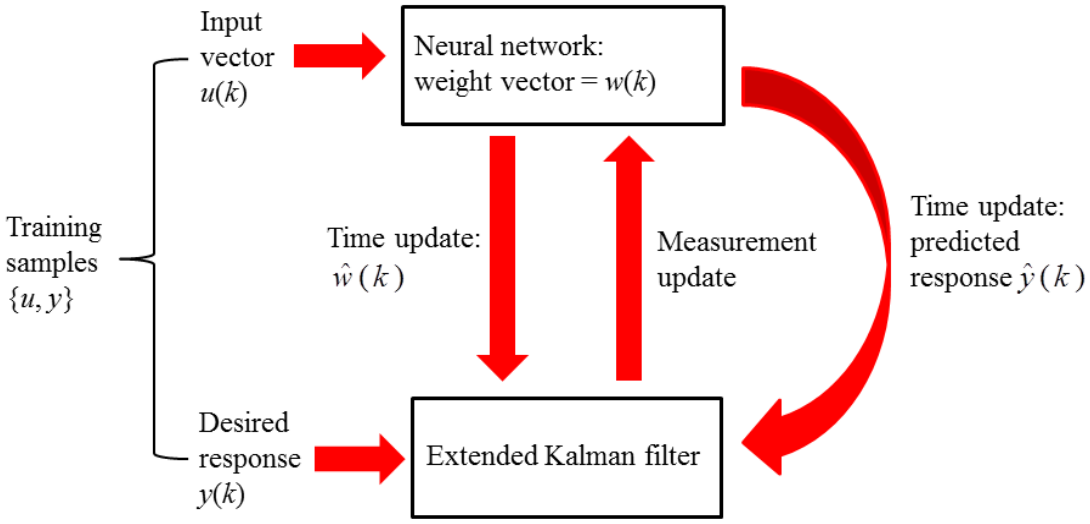

Figure 6.9 Schematic chart of EKF trained artificial neural network

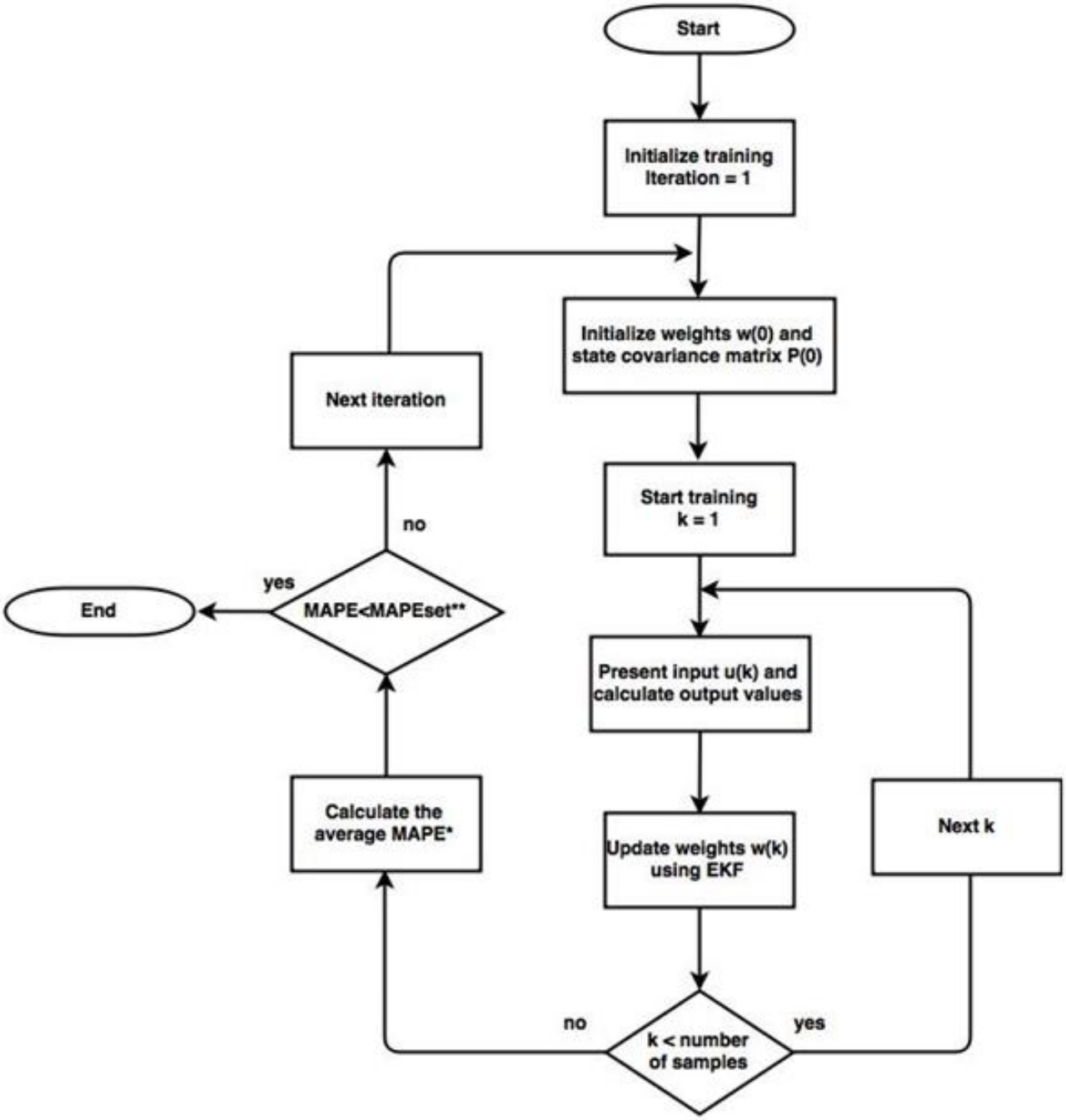

*: Mean absolute percentage error (MAPE) is used to evaluate the training;
**: MAPEset is a threshold set to stop the NN training.

Figure 6.10 Flow chart of EKF trained artificial neural network

6.3.3 Two-sigma confidence interval for NN learning

If a bridge is in good condition without damage, the nature frequency should fluctuate slightly within a normal range. However, when damage occurs, the nature frequency may jump outside the normal ranges and the changes can be captured by the confidence intervals derived from EKFNN. The means and standard deviations of natural frequency predictions are calculated iteratively in each time step from EKF algorithm to form two-sigma confidence interval for the damage detection.

As depicted in Figure 6.8, the natural frequency prediction is the output of the developed EKFNN model. The standard deviation of the natural frequency prediction can be derived from the diagonal element of the innovation covariance matrix in EKF algorithm as in Equation 6.13.

$$\sigma(k) = \sqrt{diag(S(k))} \tag{6.13}$$

The estimation error of EKF is assumed as a normal distribution, thus two-sigma ranges can be used to guarantee a 95% confidence level. The damage detection rule adapted in this paper is that bridge damage is detected if consecutive measurements of any structural parameter fall outside of the two-sigma range.

6.4 Structural damage simulation in finite element model

The Meriden Bridge is currently operating in good conditions. To validate the damage detection capacity of the developed method, numerical simulation techniques can be performed to simulate the real damage scenarios on the bridge structure (Bagchi *et al.*, 2010). In this section, real damage conditions are simulated in finite element analyses to observe their influences on the changes of natural frequencies. The change of natural frequencies will then be applied in the testing phase to validate the developed damage detection method.

6.4.1 Finite element model

The finite element model for the structure of Meriden Bridge is developed using SAP 2000 software as depicted in Figure 6.11. The FE model contains 1464 frame elements and 4758 shell elements, with total 5313 nodes. 2D shell elements were used for the concrete deck and steel girders. The cross bracing is

modelled using 1D frame elements. The composite actions between deck and girder elements are also modelled by 1D frame elements. For the boundary conditions of the one-span bridge structure, fixed supports are assigned at the north end, and roller supports are assigned at the south end. The material for concrete deck, steel girder and steel bracing are assumed 4,000 psi concrete, A36 steel and A992 steel respectively. The FE model for Meriden Bridge is updated with the natural frequencies obtained from the field test, and is used as the baseline model for undamaged condition (Li, 2014).

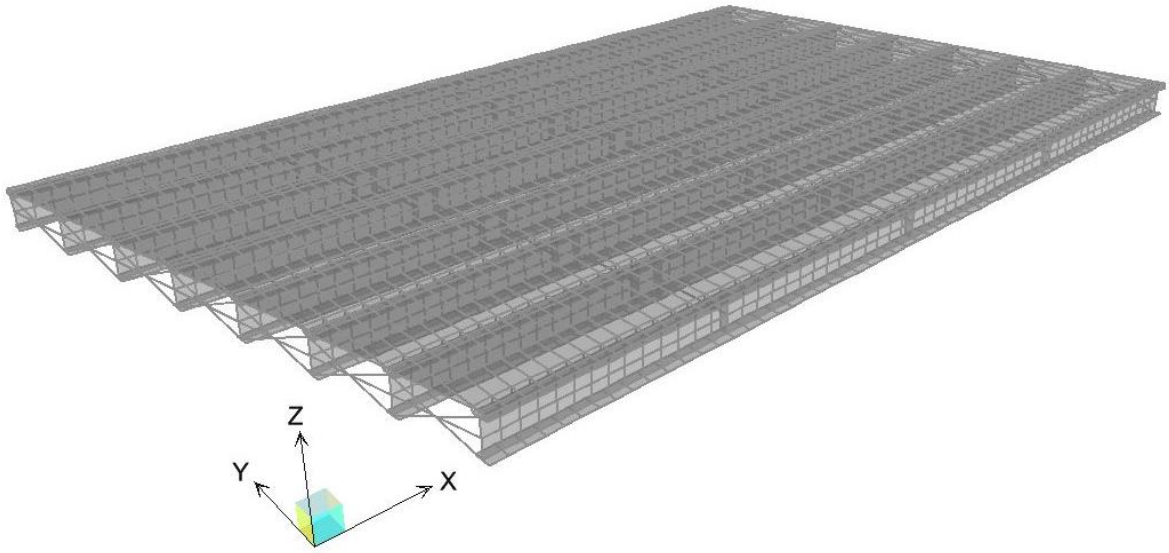

Figure 6.11 FE model for Meriden Bridge

A composite steel girder bridge may encounter many types of structural damages during operation, and the occurrence of these damages will threat the service and life span of highway bridges. In this paper, two common damage scenarios are considered: the impact damage due to vehicles passing under the bridge, and the static loading test using full-loaded truck.

6.4.2 Damage scenario 1: Removal of composite action

Bridge damage resulted from underneath cross traffic collision is one of the major threads to bridge structures. The composite action between steel girder and concrete deck may be lost or diminished after the bridge undertakes the impact on the exterior lateral side. Plude studied the effects of potential damage

scenarios on a composite steel girder bridge using finite element model (Plude, 2011). Three damage types were considered, including fatigue cracking due to truck traffic, loss of composite action on exterior girder and deterioration of the bridge deck. The FE analysis results showed that the change of natural frequencies caused by loss of composite action in exterior girder is much more significant than the other two damage scenarios.

To simulate the damage scenario that the exterior girder becomes non-composite, the composite action of exterior girder is removed in the finite element model by releasing the moments at both ends of the frame elements connecting steel girder and concrete deck. The location of damaged exterior girder is shown in Figure 6.12. Then the natural frequencies of bridge with non-composite exterior girder are obtained using modal analysis in SAP 2000. The seven natural frequencies of bridge in damaged scenario 1 are listed and compared with undamaged case in Table 6.1, from which conclusion can be made that all the seven natural frequencies have reduced because of the damage of removal of composite action in the exterior girder. In particular, the reduction ratio for the first natural frequency is 5.23%.

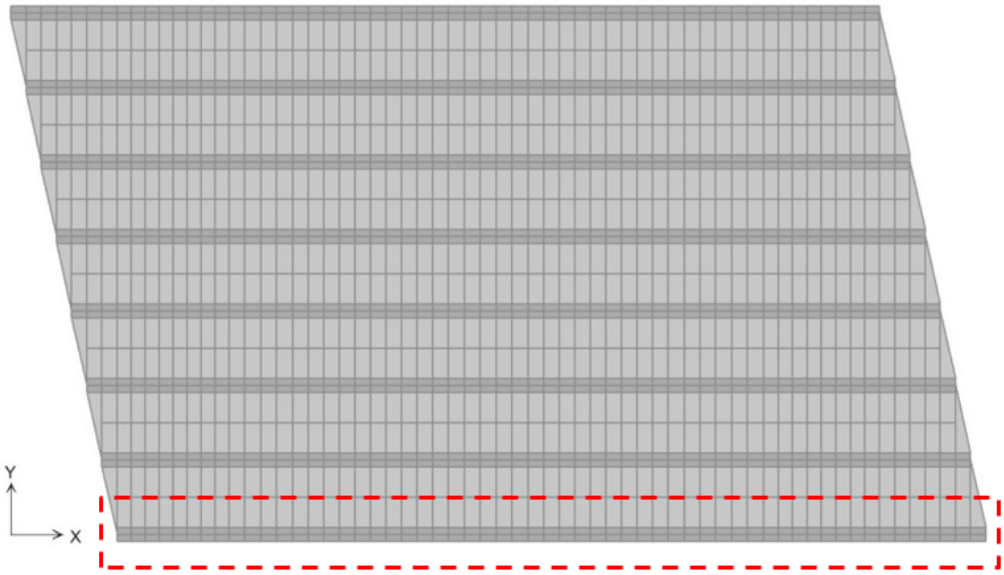

Figure 6.12 Removal of composite actions on exterior girder in FE model

Table 6.1 Comparison of the natural frequencies before and after losing composite action on exterior girder

Mode	Undamaged (Hz)	Damage 1 (Hz)	Damage 1 Diff (%)
1	4.44	4.21	-5.23
2	5.57	4.74	-14.87
3	6.78	6.25	-7.79
4	9.77	9.27	-5.07
5	14.17	14.02	-1.05
6	14.89	14.43	-3.10
7	16.72	16.52	-1.20

6.4.3 Damage scenario 2: Static loading test

Static loading tests are frequently performed to verify the actual structural behavior of bridge compared with designs. The results of static load tests also produce an initial baseline for future condition assessment. Static loading tests using finite element model simulation (Samali *et al.*, 2007) and real truck experiment (Karoumi *et al.*, 2006) reported that the static loading tests can cause decreased natural frequencies for bridge structures.

To simulate the Meriden Bridge under static loading test, the load of a fully loaded five-axle truck, i.e., 68,600 lbs, is added on the right lane at the mid-span of the bridge in the FE model. The detailed information of the test truck was obtained in the previous calibration test for the bridge monitoring system, as shown in Table 6.2. The loadings due to the weight of truck are modelled as five static loading on each axle applied on the deck of bridge in the FE model, as shown in Figure 6.13 and 6.14. The identified natural frequencies of bridge under static loading test are listed and compared with undamaged case in Table 6.3, which also shows a reduction of natural frequencies caused by the static loading test. In particular, the first natural frequency reduced 5.9%.

Table 6.2 Length and weight characteristics of the five-axle test truck (Christenson *et al.*, 2011).

–	SI	US
Gross Vehicle Weight	305.15 kN	68,600 lbs
Wheelbase length (Axle 1-5)	13.58 m	44.55 feet
Number of axles	5	5
Axle Space (1-2)	3.59 m	11.78 feet
Axle Space (2-3)	1.34 m	4.40 feet
Axle Space (3-4)	7.42 m	24.34 feet
Axle Space (4-5)	1.23 m	4.04 feet
Axle Weight (1)	45.19 kN	10,160 lbs
Axle Weight (2)	58.98 kN	13,260 lbs
Axle Weight (3)	57.83 kN	13,000 lbs
Axle Weight (4)	73.04 kN	16,420 lbs
Axle Weight (5)	70.10 kN	15,760 lbs

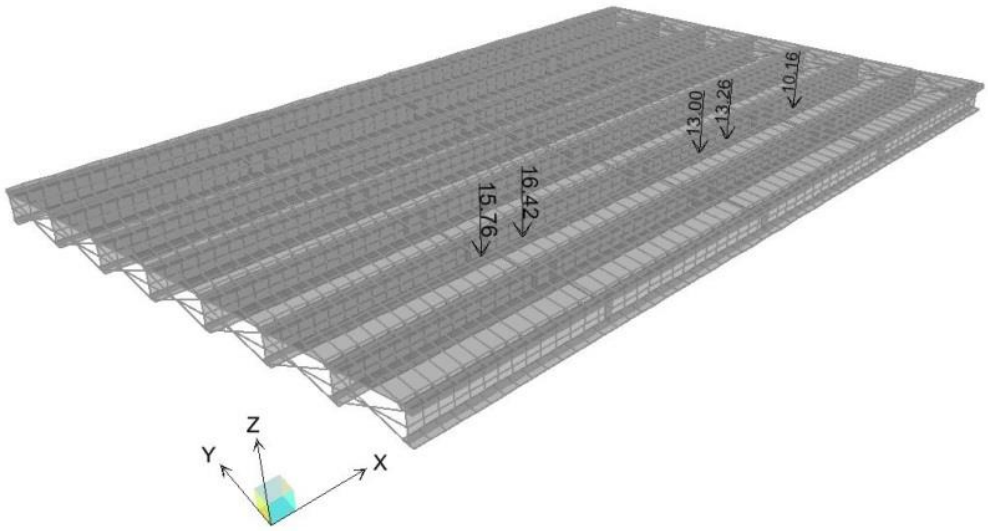

Figure 6.13 Global view of FE model under static loading

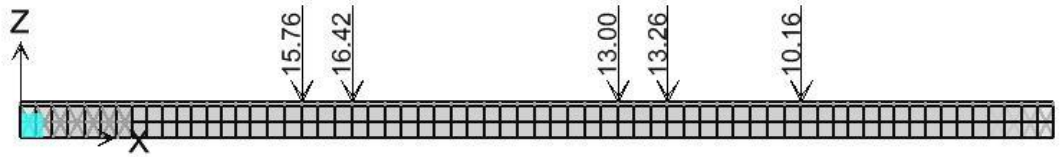

Figure 6.14 Side view of static loadings on FE model

Table 6.3 Comparison of the identified natural frequencies before and after static loading test

Mode	Undamaged (Hz)	Damage 2 (Hz)	Damage 2 Diff (%)
1	4.44	4.18	-5.90
2	5.57	5.33	-4.32
3	6.78	6.65	-1.92
4	9.77	9.08	-6.97
5	14.17	12.42	-12.39
6	14.89	13.94	-6.42
7	16.72	15.54	-7.05

6.5 Numerical testing

The results of FE model analysis showed that the two damage scenarios cause a decrease on natural frequencies for Meriden Bridge, and with 5.23% and 5.9% reduction on the first natural frequencies, respectively. When the above two damage scenarios occur, the real-time structural health monitoring system is expected to detect the damage considering temperature effects, and send out alarm immediately. To validate whether this requirement is satisfied in the developed method, the second half of the first mode natural frequency samples during the testing phase were reduced 5% to simulate the damages. The synthesized data are then fed into NN to test whether the EKF algorithm can eliminate the temperature effects and catch the abnormal changes automatically.

The NN used to predict the natural frequency is represented by a three-layer perceptron, with the number of input neurons and output neuron defined as 7 and 1 respectively. Selecting the number of neurons in the hidden layer is an important part to establish the overall neural network architecture. Using too few

hidden neurons can result in under-fitting, while using too many neurons can result in over-fitting and significantly increase computational efforts. In this paper, the number of hidden neuron is determined through extensive training and validation processes (Gutierrez-Osuna, 2015) to achieve good generalization performance for NN.

Hourly data of the first mode natural frequency and temperature obtained on Meriden Bridge from March 2013 to May 2014 are used to examine the developed EKFNN method for structural damage detection. Among them, the first eleven-month data (03/2013-01/2014) are used for training, the following one-month data (02/2014) are used for validation, and the last one-month data (03/2014) are used for the testing. The number of hidden neurons is determined through the training and validation process. The damage detection capability is evaluated in the testing phase.

The following three testing cases are performed. Case 1 demonstrates the selection of number of hidden neurons. Case 2 compares the prediction results of EKFNN with and without considering the temperature effects. Case 3 validates the damage detection capability using simulated damage data. The natural frequency prediction performance is evaluated by using the standard mean absolute percentage error (MAPE), which is a measure of accuracy for a forecasting method. A smaller MAPE indicates a better forecasting performance. MAPE is defined by Equation 6.14.

$$MAPE = \frac{1}{T}\sum_{t=1}^{T}\frac{\left|\hat{f}(t) - f_A(t)\right|}{f_A(t)} \times 100\% \tag{6.14}$$

where $\hat{f}(t)$ and $f_A(t)$ are the predicted and actual first mode natural frequency, respectively.

6.6.1 Case 1: Selection of the number of hidden neurons

This case demonstrates the selection of the number of hidden neurons N_h through training and validation process. There are several rules to set N_h, for instance, using the half of the sum of input and output neurons. To effectively determine this parameter, intensive training-validation experiments are conducted. The NN is trained with the initialized N_h (starting from 2) through training set data, and the prediction performance is then evaluated on the validation set by calculating the validation MAPE. The

value of N_h is increased until the minimum validation MAPE is achieved. For each N_h, the algorithm runs 10 times, and the averaged MAPEs are then calculated to select the best N_h. The MAPEs of the EKFNN using first natural frequency in validation phase with N_h ranging from 2 to 7 are depicted in Figure 6.15. The number of hidden neurons is thus selected as 6 to achieve the minimum validation error and superior prediction capability.

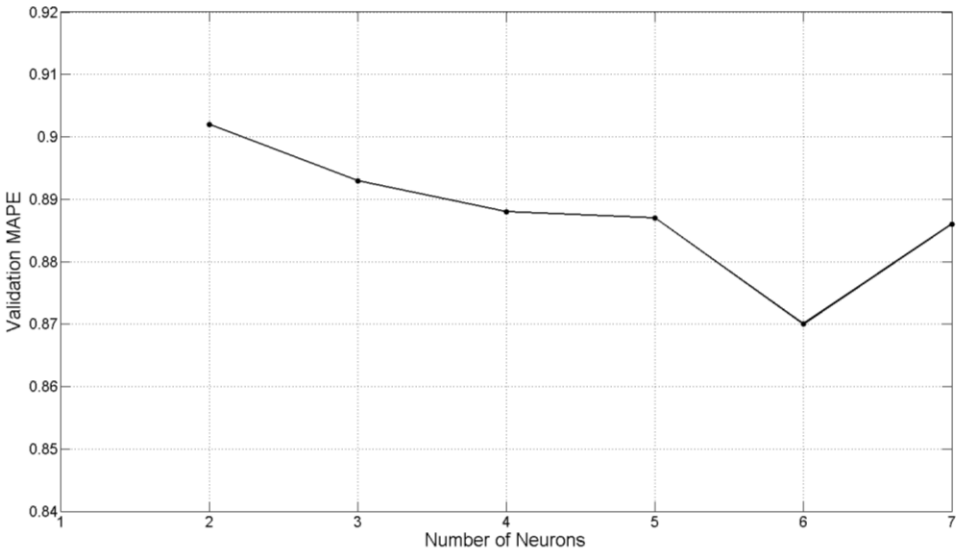

Figure 6.15 Validation MAPEs with the number of hidden neurons

6.5.2 Case 2: Comparison of NNs with and without temperature inputs

This case compares results of the developed EKFNN model with and without considering temperature as input factors. When temperature factor is not considered as inputs for NN model, the number of input variables decreases to 4. By following the same training and validation processes as discussed in Case 1, the number of hidden neurons is selected as 3. As summarized in Table 6.4, the NN model without considering temperature factor produces a higher MAPE 1.15 and a lower two-sigma coverage rate 90% as compared with the MAPE 1.06 and two-sigma coverage rate 100% when temperature inputs are involved. The results are reasonable because NN model without temperature inputs could result in lower accuracy

performance and false alarm problems. The actual measurements, predictions as well as two-sigma ranges with and without considering temperature factor are depicted in Figures 6.16 and 6.17, respectively.

Table 6.4 Comparison of EFKNN method with/without using temperature inputs

Inputs	Number of Hidden Neuron	MAPE during testing period	Two-sigma coverage rate
With Temp	6	1.06	100%
Without Temp	3	1.15	90%

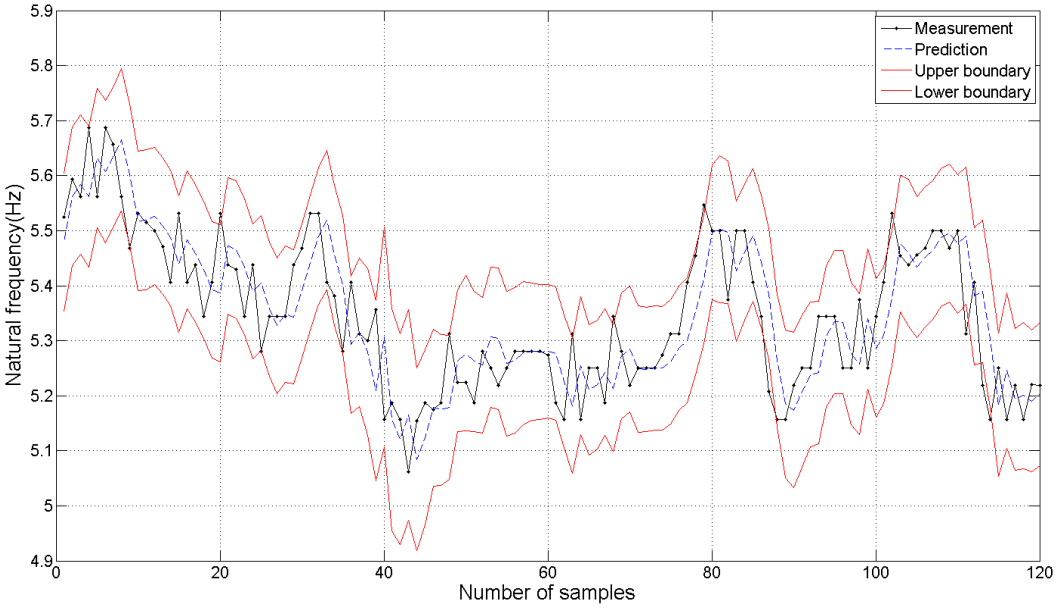

Figure 6.16 Performance of EKFNN without using temperature inputs

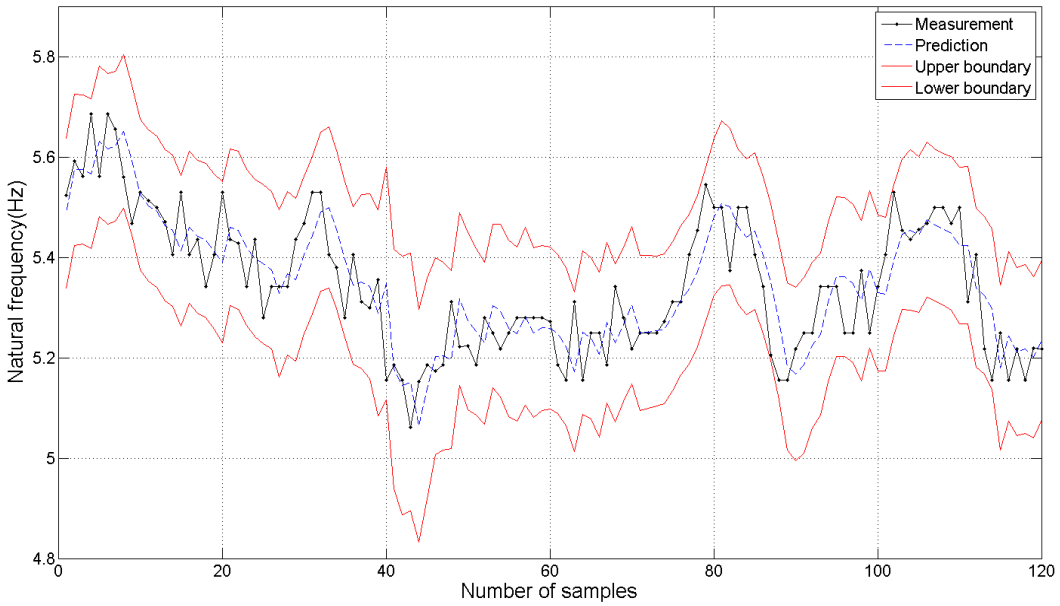

Figure 6.17 Performance of EKFNN with using temperature inputs

6.5.3 Case 3: Validation of EKFNN damage detection capability

This case validates the efficiency and capability of damage detection of the developed EKFNN method using simulated damage data. When structural damage occurs, the online monitoring system is expected to detect the damage and send out alarms in a very short time. In this testing case, the first half samples represent undamaged structure, and last half samples are synthesized damaged data by decreasing original data by 5%. As shown in Figure 6.18, when structural damage occurs at 61th point, the real measurements of natural frequencies jump outside of the two-sigma control limits for consecutive points. Thus the EKFNN method detects the structural damage successfully.

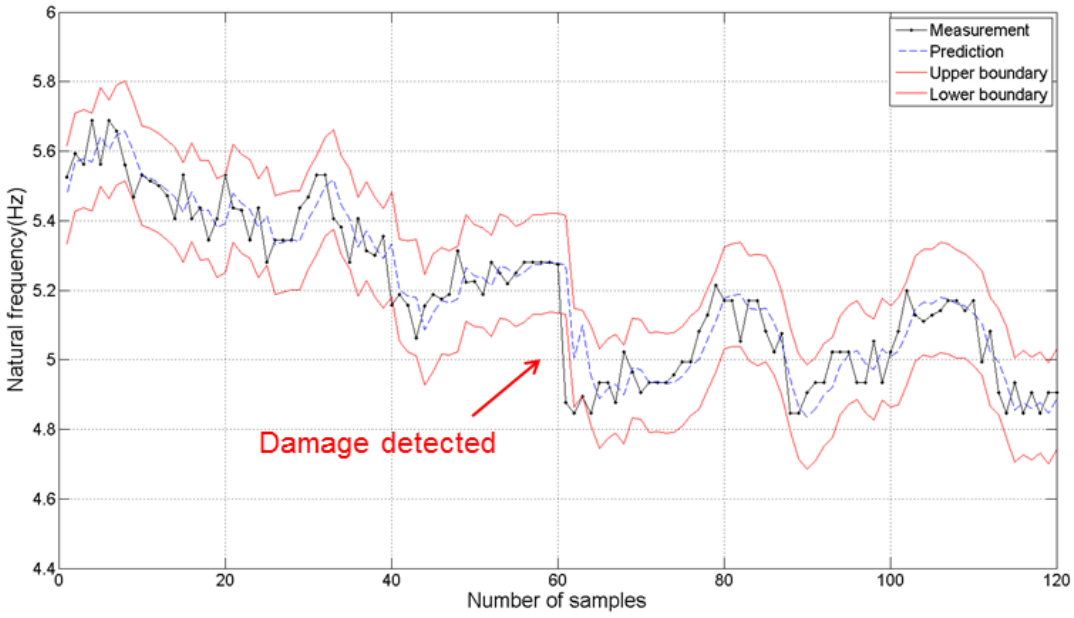

Figure 6.18 Performance of EKFNN when natural frequency reduced 5%

6.6 Comparison with multiple linear regressions (MLR)

To compare the performance of the developed EKFNN method, some regression analysis can be used, such as autoregressive integrated moving average (ARIMA), multiple linear regressions (MLR), vector auto-regression (VAR) (Shumway and Stoffer, 2013). Among them, multiple linear regression (MLR) model is one of the widely used statistical techniques to predict the relationship between a dependent variable and multiple independent variables by fitting a linear equation to observed data (Antoniadis *et al.*, 2006). In this paper, MLR is used as the benchmark to compare and evaluate the performance of EKFNN. To conduct an apple-to-apple comparison, a MLR model is created using the same input variable (f_{t-1}, f_{t-2}, f_{t-3}, T_{t-1}, T_{t-2}, T_{t-3} and Season Index) and output variable (f_t) as used in the EKFNN. The equation for the MLR model is described as:

$$f_t = \beta_0 + \beta_1 f_{t-1} + \beta_2 f_{t-2} + \beta_3 f_{t-3} + \beta_4 T_{t-1} + \beta_5 T_{t-2} + \beta_6 T_{t-3} + \beta_7 SeasonIndex + \varepsilon_\alpha \qquad (6.15)$$

where β_0, β_1, β_2,…β_7 are coefficients for each input variable and ε_α is the Gaussian error variable with zero mean.

For comparison, the same data used for training, validation and testing of EKFNN method are also used in MLR method. In the training phase, the unknown regression coefficients are estimated by minimizing the least squares errors. In the testing phase, the MLR model predicts the natural frequency in the next hour when the new input variables are given, and the 95% confidence interval of the prediction is used to detect the potential damage of the bridge. If the predicted natural frequency falls outside the 95% confidence interval generated by MLR, the damage is to be detected.

Two cases are presented in this section. Case 1 compares the performance of EKFNN and MLR under normal conditions, and Case 2 shows the prediction and damage detection performance of EFKNN and MLR under structural damage.

6.6.1 Case 1: Performance comparison of MLR and EKFNN without structural damage

The mean absolute error (MAE), standard deviation of MAE, MAPEs, standard deviation of MAPE (Std. MAPEs) of the MLR and the EKFNN under normal condition are compared in Table 6.5. It can be seen that both the mean and stand deviation of prediction errors from the EKFNN are lower than that of the MLR, which demonstrates that EKFNN has more accurate performance than MLR. Actual measurements, predictions, as well as 95% confidence interval are plotted in Figure 6.19. As can be seen, the 95% confidence interval of MLR is very conservative, which might not suitable for damage detection for bridge structures.

Table 6.5 Performance comparison between MLR and EKFNN under normal condition

Method	**MLR**	**EKFNN**
MAE (Hz)	0.06	0.0536
Std. MAE	0.0484	0.043
MAPE (%)	1.240	1.113
Std. MAPE	1.0442	0.827

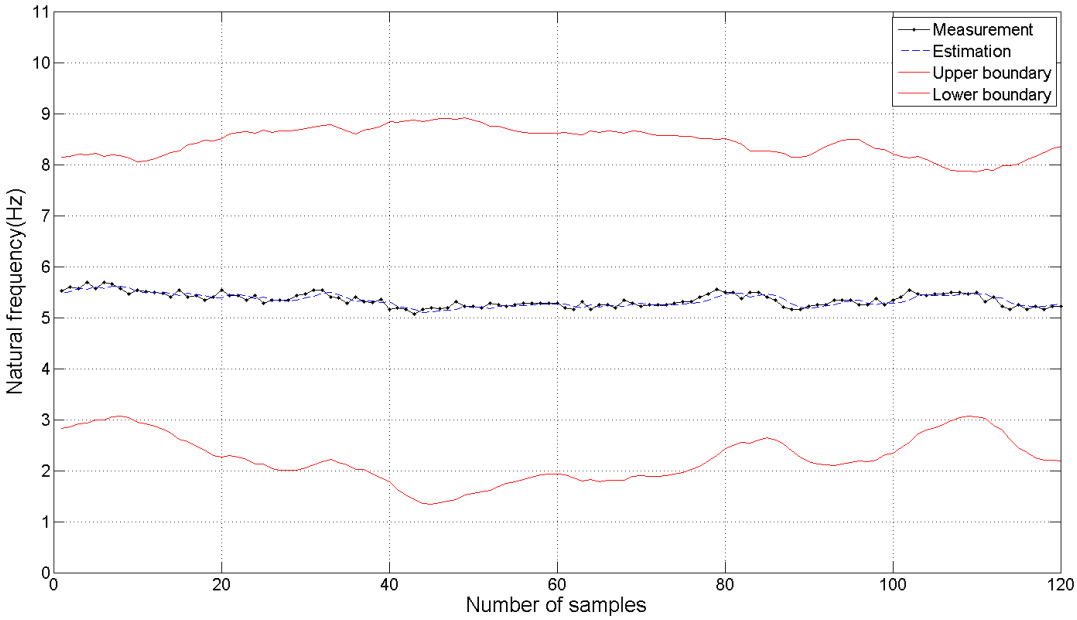

Figure 6.19 Performance of MLR under normal condition

6.6.2 Case 2: Performance comparison of MLR and EKFNN with structural damage

This case compares the performance of damage detection between MLR and developed EKF-ANN using the same damage simulation data as Case 3 in Section 6. The mean absolute error (MAE), standard deviation of MAE, MAPEs, standard deviation of MAPE (Std. MAPEs) of damage detection testing using both MLR and the EKFNN methods are compared in Table 6.6. The performance of EKFNN is more preferable than that of MLR. As the damage detection performance of MLR shown in Figure 6.20, the huge confidence interval is too conservative to capture the deviation points and to detect the damage when structural damage occurred at 61th point. Therefore, conclusions can be made that the developed EKFNN method is more effective and accurate for structural damage detection than MLR method.

Table 6.6 Performance comparison between MLR and EKFNN with structural damage

Method	MLR	EKFNN
MAE (Hz)	0.688	0.0572
Std. MAE	0.0598	0.0485
MAPE (%)	1.31	1.12
Std. MAPE	1.17	1.06

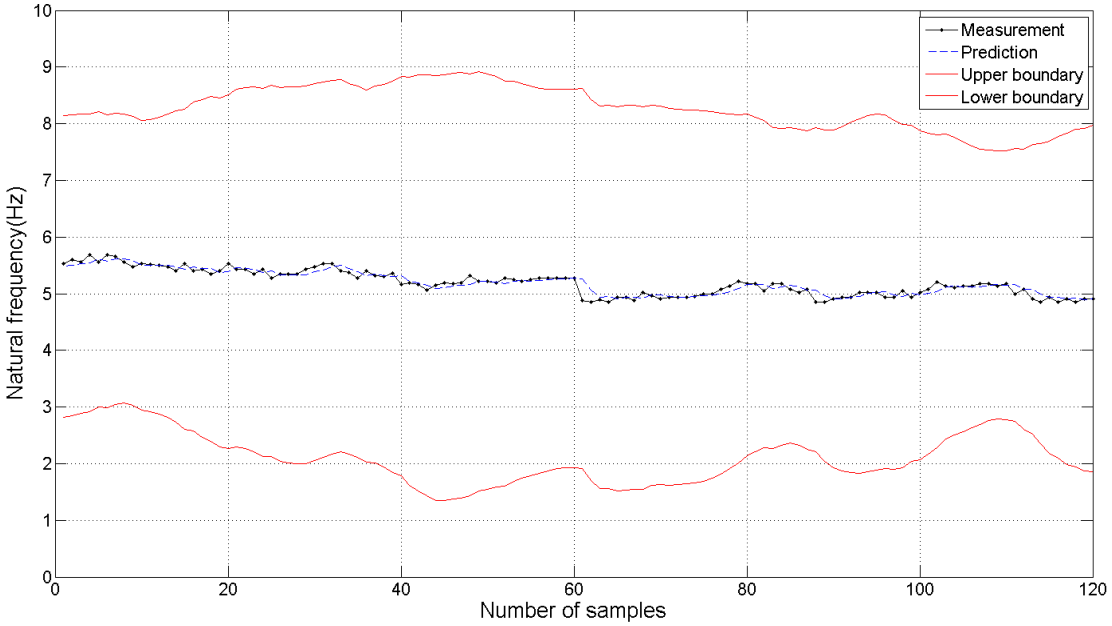

Figure 6.20 Performance of MLR with structural damage

6.7 Summary

A new damage detection method using artificial neural network aided with the extended Kalman filter is developed for a composite steel girder bridge under severe temperature change environment. Based on data analysis of long term bridge monitoring data, a systematic procedure to select input variables for NN is developed. Lagged hourly temperature, lagged hourly natural frequency, and comprehensive season index are selected as input variables for neural network. Based on the above input variables, the natural frequency in the next time step is predicted as output. Especially, a newly developed season index is added as input to represent the freezing effects for structures under severe temperature changes. Damage scenarios

are simulated using finite element analysis software SAP 2000 to obtain the change ratios of natural frequency, which are applied on two-month measurement data to simulate natural frequency of bridge in damaged situations. One-year hourly natural frequency and temperature data are used to train the developed EKFNN model. In testing phase, the damage simulation data of natural frequency time series are presented to the trained model, and the occurrence of damage can be successfully detected by the control limits provided by the damage detection model. The testing results indicate that the EFKNN has better capabilities than benchmark multiple linear regression approach. The EFKNN method shows a strong potential for real time damage detection for civil structures that are instrumented with long-term health monitoring system. This approach provides an objective manner to reduce the uncertainty in structural damage detection, and increases the ability for structural health monitoring system to aid bridge management and maintenance.

CHAPTER 7 SUMMARY, CONCLUSIONS AND RECOMMENDATIONS

7.1 Summary and conclusions

The research presented in this dissertation provided a comprehensive framework for real-time damage detection for civil structures using big data collected from long-term structural health monitoring systems.

First, in order to efficiently evaluate the condition of Meriden Bridge, long-term strain data were analyzed using reliability-based methods in Chapter 3. Two efficient approach to assess the reliability for bridge component based on strain monitoring data are presented using yield strength limit state and fatigue limit state. The yield strength limit state function considers the yield strength, and the sensor error is also included in the reliability index equation. The fitting tests of six probability distributions are compared using peak living loading from monitoring data. A parallel-series combined system is presented in order to assess the bridge reliability based on multi-sensor monitoring systems. The fatigue limit state function considers fatigue theory and miner's rule to estimate the remaining life for structures. Both methods can reflect the overview of condition for the whole bridge, and it can also assess the reliability of bridge in real time through on-line monitoring.

Secondly, a novel structural parameter identification method based on extended Kalman filter is developed for linear structures equipped with MR damper devices in Chapter 4. In order to incorporate the MR damper into the structural dynamic model, a new state-space model is established by combining hyperbolic tangent model and equation of motion of structural dynamic system. To estimate the structural variables and parameters, EKF is used to update the states based on new measurement in each time step. Based on measurements of accelerations of three stories and damper force, the EKF algorithm can produce real-time estimation for the structural parameters and state variables. The EKF based method is tested using simulated data of a three stories linear building with MR damper under earthquake excitations, and numerical results demonstrate high estimation accuracy and light computation of this presented method. The developed EKF based method can be easily replicated to other types of structures equipped with MR

dampers. And the developed EKF-based method has a good potential to be implemented in real-time SHM systems for in-service MR damper equipped structures.

Fourthly, a real-time structural damage detection method for civil structures is developed based on the combination of EKF and DSPC in Chapter 5. Based on measurements of damage-sensitive parameters involved in the state-space model of structural dynamic systems, the EKF algorithm produces real-time estimation means and standard deviations for the identified structural parameters to form the dynamic control limits to detect any abnormality in the selected parameters. The developed EKF-DSPC damage detection method is validated using simulation response data of a three-story linear structure and a two-story nonlinear hysteretic structure under earthquake excitation considering different damage scenarios, and the testing results demonstrate fast convergence rate, high damage detection accuracy and light computational costs. The EKF-DSPC method can be easily replicated in other structural damage detection problems for both linear and nonlinear structures. Moreover, since the EFK is a well-developed methodology that does not require large computation, and DPSC is capable to handle system variations caused by operational and environmental effects, the EKF-DSPC method has a good potential to be implemented in real-time SHM systems for in-service civil structures.

Finally, a new damage detection method using artificial neural network aided with the extended Kalman filter is developed for a composite steel girder bridge under severe temperature change environment in Chapter 6. Based on data analysis of long term bridge monitoring data, a systematic procedure to select input variables for NN is developed. In testing phase, the damage simulation data of natural frequency time series are presented to the trained model, and the occurrence of damage can be successfully detected by the control limits provided by the damage detection model. The testing results indicate that the EFKNN has better capabilities than benchmark multiple linear regression approach. The EFKNN method shows a strong potential for real time damage detection for civil structures that are instrumented with long-term health monitoring system. This approach provides an objective manner to reduce the uncertainty in structural damage detection, and increases the ability for structural health monitoring system to aid bridge management and maintenance.

In conclusion, this research provided a comprehensive contribution to long-term structural health monitoring and damage detection for civil structures using big data, including weight-in-motion systems, structural control devices-equipped structures, linear and nonlinear building structures, and full-scale highway bridge under severe temperature effects.

7.2 Recommendations on future work

While a comprehensive contribution has been made by the research in this study, subsequent future studies are suggested to extend the developed framework to be applicable for various types of full scale civil structures in a long-term manner using big data.

One of the biggest influence factors for reliability-based method for bridge monitoring is the traffic volume of vehicles passing through the bridge. The distribution of traffic volume is significantly influenced by weekday or weekends, hours in a day, seasons in a year, and extremely weathers. Adding these parameters into the model may improve the accuracy of reliability based models. This thesis only used data from one day (non-holiday and non-weekend) to represent the traffic pattern for the whole year. Larger size of strain monitoring data (multiple month, multiple year) are suggested to be tested using developed reliability method to calculate the structural probability of failure and bridge remaining life more accurately. A well-designed sampling method need to be designed to pick specific days within a year based on traffic pattern instead of processing all data in a whole year.

The EKF-based structural parameter estimation method can estimate structural parameters for MR damper equipped structure successfully. In the research perspective from structural control, it is also important to estimate the parameters inside the MR damper device to monitor the health condition and detect whether the MR damper is working properly. It was not tested in this research, however, the unscented Kalman filter (UKF) and particle filter could have a better estimation capability than the EKF in specific applications for highly nonlinear system identification problems. Considering the highly nonlinear characteristics and behaviors of MR damper, UKF and particle filter method may be tested for MR damper parameter estimation problems in future.

The developed EKF-DSPC based damage detection method has been verified to be effective on both linear and nonlinear structures. One key important factor for improving the high-accuracy and decreasing the false alarm rate is to select good initial values of parameters in EKF, including the initial error covariance matrix of the extended state vector, the covariance matrix of the measurement noise, and the covariance matrix of the process noise. In this research, the initial parameters of EKF are obtained through extensive testing. Some EKF parameter initialization methods have been proposed and show good results on specific testing cases, but these methods usually require rich empirical experience or complex mathematical derivations and calculation. Systematic method to initialize EKF parameters could be developed from other driplines for general use of EKF-based methods in various engineering problems. In order to apply the developed EKF-DSPC method in damage detection problems for civil structures, a simple, reliable and systematic approach to initialize these EKF parameters need to be investigated in future.

The EKF-trained neural network method has been verified to successfully detect a simulated damage of 5% decrease on natural frequency for an in-service highway bridge in real time. The decrease of natural frequency damage is obtained by simulating two common damage cases in finite element model. Further testing is suggested to verify whether this method can be sensitive to smaller damages, and optimize this model to detect minor damages to improve the sensitivity of the whole damage detection system. Some challenges still exist to detect structural damage for bridge structures experimentally. It is difficult to detect small damages only based on changes in natural frequency. Also for some damage scenarios, one single change in the finite element model cannot represent damaged status accurately, thus we need to incorporate multiple changes in the finite element to model the structural damage more accurately.

APPENDIX A EXPERIMENTAL DATA ANALYSIS FOR TRUCK TEST ON MERIDEN BRIDGE

A-1 Experimental data measurement

To explore the influence of structural damage on the natural frequency of bridge, a heavy truck is used for static loading test on Meriden Bridge. The truck test on Meriden Bridge was implemented from 9:39am to 11:34am on June 16, 2014. Totally 7 sets of valid 10-mins data were collected. The first four data sets were recorded before the truck test started. The fifth data set (10_42_29) measured the process that truck was moving to the center of bridge and started the test. The first 6 mins in the fifth data set has no truck and the last 4 mins has truck loading applied at the center of the bridge. And the last two data sets measured the data when truck was parking on bridge. The time for truck parking on bridge could be identified from the time history in the fifth data set, based on strain measurement of the sensor under the slow lane at the center of the bridge, see Figure A-1. The peaks are introduced by passing of vehicle wheels, and the rapid increase of strain level indicates the start time for truck test.

Table A-1. Data sets description

File Name (hour_min_sec)	Is truck on bridge?
9_39_41	No
9_50_1	No
10_0_22	No
10_13_25	No
10_42_29	first 6 mins No, last 4 mins Yes
11_13_46	Yes
11_24_22	Yes

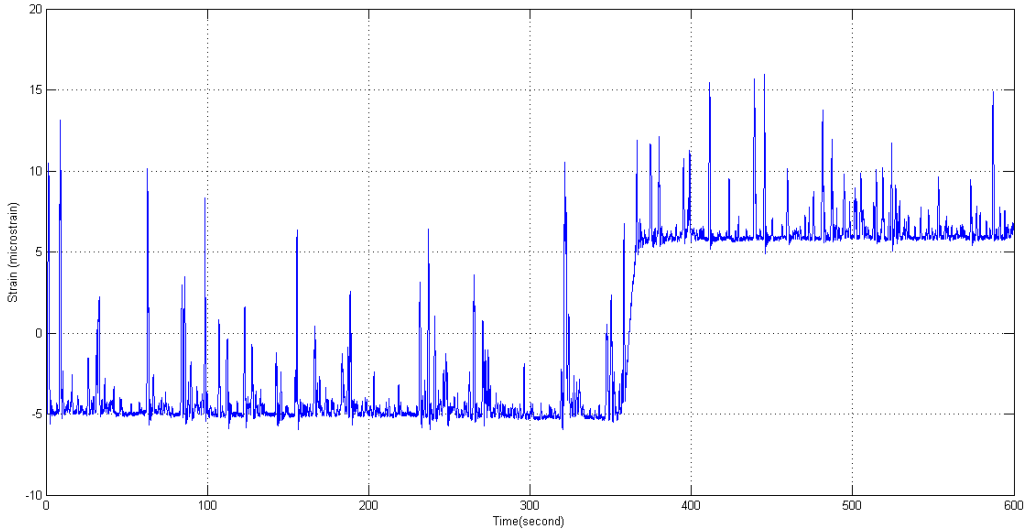

Figure A-1. Time history of strain sensor under lane 1 during truck test

A-2 Power spectral density graphs

A-2.1 PSD comparison between undamaged and damaged scenario in 5th data set

Special attention is paid to 5th data set because it has both data with and without truck parking test. The first three and last three-minute data are used for undamaged and damaged scenario, respectively. The PSD graphs for all 8 sensors in 5th data are plotted in figure 2. The blue curves represent before truck test, and the red curves represent after truck test. And the final PSD graph is plotted using Singular Value Decomposition (SVD) method. As shown in figure 3, the peaks representing natural frequencies on PSD graph show a tendency of increase after the truck parking test. In particular, the first natural frequency has a 2.8% increase after damage.

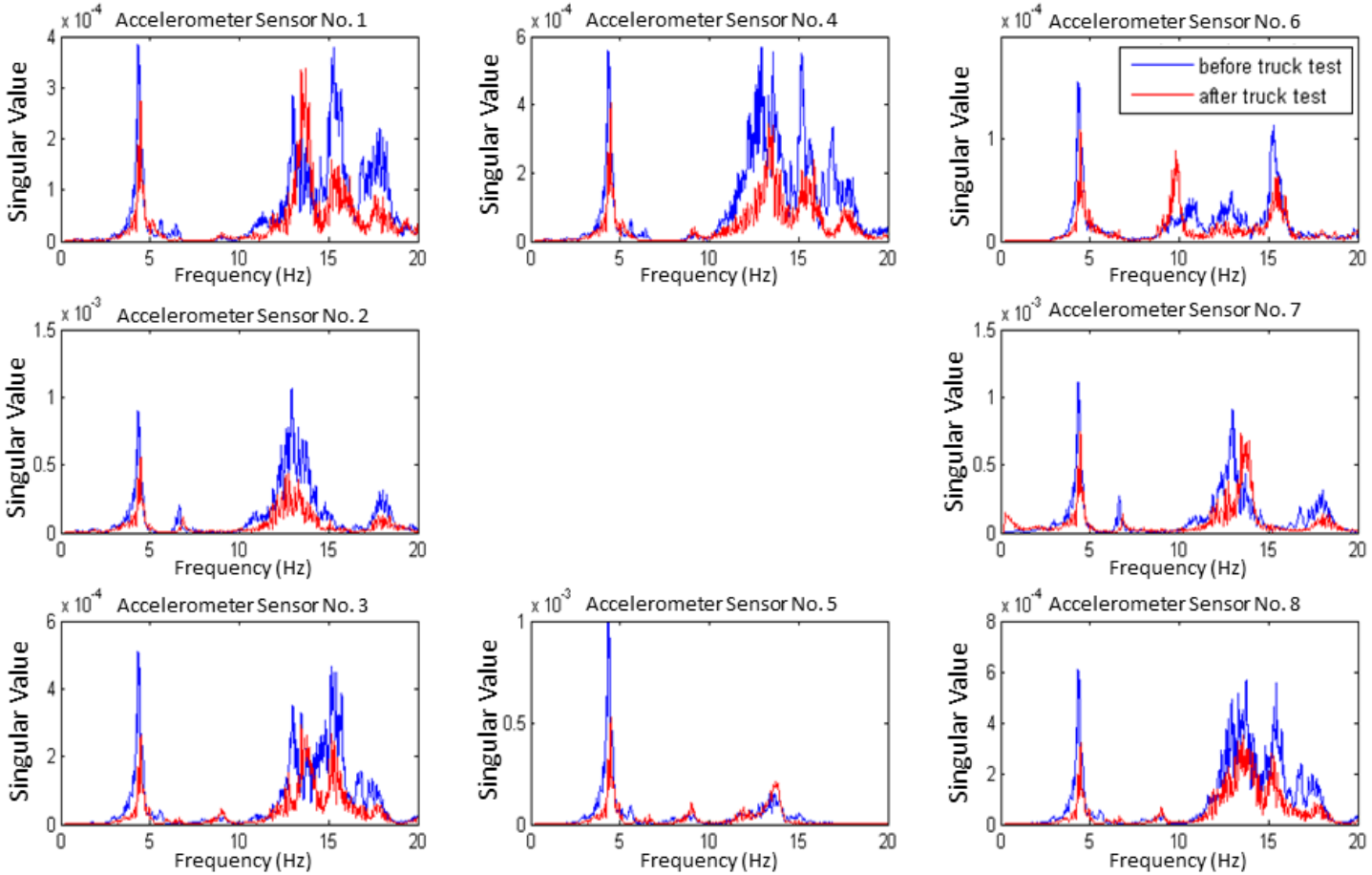

Figure A-2. Power spectral density graphs for 8 sensors in 5th data

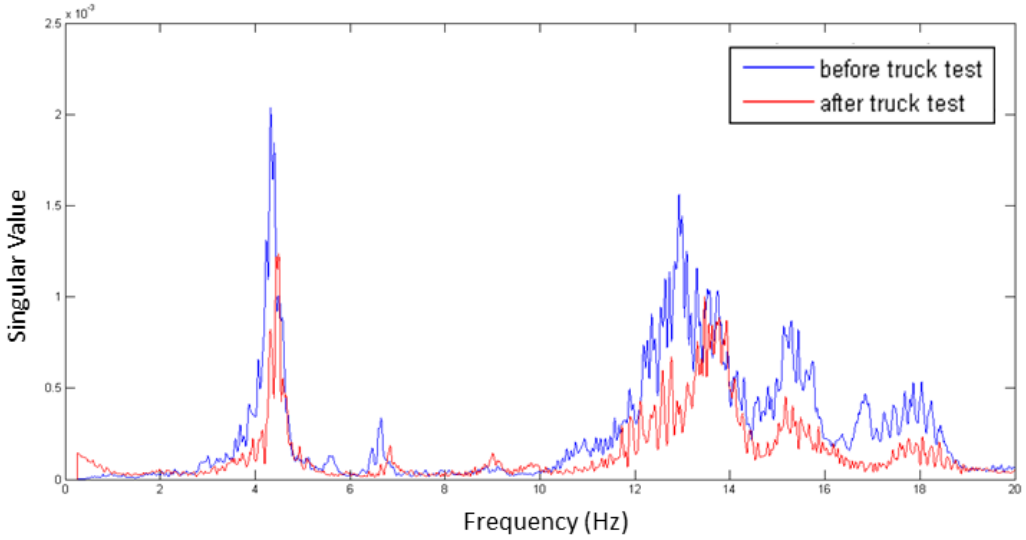

Figure A-3. Power spectral density graphs for 5th data

A-2.2 PSD comparison for all data sets

Similar to previous analysis, the PSD graphs for all data sets are plotted as shown in figure 4. The undamaged data sets include data set 1-4 and the first three minutes of 5th data. And the damaged data include the last three minutes of 5th data and data 6-7. To have a better understanding of the trends of change on natural frequency, the average PSD for undamaged and damaged data sets are plotted in figure 5. The same trend of increasing natural frequency after truck test is observed, and the first natural frequency has an increase around 3%.

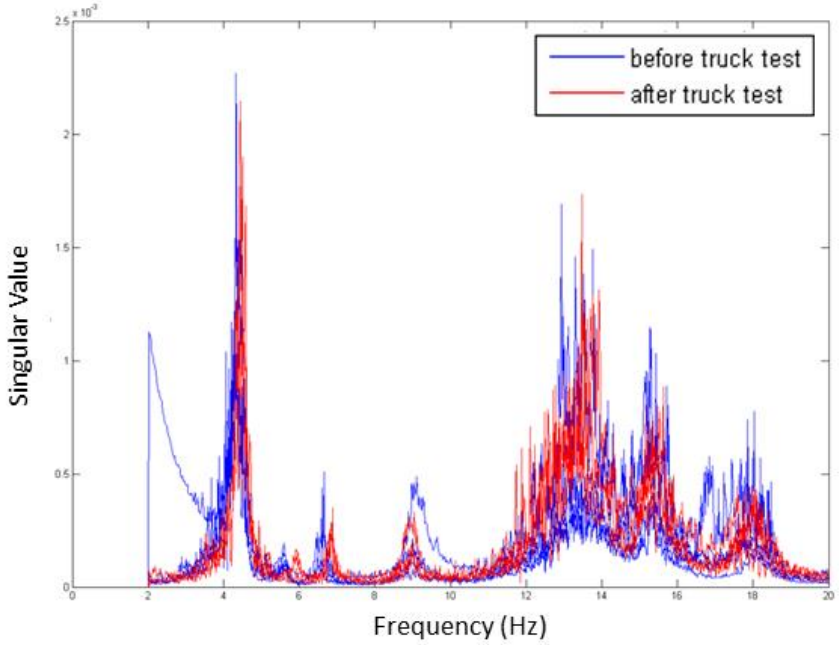

Figure A-4. Power spectral density graphs for all data sets

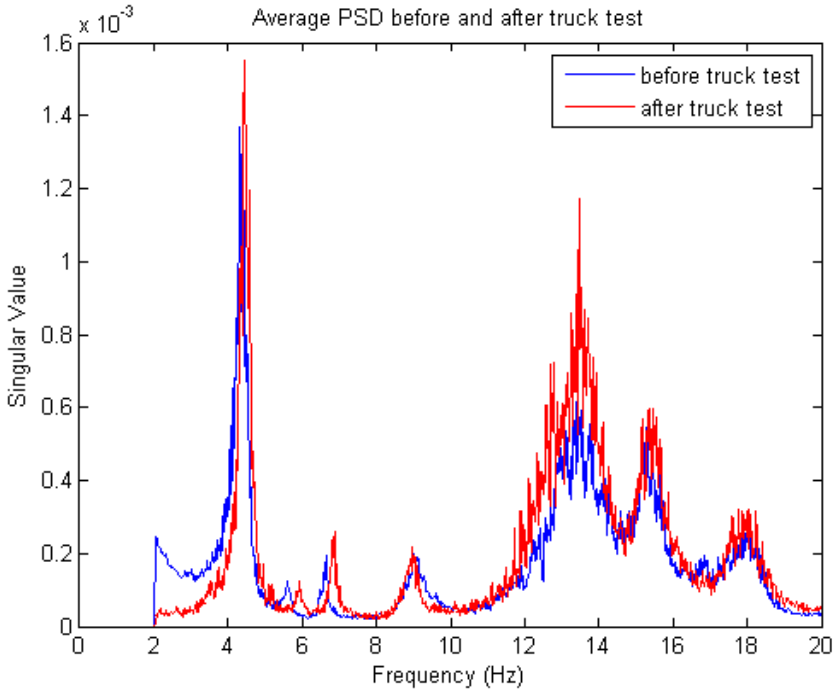

Figure A-5. Average power spectral density graph comparison for all data sets

A-3 Finite element analysis

Many researches have reported that adding mass will change the natural frequency of the bridges using simulation tests on finite element model. To simulate the previous truck test, a fully loaded five-axle truck is used to add static loading on the FE bridge model. The total gross weight, weight of each axle, and length between each axle of the truck for experiment were measured and listed in Table A-2. In this damage scenario, the full loaded truck is parking on the right lane at the center of the bridge. The loadings due to the weight of truck are modelled as five static loading on each axle applied on the deck of bridge, see Figure A-6 and A-7. The identified natural frequencies of bridge under truck loading are listed in Table A-3, which also shows a reduction of natural frequencies compared with undamaged scenario due to the weight of truck. In particular, the first natural frequency reduced 5.9%.

Table A-2. Length and weight characteristics of the five-axle test truck

–	SI	US
Gross Vehicle Weight	305.15 kN	68,600 lbs
Wheelbase length	13.58 m	44.55 feet
(Axle 1 to 5)		
Number of axles	5	5
Axle Space (1-2)	3.59 m	11.78 feet
Axle Space (2-3)	1.34 m	4.40 feet
Axle Space (3-4)	7.42 m	24.34 feet
Axle Space (4-5)	1.23 m	4.04 feet
Axle Weight (1)	45.19 kN	10,160 lbs
Axle Weight (2)	58.98 kN	13,260 lbs
Axle Weight (3)	57.83 kN	13,000 lbs
Axle Weight (4)	73.04 kN	16,420 lbs
Axle Weight (5)	70.10 kN	15,760 lbs

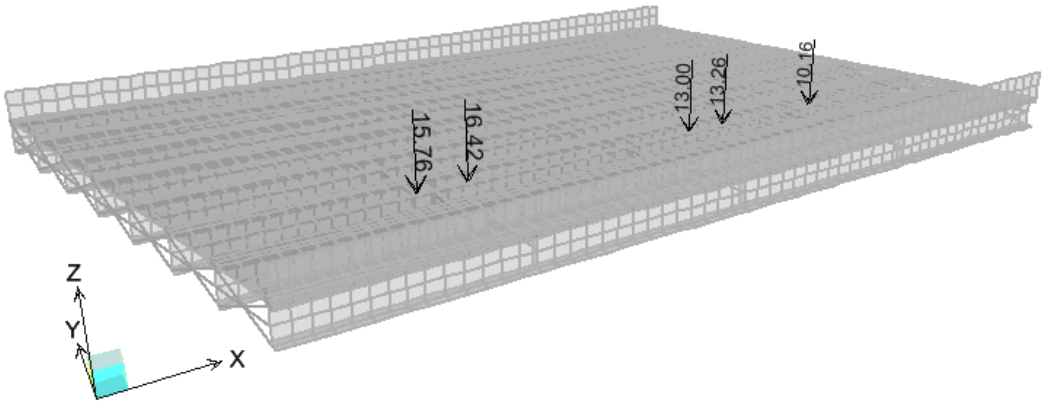

Figure A-6. SAP 2000 model for full loaded five-axle truck parking

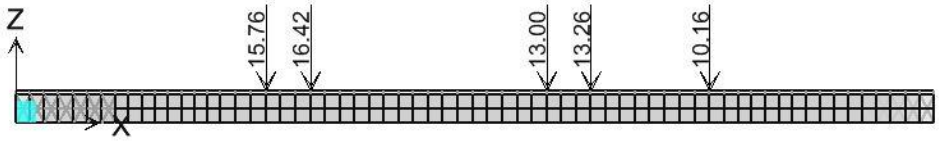

Figure A-7. Side view of SAP 2000 model for bridge under truck test

Table A-3. Comparison of the identified natural frequencies before and after truck test in SAP 2000

Mode Number	Undamaged	Truck test	
	Nf (Hz)	Nf (Hz)	Diff (%)
1	4.44	4.18	-5.90
2	5.57	5.33	-4.32
3	6.78	6.78	-0.12
4	9.77	9.08	-6.97
5	14.17	12.42	-12.39
6	14.89	13.94	-6.42
7	16.72	15.54	-7.05

A-4 Discussions

The experimental data analysis result for truck test on Meriden Bridge is contrary to the finite element analysis and the common sense that increasing mass will decrease the natural frequency, based on equation $f = \sqrt{\frac{k}{m}}$. Two reasons could explain the testing results for increasing natural frequency: boundary condition and stiffness.

A-4.1 Boundary condition

According to the design graph in Figure A-8 and A-9, the boundary conditions for Meriden Bridge are fixed bearing on south abutment, and expansion bearing on the north abutment. As shown in the notes on figure 9, the expansion bearing has "*slotted holes in flange and sole plate, and anchor bolts are set at center of the slot at 50ºF*", which allows horizontal expansion of bridge under thermal and operational effects. However, in the finite element model in SAP 2000, the boundary condition is simple supported with one end roller and another end pin fixed, which does not consider the expanding movement in real case.

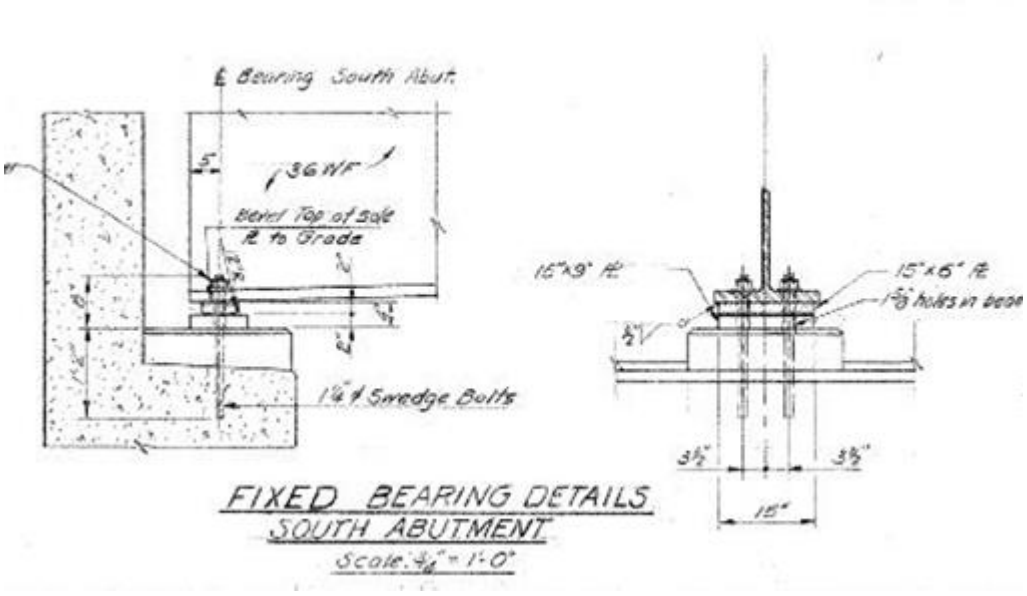

Figure A-8. Design graph for fixed bearing at south abutment (Li, 2014)

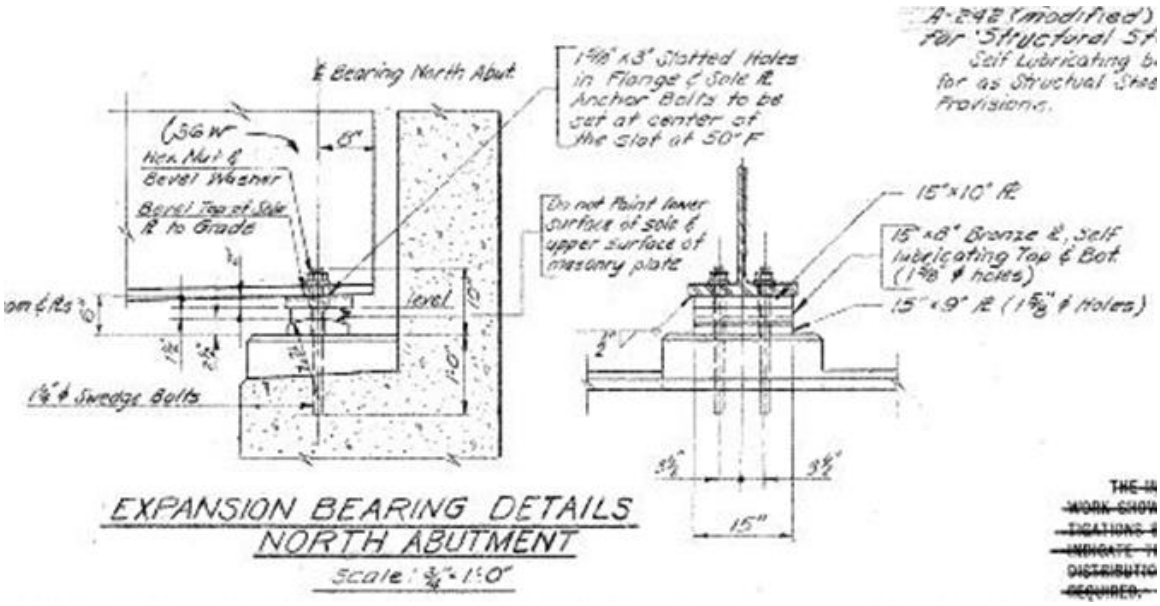

Figure A-9. Design graph for expansion bearing at north abutment (Li, 2014)

A-4.2 Stiffness

The loading acting on the center of bridge structure cause a bending moment, which results expanding force in steel girder and compression force in concrete. Cracks are commonly existed inside the concrete components of civil structures. As shown in Figure A-10, these cracks will shrink and close under such compression forces, which make the stiffness of concreate increased under the loads and possibly result an increase in natural frequency.

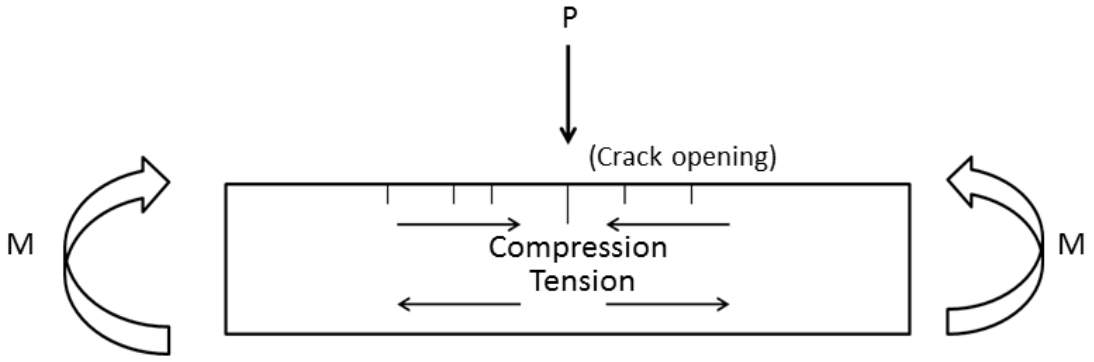

Figure A-10. Crake closing due to bending

APPENDIX B SENSITIVITY ANALYSIS FOR STRUCTURAL DAMAGES ON BRIDGE GIRDERS USING FINITE ELEMENT TOOLS

Girders are vulnerable part for bridge structures. Damage events such as collision, fire, corrosion and fatigue often occur on girder structures. In this research, various damage scenarios are considered in SAP 2000 finite element modeling for Meriden Bridge. After damage are modelled in the model, modal analysis is implemented to compare the natural frequency results with undamaged baseline. This study will be helpful to researchers to understand how much natural frequency will change under different damage scenarios.

B-1 Damage on the center of all 8 girders

In this part, structural damages are simulated by cutting the web and bottom flange at the center of all 8 girders. The drawings of the three damage cases can be seen in Figure B-1.

Scenario All-1: lower half of the center element on web is cut, the height is 17.32 in (0.44 m), and the width is 17.81 in (0.45 m).

Scenario All-2: Both lower half of web and bottom flange are cut.

Scenario All-3: The whole web and bottom flange are cut.

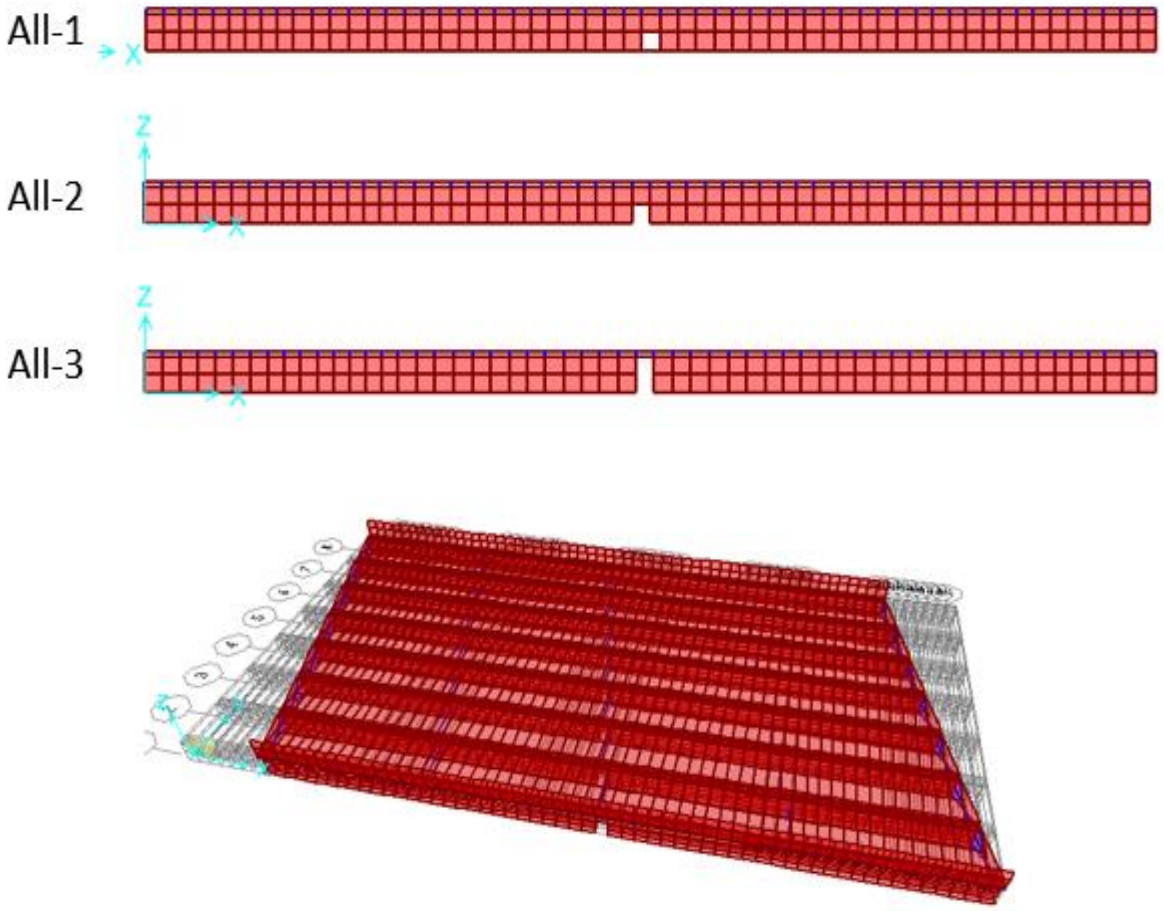

Figure B-1. Damage on center for all 8 girders

Table B-1. Change of natural frequency due to damage on center of all 8 girders

Undamaged		All-1		All-2		All-3	
Num	**Freq(Hz)**	**Freq(Hz)**	**Change**	**Freq(Hz)**	**Change**	**Freq(Hz)**	**Change**
1	4.44	4.44	-0.10%	3.5625	-19.82%	3.01	-32.15%
2	5.57	5.57	-0.05%	5.031	-9.69%	4.71	-15.47%
3	6.78	6.78	-0.10%	6.2533	-7.81%	5.87	-13.49%
4	9.77	9.75	-0.13%	9.2578	-5.20%	8.62	-11.74%
5	14.17	14.13	-0.27%	14.138	-0.24%	13.78	-2.74%
6	14.89	14.88	-0.11%	14.833	-0.41%	13.99	-6.06%
7	16.72	16.68	-0.22%	16.666	-0.29%	16.52	-1.14%
	Average change		-0.14%		-6.21%		-11.83%

B-2 Damage throughout Girder 3

In Meriden Bridge, No. 3 girder is under slow land and undertakes largest loadings among all girders. Thus No.3 girder is selected in this study to simulate various damage scenarios. Two damage scenarios are simulated consider damage throughout all length of Girder 3. Five damage scenarios are simulated consider single small damage on different locations on girder 3.

Scenario G3-1: lower half of the web is cut throughout girder No. 3, its height is 17.32 in (0.44 m).

Scenario G3-2: Both lower half of web and bottom flange are cut throughout girder No. 3.

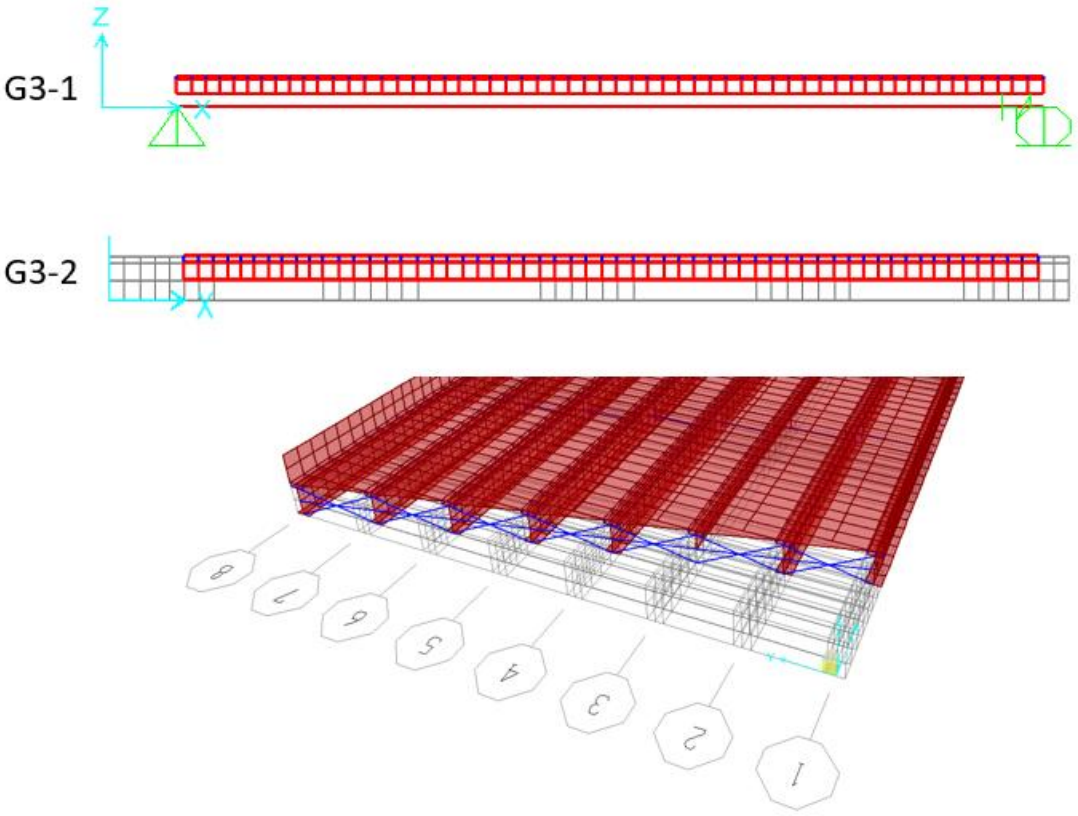

Figure B-2. Damage throughout Girder 3

Table B-2. Change of natural frequency due to damage throughout Girder 3

Undamaged		**G3-1**		**G3-2**	
Num	**Freq(Hz)**	**Freq(Hz)**	**Change**	**Freq(Hz)**	**Change**
1	4.44	4.2105	-5.24%	4.28	-3.62%
2	5.57	5.4133	-2.83%	5.46	-1.97%
3	6.78	6.614	-2.49%	6.67	-1.70%
4	9.77	9.3014	-4.75%	9.26	-5.17%
5	14.17	12.454	12.12%	12.67	10.62%
6	14.89	14.7	-1.30%	14.79	-0.71%
7	16.72	18.254	9.21%	15.79	-5.54%
Average			-2.79%		-4.19%

B-3 Single damage on different locations on Girder 3

Damage G3-3: The height of the cut is 17.32 in (0.44 meter), and the width is 17.81 in (0.45 meter).

Damage G3-4: The 14th element is cut for both lower web and bottom flange. Its distance to left edge is 222.75 in (5.66 meter).

Damage G3-5: The damage element is 28th from the left. Its distance to left end is 480.72 in (12.21 meter).

Damage G3-6: The damage element is 42th from the left. Its distance to left end is 776.03 in (19.71 meter), to the right is 215.18 in (5.47 meter).

Damage G3-7: The width is 17.81 in (0.45 meter), and height is 17.32 in (0.44 meter).

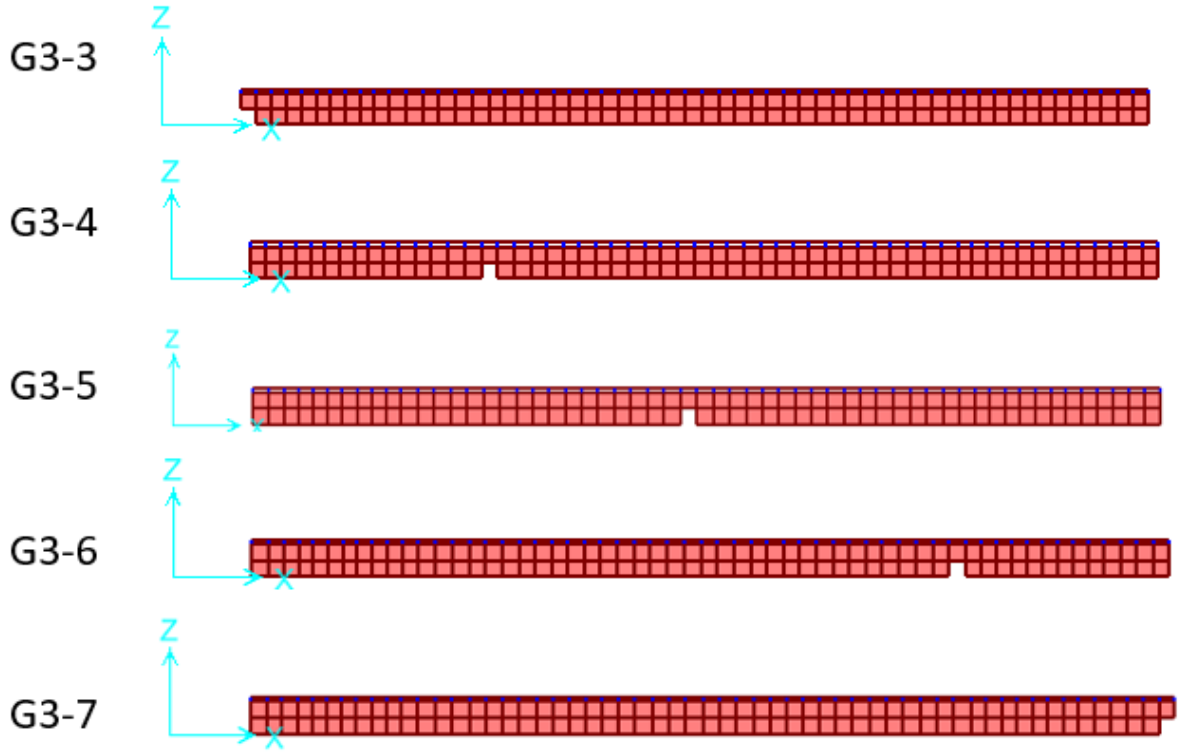

Figure B-3. Single damage on different locations on Girder 3

Table B-3. Change of natural frequency due to damage through Girder 3

Undamaged		**G3-3**		**G3-4**		**G3-5**		**G3-6**		**G3-7**	
Number	**Freq(Hz)**	**Freq(Hz)**	**Change**	**Freq(Hz)**	**Change**	**Freq(Hz)**	**Change**	**Freq(Hz)**	**Change**	**Freq(Hz)**	**Change**
1	4.44	4.44	-0.18%	4.41	-0.74%	4.36	-1.82%	4.41	-0.66%	4.41	-0.77%
2	5.57	5.54	-0.53%	5.57	-0.10%	5.53	-0.77%	5.55	-0.44%	5.54	-0.50%
3	6.78	6.73	-0.79%	6.78	-0.02%	6.76	-0.29%	6.77	-0.17%	6.78	-0.07%
4	9.77	9.58	-1.85%	9.75	-0.13%	9.65	-1.14%	9.68	-0.92%	9.72	-0.43%
5	14.17	14.09	-0.56%	13.76	-2.88%	14.16	-0.08%	13.82	-2.47%	14.11	-0.45%
6	14.89	14.88	-0.10%	14.92	0.17%	14.91	0.11%	14.85	-0.27%	14.86	-0.23%
7	16.72	16.54	-1.04%	16.53	-1.12%	16.7	-0.07%	16.38	-2.00%	16.63	-0.52%
Average			-0.72%		-0.69%		-0.58%		-0.99%		-0.43%

REFERENCES

[1] Aguirre, N., Ikhouane, F., Rodellar, J. and Christenson, R. (2012). "Parametric identification of the Dahl model for large scale MR dampers." *Structural Control and Health Monitoring*, 19(3), 332-347.

[2] American Road & Transportation Builders Association (2016). "2016 Structurally Deficient Bridges." http://www.artba.org/economics/2016-u-s-deficient-bridges/, Data Source: Federal Highway Administration, 2015 National Bridge Inventory ASCII files, January 2016.

[3] Anastasopoulos, A., Lekou, D. J. and Mouzakis, F. (2012). "Health monitoring of a neg-miconnm48/750 wind turbine blades with acoustic emission." *In European conference on acoustic emission testing & 7th international conference on acoustic emission*, 12-15, University of Granada, Granada, Spain.

[4] Antoniadis, A., Paparoditis, E. and Sapatinas, T. (2006). "A functional wavelet-kernel approach for time series prediction." *J. Royal Stat. Soc. B*, 68, 837–857.

[5] Atray, V.S. and Roschke, P.N. (2004). "Neuro-fuzzy control of railcar vibrations using semiactive dampers." *Computer-Aided Civil and Infrastructure Engineering*, 19(2), 81-92.

[6] Bagchi, A., Humar, J., Xu, H. and Noman, A.S. (2010). "Model-based damage identification in a continuous bridge using vibration data." *Journal of Performance of Constructed Facilities*, 24(2), 148-158.

[7] Bass, B.J. and Christenson, R.E. (2007). "System identification of a 200 kN magneto-rheological fluid damper for structural control in large-scale smart structures." American Control Conference 2007, New York City, USA.

[8] Bouc, R. (1971). "A mathematical model for hysteresis." *Acta Acustica united with Acustica*, 24(1), 16-25.

[9] Cai, G. and Mahadevan, S. (2016). "Big data analytics in online structural health monitoring." International Journal of Prognostics and Health Management, 7, 1-11.

[10] Cao Y., Yim J., Zhao Y. and M.L. Wang (2011). "Temperature effects on cable stayed bridge using health monitoring system: a case study." *Structural Health Monitoring*, 10(5), 523-537.

[11] Chang, C.C. and Roschke, P. (1998). "Neural network modeling of a magnetorheological damper." *Journal of intelligent material systems and structures*, 9(9), 755-764.

[12] Chatzi, E. and Smyth, A.W. (2009). "The unscented Kalman filter and particle filter methods for nonlinear structural system identification with non-collocated heterogeneous sensing." *Structural Control and Health Monitoring*, 16(1), 99-123.

[13] Chatzis, M.N., Chatzi, E.N. and Smyth A.W. (2014). "An experimental validation of time domain system identification methods with fusion of heterogeneous data." *Earthquake Engineering & Structural Dynamics*, 44(4), 523–547.

[14] Choi, S.B., Lee, S.K. and Park, Y.P. (2001). "A hysteresis model for the field-dependent damping force of a magnetorheological damper." *Journal of Sound and Vibration*, 245(2), 375–383.

[15] Christenson, R. and Motaref, S. (2016). "Dual purpose bridge health monitoring and weigh-in-motion (BWIM)." Final Report, Connecticut Department of Transportation, Report No. CT-2265-F-15-7, July 7, 2016.

[16] Christenson, R., Bakulski, S.K. and McDonnell, A.H. (2011). "Establishment of a dual-purpose bridge health monitoring and weigh-in-motion system for a steel girder bridge." In: Transportation Research Board 90th Annual Meeting, Washington, D.C., USA, 23-27 January 2011, paper no. 11-1598.

[17] Christenson, R., Kolev, V., Motaref, S. and Jang, S. (2016). "Development and evaluation of a dual purpose bridge health monitoring and weigh-in-motion system for a steel girder." Final Report, Connecticut Department of Transportation, Report No. CT-2271-F-15-10, June 30, 2016.

[18] Constantinou, M. and Tadjbakhsh, I.G. (1985). "Hysteretic dampers in base isolation: random approach." Journal of Structural Engineering, 111(4), 705-721.

[19] Cornwell, P., Farrar, C.R., Doebling, S.W. and Sohn, H. (1999). "Environmental variability of modal properties." *Experimental Techniques*, 23(6), 45-48.

[20] Cross, E.J., Koo, K.Y., Brownjohn, J.M.W. and Worden, K. (2013). "Long-term monitoring and data analysis of the Tamar Bridge." *Mechanical Systems and Signal Processing*, 35(1-2), 16-34.

[21] Dahl, P. R. (1968). "A solid friction model." Technical report, (No. TOR-0158 (3107-18)-1). Aerospace Corp, El Secundo, CA.

[22] Dahl, P. R. (1976). "Solid friction damping of mechanical vibrations." *AIAA Journal*, 14(12), 1675-1682.

[23] Deraemaeker, A., Reynders, E., De Roeck, G. and Kullaa, J. (2008). "Vibration-based structural health monitoring using output-only measurements under changing environment." *Mechanical Systems and Signal Processing*, 22(1), 34-56.

[24] Desjardins, S. L., Londono, N. A., Lau, D. T. and Khoo, H. (2006). "Real-time data processing, analysis and visualization for structural monitoring of the confederation bridge", *Advances in Structural Engineering*, 9(1), 141-157.

[25] Ding, Y. and Li, A. (2011). "Temperature-induced variation of measured modal frequencies of steel box girder for a long-span suspension bridge." *International Journal of Steel Structure*, 11(2): 145-155.

[26] Doebling, S.W., Farrar, C.R. and Prime, M.B. (1998). "A summary review of vibration-based damage identification methods." *Shock and Vibration Digest*, 30(2), 91–105.

[27] Dyke, S.J. (2010). "2020 vision for earthquake engineering research: Rep. on an OpenSpace Technology Workshop on the future of Earthquake Engineering." https://nees.org/resources/1636.

[28] Eftekhar Azam, S., Bagherinia, M. and Mariani, S. (2012). "Stochastic system identification via particle and sigma-point Kalman filtering." *Scientia Iranica*, 19(4), 982-991.

[29] Fugate, M.L., Sohn, H. and Farrar, C.R. (2001). "Vibration-based damage detection using statistical process control", *Mechanical System and Signal Processing*, 15(4), 707-721.

[30] Gamota, D.R. and Filisko, F.E. (1991). "Dynamic mechanical studies of electro-rheological materials: moderate frequencies." *Journal of Rheology*, 35(3), 399-342.

[31] Gavin, H.P. (2001). "Multi-duct ER dampers." *Journal of Intelligent Material Systems and Structures*, 12(5), 353-366.

[32] Gonzales I., Ülker-Kaustell, M. and Karoumi, R. (2013). "Seasonal effects on the stiffness properties of a ballasted railway bridge." *Engineering structures*, 57, 63-72.

[33] Gutierrez-Osuna, R. "Intelligent sensor systems Lecture 13." http://research.cs.tamu.edu/prism/lectures/iss/iss_l13.pdf (accessed 14 June 2015)

[34] Hoshiya, M. and Saito, E. (1984). "Structural identification by extended Kalman filter." *Journal of Engineering Mechanics*, 110(12), 1757–1770.

[35] Ismail, M., Ikhousne, F. and Rodellar, J. (2009). "The hysteresis Bouc-Wen model, a survey." *Arch Comput Methods Eng*, 16, 161-188.

[36] Jameson, A., Schmidt, W. and Turkel, E. (1981). "Numerical solutions of the Euler equations by finite volume methods using Runge-Kutta time-stepping schemes." *AIAA 14th Fluid and Plasma Dynamic Conference*, CA, USA.

[37] Jiang, Z., and Christenson, R. (2011). "A comparison of 200 kN magneto-rheological damper models for use in real-time hybrid simulation pretesting." *Smart Materials and Structures*, 20(6), 065011.

[38] Jiang, Z., and Christenson, R. (2012). "A fully dynamic magneto-rheological fluid damper model," *Smart Materials and Structures*, 21(6), 065002.

[39] Jiménez, R. and Álvarez-Icaza, L. (2005). "LuGre friction model for a magnetorheological damper." *Structural Control and Health Monitoring*, 12(1), 91-116.

[40] Jin, C., Jang, S. and Sun, X. (2015a). "Structural damage detection using extended Kalman filter combined with statistical process control." *Proceedings of SPIE Smart Structures/NDE 2015*, San Diego, CA.

[41] Jin, C., Jang, S. and Sun, X. (2015b). "Structural damage detection using extended Kalman filter combined with statistical process control in nonlinear systems." *Proceedings of the 10th International Workshop on Structural Health Monitoring 2015: System Reliability for Verification and Implementation*, Stanford, CA.

[42] Jin, C., Jang, S. and Sun, X. (2016a). "An integrated real-time structural damage detection method based on extended Kalman filter and dynamic statistical process control." *Advances in Structural Engineering*, July 5, 2016, doi: 10.1177/1369433216658484

[43] Jin, C., Jang, S., Sun, X., Jiang, Z. and Christenson, R. (2015c). "Application of MR damper in real-time structural damage detection using extended Kalman filter." *The Joint 6th International Conference on Advances in Experimental Structural Engineering (6AESE) and 11th International Workshop on Advanced Smart Materials and Smart Structures Technology (11ANCRiSST)*, Urbana Champaign, IL.

[44] Jin, C., Jang, S., Sun, X., Jiang, Z. and Christenson, R. (2016b). "Extended Kalman filter based structural damage detection for MR damper controlled structures." *Proceedings of SPIE Smart Structures/NDE 2016*, Las Vegas, NV.

[45] Jin, C., Li, J., Jang, S., Sun, X. and Christenson, R. (2015d). "Structural damage detection for in-service highway bridge under operational and environmental variability." *Proceedings of SPIE Smart Structures/NDE 2015*, San Diego, CA.

[46] Jin, C., Li, J., Jang, S., Sun, X. and Christenson, R. (2016c). "Damage detection of a highway bridge under severe temperature changes using extended Kalman filter trained neural network." *Journal of Civil Structural Health Monitoring*, 6 (3), 545-560.

[47] Kallinikidou, E., Yun, H. B., Masri, S. F., Caffrey, J. P. and Sheng, L. H. (2013). "Application of orthogonal decomposition approaches to long-term monitoring of infrastructure systems", *Journal of Engineering Mechanics*, 139(6), 678-690.

[48] Karoumi, R., Andersson, A. and Sundquist, H. (2006). "Static and dynamic load testing of the New Svinesund Arch Bridge." *The International Conference on Bridge Engineering – Challenges in the 21st Century*, 1-3 November 2006, Hong Kong.

[49] Kullaa, J. (2003). "Damage Detection of the Z24 Bridge using control charts." *Mechanical Systems and Signal Processing*, 17(1), 163-170.

[50] Lee, G. C., Mohan, S. B., Huang, C. and Fard, B. N. (2013). "A study of U.S. bridge failures (1980-2012)." Technical Report, MCEER-13-0008, MCEER University at Buffalo, State University of New York, June 15, 2013.

[51] Lei, Y., Jiang, Y. and Xu, Z. (2012). "Structural damage detection with limited input and output measurement signals." *Mechanical System and Signal Processing*, 28, 229-243.

[52] Li J. (2014). "Structural health monitoring of an in-service highway bridge with uncertainties." PhD Thesis, University of Connecticut, USA.

[53] Liang, Y., Wu, D., Liu, G., Li, Y., Gao, C., Ma, Z.J. and Wu, W. (2016). "Big data-enabled multiscale serviceability analysis for aging bridges." Digital Communications and Networks, 2(3), 97-107.

[54] Liu, C. and DeWolf, J.T. (2007). "Effect of temperature on modal variability of a curved concrete bridge under ambient loads." *Journal of Structural Engineering*, 133(12), 1742-1751.

[55] Liu, X., Escamilla-Ambrosio, P.J. and Lieven, N.A.J. (2009). "Extended Kalman filtering for the detection of damage in linear mechanical structures." *Journal of Sound and Vibration*, 325(4), 1023-1046.

[56] Magalhães, F., Cunha, A. and Caetano, E. (2012). "Vibration based structural health monitoring of an arch bridge: from automated OMA to damage detection." *Mechanical Systems and Signal Processing*, 28, 212-228.

[57] Mariani, S. and Corigliano, A. (2005). "Impact induced composite delamination: state and parameter identification via joint and dual extended Kalman filters." *Computer Methods in Applied Mechanics and Engineering*, 194(50–52), 5242–5272.

[58] Mariani, S. and Ghisi, A. (2007). "Unscented Kalman filtering for nonlinear structural dynamics." *Nonlinear Dynamics*, 49(1-2), 131-150.

[59] Mata J. (2011). "Interpretation of concrete dam behaviour with artificial neural network and multiple linear regression models." *Engineering Structures*, 33(3), 903-910.

[60] Meko, T. (2016). "Six maps that show the anatomy of America's vast infrastructure." The Washington Post, Dec. 1, 2016, https://www.washingtonpost.com/graphics/national/maps-of-american-infrastrucure/

[61] Nayyerloo, M. (2011), "Real-time structural health monitoring of nonlinear hysteretic structures." PhD thesis, University of Canterbury, New Zealand.

[62] Peeters, B. and Roeck, G.D. (2001). "One-year monitoring of the Z24-Bridge: environmental effects versus damage events." *Earthquake Engineering and Structural Dynamics*, 30, 149-171.

[63] Peeters, B., Maeck, J. and De Roeck, G. (2001). "Vibration-based damage detection in civil engineering: excitation sources and temperature effects." *Smart Materials and Structures*, 10(3), 518-527.

[64] Plude, S. (2011). "Implementing a long-term bridge monitoring strategy for a composite steel girder bridge." Master Thesis, University of Connecticut, USA.

[65] Pukelsheim, F. (1994). "The three sigma rule." *The American Statistician*, 48(2), 88-91.

[66] Reynders, E., Wursten, G. and De Roeck, G. (2014). "Output-only structural health monitoring in changing environmental conditions by means of nonlinear system identification." *Structural Health Monitoring*, 13(1), 82-93.

[67] Ruangrassamee, A., Srisamai, W. and Lukkunaprasit, P. (2006). "Response mitigation of the base isolated benchmark building by semi-active control with the viscous-plus-variable-friction damping force algorithm", *Journal of Structural Control and Health Monitoring*, 13(2-3), 809-822.

[68] Samali, B., Li, J., Crews, K.I. and Al-dawod, M. (2007). "Load Rating of impaired bridges using a dynamic method." *Electronic Journal of Structural Engineering Special Issue: Loading on Structures*, 66-75.

[69] Shirazi, F.A., Mohammadpour, J., Grigoriadis, K.M. and Song, G. (2012). "Identification and control of an MR damper with stiction effect and its application in structural vibration mitigation." *IEEE Transactions on Control Systems Technology*, 20(5), 1285-1301.

[70] Shumway, R.H. and Stoffer, D.S. (2013). "*Time series analysis and its applications*." Springer Science & Business Media.

[71] Sohn, H. (2007). "Effects of environmental and operational variability on structural health monitoring." *Philosophical Transactions of the Royal Society*, 365(1851), 539-560.

[72] Sohn, H., Czarnecki, J.A. and Farrar, C.R. (2000). "Structural health monitoring using statistical process control." *Journal of Structural Engineering*, 126(11), 1356-1363.

[73] Sohn, H., Farrar, C.R., Hemez, F.M. and Czarnecki, J.J. (2004). "A review of structural health monitoring literature: 1996-2001." Rep. No. LA-13976-MS, Los Alamos National Laboratory, Los Alamos, NM.

[74] Sohn, H., Worden, K. and Farrar, C.R. (2002). "Statistical damage classification under changing environmental and operational conditions." *Journal of Intelligent Material Systems and Structures*, 13, 561-574.

[75] Song, X., Ahmadian, M. and Southward, S.C. (2005). "Modeling magnetorheological dampers with application of nonparametric approach." *Journal of Intelligent Material Systems and Structures*, 16(5), 421-432.

[76] Soyoz, S. and Feng, M.Q. (2008). "Instantaneous damage detection of bridge structures and experimental verification." *Structural Control and Health Monitoring*, 15(7), 958-973.

[77] Soyoz, S. and Feng, M.Q. (2009). "Long-term monitoring and identification of bridge structural parameters." *Computer-Aided Civil and Infrastructure Engineering*, 24, 82-92.

[78] Spencer, B.F., Dyke, S.J., Sain, M.K. and Carlson, J.D. (1997). "Phenomenological model for magnetorheological dampers." *Journal of Engineering Mechanics*, 123(3), 230-238.

[79] Spiridonakos, M. and Chatzi, E. (2014). "Polynomial chaos expansion models for SHM under environmental variability." *In Proceedings of European 2014, 9th International Conference on Structural Dynamics*, June 30-July 2, 2014, Porto, Portugal.

[80] Stanway, R., Sproston, J.L. and Stevens, N.G. (1985). "Non-linear identification of an electrorheological vibration damper." In IFAC Identification and System Parameter Estimation, 7, 195-200.

[81] Stanway, R., Sproston, J.L. and Stevens, N.G. (1987). "Non-linear modelling of an electro-rheological vibration damper." *Journal of Electrostatics*, 20(2), 167-184.

[82] Sun, B., Luh, P.B., Jia, Q. and O'Neill, Z. (2012). "Building Energy Doctors: an SPC and Kalman filter-based method for system-level fault detection in HVAC systems." *IEEE Transaction on Automation Science and Engineering*, 11(1), 215-229.

[83] Wang, D.H. and Liao, W.H. (2004). "Modeling and control of magnetorheological fluid dampers using neural networks." *Smart Materials and Structures*, 14(1), 111-126.

[84] Welch, G. and Bishop, G. (2002). "An Introduction to The Kalman Filter." technical report, Dept. of Computer Science, Univ. of North Carolina at Chapel Hill.

[85] Wen, Y. K. (1976). "Method for random vibration of hysteretic systems." *Journal of the engineering mechanics division*, 102(2), 249-263.

[86] Wheeler, D.J. and Chambers, D.S. (1992). "Understanding statistical process control." SPC press, Tennessee, USA.

[87] Wiborg, E., Hulaas, H., Francke, H., Bureau, F.D. and Nielsen, T.K. (2014). "Applied statistical quality control on field measurement data." *10th International Conference of Hydraulic Efficiency Measurement*, Brazil.

[88] Wu, M. and Smyth, A.W. (2007). "Application of the unscented Kalman filter for real-time nonlinear structural system identification." *Structural Control and Health Monitoring*, 14(7), 971-990.

[89] Xia, Y., Chen, B., Weng, S., Ni, Y. and Xu, Y. (2012). "Temperature effect on vibration properties of civil structures: a literature review and case studies." *Journal of civil structural health monitoring*, 2(1), 29-46.

[90] Xu, H. and Humar, J. (2006). "Damage detection in a girder bridge by artificial neural network technique." *Computer-Aided Civil and Infrastructure Engineering*, 21(6), 450-464.

[91] Yan, Y.J., Cheng, L., Wu, Z.Y. and Yam, L.H. (2007). "Development in vibration-based structural damage detection technique." *Mechanical Systems and Signal Processing*, 21(5), 2198-2211.

[92] Yang, J.N., Lin, S., Huang, H. and Zhou, L. (2006). "An adaptive extended Kalman filter for structural damage identification." *Structural Control and Health Monitoring*, 13(4), 849-867.

[93] Yang, J.N., Pan, S. and Huang, H. (2007). "An adaptive extended Kalman filter for structural damage identifications II: unknown inputs." *Structural Control and Health Monitoring*, 14(3), 497-521.

[94] Yin, Q., Zhou, L., Mu, T. and Yang, J.N. (2013). "Experimental study on damage detection of base-isolated structure using an adaptive extended Kalman filter." *Journal of Theoretical and Applied Mechanics*, 51(4), 1013-1026.

[95] Zapico-Valle, J.L., García-Diégueza, M., González-Martíneza, M.P. and Wordenb, K. (2011). "Experimental validation of a new statistical process control feature for damage detection." *Mechanical Systems and Signal Processing*, 25(7), 2513-2525.

[96] Zhang, J., Qiu, H., Shamsabadi, S. S., Birken, R. and Schirner, G. (2014). "SIROM3 -- A scalable intelligent roaming multi-modal multi-sensor framework", In IEEE 38th Annual Computer Software and Applications Conference (COMPSAC), pp. 446-455.

[97] Zhang, W., Cai, C. S., Pan, F. (2012). "Fatigue reliability assessment for long-span bridges under combined dynamic loads from winds and vehicles." *ASCE Journal of Bridge Engineering*, 18(8), 735-747.

[98] Zhou, H.F., Ni, Y.Q. and Ko, J.M. (2010). "Constructing input to neural networks for modeling temperature-caused modal variability: mean temperatures, effective temperatures, and principal components of temperatures." *Engineering Structures*, 32(6), 1747-1759.

[99] Zhou, H.F., Ni, Y.Q. and Ko, J.M. (2011). "Eliminating temperature effect in vibration-based structural damage detection." *Journal of Engineering Mechanics*, 137, 785-796.

[100] Zhou, L., Wu, S. and Yang, J.N. (2008). "Experimental study of an adaptive extended Kalman filter for structural damage identification." *Journal of Infrastructure Systems*, 14(1), 42-51.